Universitat de les
Illes Balears

Doctoral Thesis
2014

MESOSCALE HYDRODYNAMICS AROUND THE BALEARIC ISLANDS: SPATIO-TEMPORAL VARIABILITY AND ITS RELATION WITH FISHING RESOURCES

Ángel M. Amores Maimó

Universitat de les Illes Balears

Doctoral Thesis
July 2014

Programa de Doctorat en Física

MESOSCALE HYDRODYNAMICS AROUND THE BALEARIC ISLANDS: SPATIO-TEMPORAL VARIABILITY AND ITS RELATION WITH FISHING RESOURCES

Ángel M. Amores Maimó

Director: Sebastià Monserrat Tomàs

List of Publications included in the Doctoral Thesis:

- Amores, A. and S. Monserrat. Hydrodynamic comparison between the north and south of Mallorca Island. *J. Marine Systems*, 2014. doi: 10.1016/j.jmarsys.2014.01.005.
- Amores, A., S. Monserrat, and M. Marcos. Vertical structure and temporal evolution of an anticyclonic eddy in the Balearic Sea (western Mediterranean). *J. Geophys. Res. Oceans*, 118:2097–2106, 2013a. doi: 10.1002/jgrc.20150.
- Pasqual,C., A. Amores, M. M. Flexas, S. Monserrat and A. Calafat. Environmental factors controlling particulate mass fluxes on the Mallorca continental slope (Western Mediterranean Sea). Accepted in *J. Marine Systems*, 2014.
- Amores, A., L. Rueda, S. Monserrat, B. Guijarro, C. Pasqual, and E. Massutí. Influence of the hydrodynamic conditions on the accessibility of Aristeus antennatus and other demersal species to the deep water trawl fishery off the Balearic Islands (western Mediterranean). *J. Marine Systems*, 2013b. doi: 10.1016/ j.jmarsys.2013.11.014.

The 2012 quality features of the journals where the articles were published are:

Journal	Impact Factor	Category Name	Total Journals in Category	Journal Rank in Category	Quartile in Category
JMS[1]	2.655	Geosciences, Multidisciplinary	172	39	Q1
		Marine & Freshwater Biology	100	12	Q1
		Oceanography	60	12	Q1
JGR[2]	3.174	Geosciences, Multidisciplinary	172	23	Q1

[1]Journal of Marine Systems
[2]Journal of Geophysical Research

A Ángeles por ser la alegría de mi vida.

A mis Padres, Ángel y Margarita, por haber estado ahí siempre.

Agraïments

En primer lloc haurem d'agraïr al qui ha pagat sa festa. Aquesta tesi ha estat duita a terme a l'Institut Mediterrani d'Estudis Avanats (IMEDEA) i ha estat possible gràcies al finançament rebut a través d'una beca JAE-PreDoc del CSIC cofinançada pel "Programa Operativo FSE 20072013". També he d'agraïr al projecte IDEADOS (proyecto del Plan Nacional CMT2008-04489-C03-03), gràcies al qual hem pogut disposar del finançament necessari per recopilar les dades emprades a aquesta tesi entre d'altres coses.

Ara que ja hem agraït a les institucions, anem a per lo important, que són les persones.

A nen Sebastià Monserrat li dec aquesta tesi. És tan seva (si no més) com meva. Sense la seva ajuda (acadèmica, moral, institucional, en persona, per Skype,...) aquest treball no hagués estat possible. He après molt treballant al seu costat i esper seguir aprenent d'ell. No sé a quina fase ens trobam ara, però crec que estam acabant sa B i començarem en breu sa C.

Amb na Marta Marcos he après el que sé de models, simulacions i sèries climàtiques. Ha estat un plaer poder treballar amb ella i esper poder seguir fent-ho al futur. Moltes gràcies pel teu temps i pel que m'has ensenyat.

També vull agraïr el seu temps que han dedicat amb jo als altres membres del grup, en Damià Gomis, en Biel Jordà i n'Antonio Sánchez.

I also want to thank Richard Thomson for the possibility of visiting the Institute of Oceanographic Sciences in Sidney, Canada, during one month. Thank you for your hospitality, your help and your time wasted with me.

No em puc oblidar de tot l'equip del projecte IDEADOS (Rosa Balbín, Jose Luís López Jurado, Alberto Aparicio,...) amb els que vaig compartir hores de vaixell, tant en la instalació i manteniment dels fondejos així com en les campanyes oceanogràfiques. Són els únics que poden dir que m'han vist "tirat" a sa coberta d'un vaixell.

Encara que només hagi passat la darrera part de la meva tesi amb ells, estic molt agraït als meus companys de despatx. Els presentarem com una banda de rock (s'ha de llegir com presentant a cada integrant). A la meva esquena trobam en Josep Llasses, responsable d'haver-me inoculat el virus FIFA ☺ i d'aixecar-me cada dia abans de que surti el Sol per anar a aixecar pes. Amb ell he passat moltes hores de discussió científica i no tant científica. A més, he après molt d'ell, de la seva manera de veure i viure la vida. A la meva esquerra es seu na Maribel Cerezo. Amb ella he pres molts cafès i hem fet moltes hores de tertúlia. Ella va aconseguir el que no havia aconseguir ningú: treure'm de festa un dijous! Més a l'esquerra trobam s'únic doctor entre noltros, en Jorge Arrieta. En ell veig s'evolució d'un doctorant com jo cap a investigador postdoctoral i m'ha obert els ulls de lo complicat que és obrir-se pas a aquest món tan competitiu. A la meva dreta es seu na Laura Ramajo, a sa que sempre tortur amb imatges mentals que no li agrada visualitzar. I finalment, i no per això menys important, en Miquel Cabanellas. Amb ell hem discutit molt sobre futbol, possibles inversions i junts hem après LaTeX. M'hauré quedat amb ses ganes d'anar a pescar bons calamars de potera amb algú que realment sap de pesca i de calamars.

Tampoc m'he d'oblidar dels companys del despatx del costat, que encara que no estiguem tan plegats també han estat allà. Entre ells hi ha n'Adrián Martínez, en Romain Escudier, en Juanma Sayol, na Bàrbara Barceló, en Dani Conti, ...

Els dinars a la UIB no serien el mateix sense en David Martinez, Diego Carrió i Maria Tous (que ens acompanya menys, per ho fa).

Encara que per coses del destí no ens veim tant com m'agradaria, durant aquets anys de tesi he fet bons amics i companys entre els estudiants de l'IFISC. Destaquen sobretot en Ricardo Martínez ("alias *el canario*"), en Pablo Fleuquín ("*el charrúa*") i en Miguel Ángel Escalona ("*el venezolano*"). Amb ells, entre molts altres bons moments, sempre recordaré ses incursons de pesca submarina, els partidets de futbol així com ses torrades a l'estil d'Uruguay.

Quan vaig començar Física vaig conèixer a n'Andreu Adrover, en Diego Carrió (ya vuelves a salir!!) i en Nico Villalonga. Amb ells he passat molts bons moments durant la carrera i els seguim passant en l'actualitat. Esper que la nostra amistat duri per molts d'anys encara que les nostres feines ens separin kilòmetres enfora.

També estic molt agraït a la totalitat de la meva família, els que hi són

i els que ja no. Gràcies a ells he arribat on som ara mateix. La meva tia Maria sempre s'ha preocupat per jo i ha estat com una segona mare. Moltes gràcies per tot el que has fet i fas. No em puc oblidar de sa meva padrina Francisca, que sempre m'ha cuidat, encara que de tant en tant corria darrera jo amb sa sabata. Si hagués d'escriure una frase per tothom no acabaria mai, per això vos incloc a tots dins aquest gràcies!

Als meus Pares, n'Àngel i na Margalida, els ho dec tot. Si he arribat on som ha estat per sa seva feina, la seva ajuda i les hores que han passat amb jo. Tot el que digui no serà suficient per agraïr el que heu fet per jo. Moltes gràcies.

Ángeles, aunque llevamos poco tiempo juntos, puedo asegurar que este tiempo contigo ha sido del mejor y más feliz de mi vida. La vida és, simplemente, mejor contigo. Tu optimismo se contagia, exhalas alegría por cada uno de tus poros y me haces ser mejor persona. Espero que el futuro nos depare muchas alegrías y buenos momentos durante mucho tiempo, y no dudes que también estaré ahí en los malos momentos que nos toque vivir. Por eso no puedo dejar de agradecerte que estés conmigo apoyándome en todo momento, dándome ánimos constantemente y preocupándote por mí siempre. Gracias por estar a mi lado!

Abstract

The Balearic Islands, located in the Western Mediterranean Sea, are the natural limit between the Balearic subbasin, at the noth and the Algerian subbasin, at the south. Previous studies based on hydrographic data have revealed that each of the basins have a different oceanographic climatology. One one hand, the Balearic subbasin has colder and saltier waters as a result of the water modification during the cyclonic circulation of the Mediterranean Sea. On the other, the Algerian subbasin waters are warmer and fresher, incoming directly from the Atlantic Ocean and entering into the Mediterranean through the Strait of Gibraltar. These two subbasins are connected via the topographic channels between the islands, whose hydrodynamic properties are governed by the mesoscale situation: non-permanent small scale phenomena ($\lesssim$100 km). Studying the mesoscale situation around the Balearic Islands can be useful for understanding how the water exchanges between the two subbasins are. Moreover, mesoscale structures, such as eddies, filaments or fronts, can temporarily change the hydrodynamic conditions. When it occurs, mesoscale variability not only affects the hydrodynamic conditions (water exchanges, alteration of the main currents, ...), but may also impact on the local ecosystems.

Understanding how the fishing resources from the Balearic Islands are affected by the mesoscale hydrodynamic situation has been one of the objectives of the IDEADOS project (CMT2008-04489-C03-01), the framework in which this thesis has been developed. The project focused in two areas of fishing interest: one located northwards of Mallorca Island, in the Balearic subbasin (Sóller), and another placed southwards, inside the Mallorca Channel (Cabrera). As part of the above mentioned research project, two mooring lines were deployed, one in the limit of each fishing ground and were maintained during 15 months. Using recorded data from the moorings, together with satellite observations and landing data from different species, we addressed questions such as: How is the hydrodynamic activity in each zone and which are the similarities and/or differences between both places

from an oceanographic perspective? Which are the main features of the mesoscale phenomena detected? And, how does the hydrography affect the sediment flux dynamics and the fishing resources of each zone?

The chapters of this thesis, which correspond to published articles in scientific journals, are organized following the previous questions. In the first chapter the data recorded by each mooring is analyzed with the aim of characterizing each zone and compare them. Derived from this study and in the second chapter, one of the mesoscale events detected in Sóller is deeply analyzed. This structure was an eddy which lasted about one month, reached down to the sea floor and completely changed the mean oceanographic properties in the complete water column. In the third chapter, the data collected by the sediment traps is analyzed and a relationship between the sediment fluxes measured and the possible triggering mechanisms is addressed. Finally, a study about the relationship between the observed hydrodynamics and the red shrimp (*Aristeus antennatus*) dynamics is performed. It is observed that the adult individuals of red shrimp would be affected by the bottom turbidity generated by the mesoscale phenomena. In turn, they would respond moving away from the fishing grounds, probably towards greater depths. As the main mesoscale events take place in Sóller during winter time, this could provoke the reported reduction of the amount of large individuals of red shrimp caught during this part of the year in this fishing ground.

The results of this thesis reinforce the lately recognized theory that fishing resources are not only affected by their exploitation or the self oscillations of the ecosystem (biotic factors), but they are also influenced by the changing oceanographic situation (abiotic factor).

Resumen

Las Islas Baleares, situadas en el Mar Mediterráneo Occidental, son el límite natural entre la subcuenca Balear, al norte y la subcuenca Argelina, al sur. Estudios previos basados en datos hidrográficos han revelado que cada una de las cuencas posee una climatología oceanográfica característica: la subcuenca Balear contiene aguas más frías y salinas como resultado de la modificación de las aguas durante la circulación ciclónica del Mediterráneo, mientras que la subcuenca Argelina contiene aguas más calientes y menos salinas provenientes directamente de aguas Atlánticas que entran por el estrecho de Gibraltar. Estas dos subcuencas están conectadas a través de los canales entre las islas, cuya hidrodinámica está dominada por la situación de mesoscala: fenómenos de escala pequeña ($\lesssim$100km) y que no son permanentes en el tiempo. Intentar conocer mejor la situación de mesoscala alrededor de las Islas Baleares puede ayudar a entender como son los intercambios de aguas entre las dos subcuencas. Además, los fenómenos asociados a la mesoscala, como son los vórtices, filamentos o frentes, pueden cambiar por completo la hidrodinámica temporalmente. En ese instante, los efectos de la mesoscala se extienden, no sólo a la oceanografía física (intercambio de aguas, alteración de las principales corrientes, entre otras), sino que también puede afectar a los ecosistemas de la zona.

Entender como se ven afectados los recursos pesqueros de las Islas Baleares por la situación hidrodinámica de mesoscala ha sido uno de los objetivos del proyecto IDEADOS (CMT2008-04489-C03-01), marco en el que se ha desarrollado esta tesis. El proyecto se centró en el estudio de dos zonas de pesca: una situada al norte de Mallorca, dentro de la subcuenca Balear y conocida como Sóller, y una localizada más al sur, dentro del canal de Mallorca y conocida como Cabrera. Para recoger los datos oceanográficos necesarios para la elaboración de este estudio, se instaló una línea de fondeo durante 15 meses en el límite de cada una de las zonas de pesca. Con estos datos y con la ayuda de datos de satélite y de capturas de diferentes

especies, se ha intentado dar respuesta a preguntas como: ¿cómo es la hidrografía de cada una de las zonas y cuales son las similitudes o diferencias entre las dos zonas? ¿Qué características tienen los fenómenos de mesoscala detectados? Y, ¿cómo afecta la hidrografía a la dinámica del flujo de sedimentos y a los recursos pesqueros de cada zona?

Los capítulos de resultados de esta tesis, que son reproducciones fieles de los artículos publicados en revistas científicas, están organizados para intentar responder a las preguntas acabadas de plantear. En el primer capítulo se analizan los datos recogidos por cada uno de los fondeos con el objetivo de fondo de caracterizar cada una de las zonas y compararlas entre ellas. Derivado de este estudio, ya en el segundo capítulo, se analiza en detalle uno de los eventos de mesoscala más intensos que se registró en Sóller: un vórtice que duró alrededor de un mes, llegando al fondo marino y que cambió por completo las propiedades oceanográficas promedio de la zona en toda la columna de agua. En el tercer capítulo se estudian los datos provenientes de cada una de las trampas de sedimentos presentes en los fondeos y se relacionan los flujos totales de masa recogidos con los posibles mecanismos generadores. Finalmente, se elabora un estudio sobre la relación de la hidrodinámica y las capturas de gamba roja (*Aristeus antennatus*). Se deduce que los individuos adultos de gamba roja se verían afectados por la turbidez de fondo generada por los fenómenos de mesoscala, y responderían alejándose de las zonas de pesca, probablemente hacia profundidades mayores. Ya que los eventos de mesoscala más importantes se dan en Sóller y principalmente en invierno, esto provocaría que la cantidad de gamba roja grande capturada durante esta época del año se viese reducida en este caladero.

Los resultados de esta tesis refuerzan la teoría de que los recursos pesqueros no sólo se ven afectados por su explotación o por las oscilaciones del propio ecosistema (factores bióticos) sino que también se ven influenciados por la situación oceanográfica cambiante (factor abiótico).

Resum

Les Illes Balears, situades a la Mar Mediterrània Occidental, són el límit natural entre la subconca Balear, al nord, i la subconca Algeriana, al sud. Estudis previs basats en dades hidrogràfiques han revelat que cada una de les conques posseix una climatologia oceanogràfica característica: la subconca Balear conté aigües més fredes i salines com a resultat de la modificació de les aigües durant la circulació ciclònica a la Mediterrània, mentre que la subconca Algeriana conté aigües més calentes i menys salines provenents directament d'aigües Atlàntiques que entren per l'estret de Gibaltar. Aquestes dues subconques estan connectadas a través dels canals entre les illes, la hidrodinàmica dels quals està dominada per la situació de mesoscala: fenòmens d'escala més petita ($\lesssim$ 100km) i que no són permanents en el temps. Intentar conèixer millor la situació de mesoscala al voltant de les Illes Balears pot ajudar a entendre com són els intercanvis d'aigües entre les dues subconques. A més, els fenòmens associats a la mesoscala, com són vòrtexs, filaments o fronts, poden canviar per complet la hidrodinàmica temporalment. En aquest moment, els efectes de la mesoscala s'extenen, no tan sols a la ocenografia física (intercanvi d'aigües, alteració de les principals corrents, entre d'altres), sinó que també poden afectar als ecosistemes de la zona.

Entendre com es veuen afectats els recursos pesquers de les Illes Balears per la situació hidrodinàmica de mesoscala ha estat un dels objectius del projecte IDEADOS (CMT2008-04489-C03-01), marc en el que s'ha desenvolupat aquesta tesi. El projecte es va centrar en l'estudi de dues zones de pesca: una situada al nord de Mallorca, dins la subconca Balear i coneguda con Sóller, i una localitzada més al sud, dins al canal de Mallorca i coneguda com Cabrera. Per recollir les dades oceanogràfiques necessàries per a l'elaboració de l'estudi, es va instal·lar una línia de fondeig durant 15 mesos al limit de cada una de les zones de pesca. Amb aquestes dades i amb l'ajuda de dades de satèl·lit i de captures de diferents espècies, s'ha intentat donar resposta a qüestions com: com es la hidrografia de

cada una de les zones i quines són les similituts o diferencies entre les dues zones? Quines característiques tenen els fenòmens de mesoscala detectats? I, com afecta la hidrografia a la dinàmica del fluxe de sediments i als recursos pesquers de cada zona?

Els capítols de resultats d'aquesta tesi, que són reproduccions fidels dels articles publicats en revistes científiques, estan organitzats per intentar respondre a les preguntes plantejades abans. En el primer capítol s'analitzen les dades recollides per cada un dels fondejos amb l'objectiu de fons de caracteritzar cada una de les zones i comparar-les entre elles. Derivat d'aquest estudi, en el segon capítol, s'analitza en detall un dels events de mesoscala més intens que es va enregistrar a Sóller: un vòrtex que durà al voltant d'un mes, arribant al fons marí i que canvià per complet les propietats oceanogràfiques promig de la zona en tota la columna d'aigua. En el tercer capítol s'estudien les dades provinents de cada una de les trampes de sediments presents als fondejos i es relacionen els fluxes totals de massa recollits amb els possibles mecanismes generadors. Finalment, s'elabora un estudi sobre la relació de la hidrodinàmica i les captures de gamba vermella (*Aristeus antennatus*). En ell es dedueix que els individus adults de gamba vermella es veurien afectats per la terbolesa de fons generada pels fenòmens de mesoscala, i respondrien allunyant-se fora de la zona de pesca, probablement cap a profunditats majors. Com que els events més importants de mesoscala es donen a Sóller i principalment a l'hivern, això faria que la quantitat de gamba vermella grossa capturada durant aquesta època de l'any es ves reduïda a aquest calader.

Els resultats d'aquesta tesi reforcen la teoria de que els recursos pesquers no sols es veuen afectats per la seva explotació o per les oscil· lacions del propi ecosistema (factors biòtics) sinó que també es veuen influenciats per la sitació oceanogràfica canviant (factor abiòtic).

Contents

Contents **xv**

Introduction **1**
The Region Under Study 1
Hydrodynamics around the Balearic Islands 1
Hydrodynamic vs Fishing Resources. 3
Mooring description 5
Satellite data 6
Bibliography 7

1 Hydrodynamic comparison between the north and south of Mallorca Island **11**
1.1 Introduction 12
1.2 Data Sets and Methodology 14
1.3 Results 15
1.4 Summary and Conclusions 27
Bibliography 29

2 Vertical structure and temporal evolution of an anticyclonic eddy in the Balearic Sea (western Mediterranean) **33**
2.1 Introduction 34
2.2 Data Sets and Methodology 37
2.3 Results and Discussion 38
2.3.1 Surface Description of the Eddy 39
2.3.2 Vertical Structure of the Eddy 40
2.3.3 Recurrence of the Phenomenon 47
2.4 Summary and Conclusions 49
Bibliography 51

3 Environmental factors controlling particulate mass fluxes on the Mallorca continental slope (Western Mediterranean Sea) 55
3.1 Introduction . . . 56
3.2 Data Sets and Methodology . . . 58
3.3 On the origin of the measured sediment fluxes . . . 60
3.4 Ecological Implications . . . 66
3.5 Summary and Conclusions . . . 66
Bibliography . . . 67

4 Influence of the hydrodynamic conditions on the accessibility of the demersal species to the deep water trawl fishery off the Balearic Islands (western Mediterranean) 73
4.1 Introduction . . . 74
4.2 Data and Methods . . . 77
4.2.1 Catches . . . 77
4.2.2 Hydrodynamic Data . . . 78
4.2.2.1 Satellite images . . . 78
4.2.2.2 Moorings . . . 79
4.2.3 Statistical Analysis . . . 79
4.3 Results and Discussion . . . 80
4.4 Summary and Conclusions . . . 88
Bibliography . . . 89

Summary and Discussion 95
Bibliography . . . 97

Conclusions 99

Future Work 103
Bibliography . . . 104

Appendix A: characteristics of the water masses. 107

Appendix B: features of the moored instruments. 109

List of Figures 111

List of Tables 117

Global Bibliography 119

Epíleg 133

Introduction

The Region Under Study

The Balearic Islands, located in the Western Mediterranean, are the natural limit between the Balearic and the Algerian subbasins (Fig. 1). These two areas are connected via channels between the islands. The Ibiza Channel (80 km wide, with a maximum depth of 800 m) is located between Cape La Nao (Iberian Peninsula) and Ibiza Island; the channel between Ibiza and Mallorca is known as the Mallorca Channel (80 km wide and 600 m deep); meanwhile the Menorca Channel, the shallowest (100 m deep) and narrowest (35 km wide) is located between Mallorca and Menorca Islands [*García et al.*, 1994].

The continental shelf of the Balearic subbasin ($38°45'$ to $42°30'$ N and $0°20'$ W to $4°00'$ N) is relatively narrow (15-30 km), with the exception of the Ebro River delta southwards, where it becomes wider up to 60-70 km. The slope is very steep, with depth increasing from 200 m to over 1000 m in only a few kilometers. The shelf around the Islands, at both Balearic and Algerian sea sides, is even narrower (5-20 km) and the slope becomes steeper and discontinuous due to the previous mentioned channels between the islands. Further details about the topographic characteristics of the region can be found, for example, in *García et al.* [1994].

Hydrodynamics around the Balearic Islands

The mean circulation in the Balearic subbasin, situated north of the archipelago up to the Iberian Peninsula, is driven by a density gradient between the fresher coastal water and the relatively saltier water in the center of the subbasin. This density gradients form the Catalan Front [*Font et al.*, 1988; *Violette et al.*, 1990] near the Continental slope and the Balearic front along the islands slope. The Northern Current (NC), which is associated with the Catalan front, flows southward along the Iberian Peninsula slope, following the isobaths, and coming from the northern coast of Sicily, the western Italian coastline and the Ligurian and

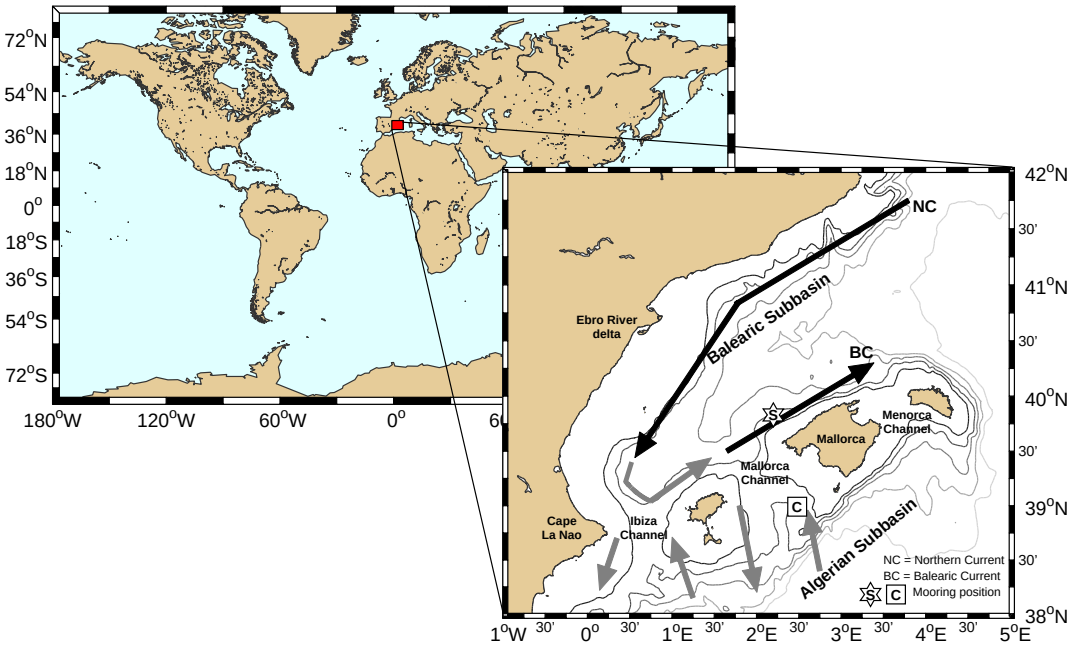

Figure 1: Map showing the main characteristics of the ocean circulation in the Balearic subbasin. The positions of the moorings are marked with an S inside a star for Sóller mooring and a C inside a square for Cabrera mooring. Isobaths are plotted between 500 m and 2500 m with a step of 500 m. Black arrows indicate the permanent currents, while the grey ones indicate the temporal features.

Provenal coast [*Millot*, 1999]. When the NC reaches the Ibiza Channel, two different behaviors are possible, depending on the mesoscale situation [*Pinot et al.*, 2002]. Normally, a portion of the NC may leave the Balearic subbasin via the Ibiza and Mallorca Channels towards the Algerian subbasin, while the rest gets reflected northward to form the Balearic Current (BC) which flows along the Islands' northern slope. In this case, the resident water between 200 m and 700 m, is mostly Levantine Intermediate Waters (LIW, refers to appendix A for further details of the water masses). When the previous winter had dry and cold winds as Mistral and Tramontane, which cause cooling and evaporation, an amount of Western Mediterranean Intermediate Waters (WIW) can be generated in the Gulf of Lion. This water mass is normally located between 100 m and 300 m and displaces the LIW forming the resident water at the intermediate depths [*Mertens and Schott*, 1998; *Millot*, 1999; *Pinot et al.*, 2002]. When these WIW reach the Balearic Channels in late spring, the NC most often gets blocked and a different configuration of flow through the channels is observed. Most of the NC reflects northwards, reinforcing the BC, and the southward flow through the channels is reduced [*Monserrat et al.*, 2008]. The deepest part of the water column, below

700 m, is occupied by Western Mediterranean Deep Waters (WMDW). Refer to *Massutí et al.* [2014]; *Millot* [1999]; *Pinot et al.* [2002] for a better description of the circulation.

The Algerian subbasin, the zone between the Balearic Islands and the north of Africa, is controlled by a completely different dynamics. The circulation of the Algerian subbasin is driven by the Algerian current which interacts with the Alboran sea gyres and spreads the Atlantic water towards the Balearic Islands. The northern part of the subbasin has no clear steady current, although its circulation is affected by the changes in the mesoscale structures in the southern part of the subbasin and the entrance of Mediterranean water coming in from the Balearic subbasin via the channels.

The mesoscale processes in the Mediterranean Sea are important since they affect to the large-scale circulation and water masses distribution pattern with important consequences on the ecosystems. These mesoscale phenomena, such as eddies, filaments or meanders, can have an horizontal scale from few km to hundreds of km and their vertical range can be superficial or extend down to the bottom. Moreover, their life span can be from a few days to several weeks [*Amores et al.*, 2013a], months [*Pascual et al.*, 2002] or even years [*Puillat et al.*, 2002]. For example, the Atlantic Water flowing in the Algerian Current can generate eddies of both signs, cyclonic or anticyclonic. Few times every year, these eddies might reach a diameter around 100 km and extend down to the seabed (more than 2000 m). Due to this vertical extension, which is deeper than the currents they were developed from, these eddies can follow the isobaths and leave the current path. The same structures are also formed in the Northern Current and the Balearic Current. These currents are strongly intensified during winter due to the deep water formation in the Gulf of Lions leading to the development of instabilities. An example of this process can be found in *Amores et al.* [2013a]. In this case, an anticyclonic eddy developed from an instability of the BC is described. It lasted for one month, reaching down to the bottom (around 900m) and modifying temporally the deep slope circulation.

Hydrodynamic vs Fishing Resources.

Population dynamics has been and still is a topic of wide interest in oceanography around the world. One of the main factors that determine its evolution is human activity, either through fishing [*Cook et al.*, 1997] or through polluting the ecosystems. Besides the human activity, the environmental variables have also been recognized as a factor affecting the population dynamics. Both types, abiotic (climate and hydrography) and biotic (trophic resources and predators) factors can produce intra- and inter-annual oscillations in the population evo-

lution of the different fishing resources [*Browman and Stergiou*, 2004]. Due to that both biotic and abiotic factors are involved, a multidisciplinary approach is advised.

Pursuing the objective of how these factors affect the deep water ecosystems and demersal resources of the Balearic Islands, the IDEA project *Influence of oceanographic structure and dynamics on demersal populations in waters of the Balearic Islands* was carried out between 2003 and 2006. On one hand, the intra-annual variability was studied through oceanographic surveys, monitoring the bottom trawl fishing fleet and studying the population dynamics of two key species, the European hake (*Merluccius merluccius*) and the red shrimp (*Aristeus antennatus*). On the other hand, long-term analysis of the parameters of these species and, climatic, meteorological and oceanographic indices were studied as inter-annual indicators of the environmental conditions.

The main results of IDEA project were:

- The development of models explaining how climatic conditions affect the hydrodynamics around the Balearic Islands [*Monserrat et al.*, 2008].
- Different hydrodynamics scenarios were found in the fishing grounds of the bottom trawl fishing fleet [*López-Jurado et al.*, 2008].
- It was observed that environmental and biological factors can influence the accessibility of the key species, as the hake [*Cartes et al.*, 2009; *Hidalgo et al.*, 2008a,b] and red shrimp [*Cartes et al.*, 2008; *Guijarro et al.*, 2008].

As a natural evolution of IDEA project, the IDEADOS project *Structure and dynamics of the bentho-pelagic slope ecosystem in two oligotrophic zones of the western Mediterranean: a multidisciplinary approach at different spatio-temporal scales in the Balearic Islands* was born in 2008 and lasted until 2013. It was designed to test the hypothesis arising from IDEA project with the main objective of determine the relationships between environmental conditions and the nekto-benthic slope communities, in two zones north (here on called Sóller) and south (referred as Cabrera) of Mallorca island (Fig. 1) at an intra-annual scale.

Among other studies, a mooring line was installed in each area (see the following section and appendix A for more details). The objective of setting these two moorings was double:

a) On one hand, to study the intra-annual hydrodynamic variability in each zone of interest and find the similarities and differences between both locations.

b) On the other hand, when the hydrodynamic features of both sides were established, seek a possible relation between the hydrodynamic and the red shrimp availability.

Moorings Description

One mooring line was deployed in each area in order to collect the required hydrodynamic data. The line from Sóller was placed northwest of Mallorca Island (39°49.682' N - 2°12.778' E) meanwhile the mooring from Cabrera was located southwest of the island, into the Mallorca Channel (38°59.484' N - 2°28.907' E) (Fig. 1).

Both moorings were deployed at about 900 m depth with a height of 600 m above the seabed. Each mooring consisted on four CTD (Conductivity, Temperature and Depth) Seabird 37 sensors placed at fixed depths at around 300 m, 500 m, 700 m and 900 m. In addition, two Nortek Aquadopp current meters were installed in the middle levels (at about 500 m) and near the bottom (around 900 m depth). A near-bottom PPS3/3 Technicap sequential sampling sediment trap (12 collecting cups, 0.125 m^2 opening and 2.5 height/diameter aspect ratio for the cylindrical part) was placed 30 m above the bottom (an scheme of the mooring is shown in Fig. 2). The lines were held at the seabed with two train wheels of 250 kg each and an acoustic release allowed their recovery. Observations of the thermohaline properties and currents were collected at sampling rates of 10 min for the CTD, 30 min for the current meters and 10 days for the sediment traps. A list of the main properties of these instruments can be found in the appendix B.

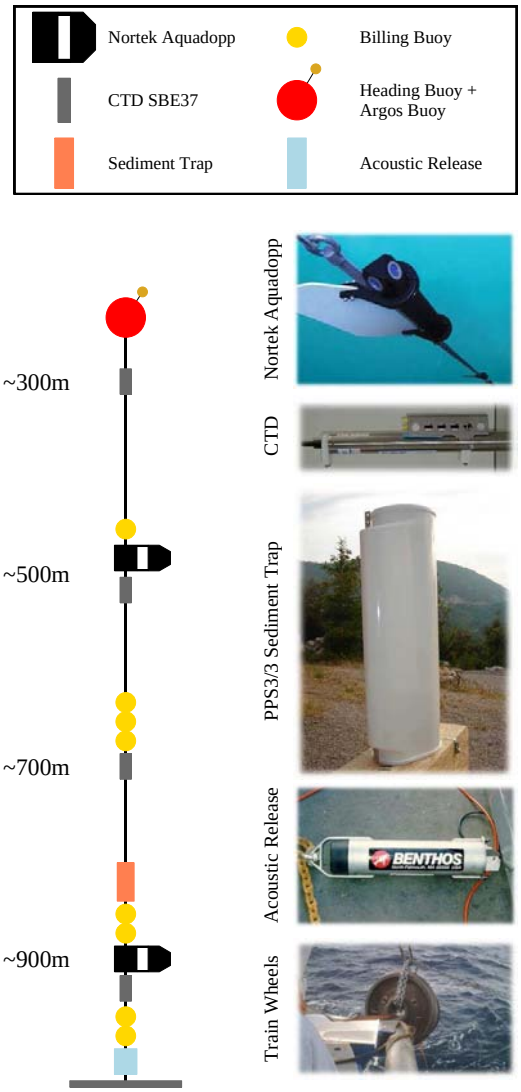

Figure 2: Scheme of the moorings configuration.

The moorings were continually recording data from mid-November 2009 until mid-February 2011. During this period, two maintenances were required because of the selected sampling rate for the sediment traps. These maintenances took place in mid-March and in mid-September 2010. The depth where

the instruments were located did not change significantly after the maintenances. The instruments encountered no significant problems during the whole period with the only exceptions of the 500m and 900m CTDs from Sóller and the 300m CTD from Cabrera which ran out of batteries around January 2011, about one month prior to the end of the experiment. The sediment trap time series have some gaps. The Cabrera sediment trap time series has a long gap in the middle of the experiment due to bad-working of the cups rotation mechanism. In addition the lack of ship availability during one of the scheduled maintenances produced another shorter gap at the time series from the trap at Sóller.

Satellite Data

From the available satellite data products, Sea Surface Heigth (SSH) and Sea Surface Temperature (SST) were used.

Daily gridded SSH fields with a map spacing of $1/8^\circ \times 1/8^\circ$ were obtained from the merged satellite AVISO products available at `www.aviso.oceanobs.com`. The absolute dynamic topography is calculated as the sum of the sea level anomalies and the mean dynamic topography [*Rio et al.*, 2007]. The regional sea level anomalies for the Mediterranean Sea available at AVISO server are a multi-mission product with up to 4 satellites at a given time, spanning the period from 1992 to present. All standard geophysical corrections were applied, including the so-called Dynamic Atmospheric Correction (DAC), produced by CLS. This correction combines the high frequency (H-F) of the Mog2D model [*Carrère and Lyard*, 2003] and the low frequency of the classical inverted barometer correction. These model outputs were used to correct the newly released altimeter data sets and therefore reducing the aliasing effects of H-F signals [*Volkov et al.*, 2007]. The regional mean dynamic topography covers the Mediterranean Sea and it is based on 7 years of observations (1993−1999). Despite its good performance in the open ocean and the wide range of applications, the altimetric products, both gridded and along-track fail when approaching to the coast, mostly due to the land contamination in the signal. Several efforts are currently devoted to the recovery and improvement of near-coastal altimetry observations. However, this new generation of observations is not fully developed for the global coastal ocean yet, not even for the Mediterranean Sea.

Daily sea surface temperature (SST) data were collected from MyOcean data base (`http://www.myocean.eu`). The regional gridded product for the Mediterranean Sea is a high resolution SST anomaly, computed using the CNR MED analysis at $1/16^\circ \times 1/16^\circ$ horizontal resolution and starting in December 2010.

*The thesis structure is the following. In the chapter 1, the data collected from both moorings is analyzed [Amores and Monserrat, 2014]. The hydrodynamic conditions of both places are studied and compared. It is observed that Sóller fishing ground is a more hydrodynamic active zone with numerous eddies, some of them reaching down to the bottom. In the next chapter, one of these eddies is analyzed in detail [Amores et al., 2013a]. It lasted around one month and clearly reached down to the seafloor, quintupling the mean near bottom currents and affecting to the resuspension of sediments and near bottom water turbidity. The quantification of the amount of sediments collected by the sediment traps at the moorings and their possible triggering mechanisms are studied in chapter 3 [Pasqual et al., 2013]. Accordingly to the greater hydrodynamic activity of Sóller, the amount of sediments collected by the sediment trap of this zone was also greater. Some evidences are shown suggesting most of these differences could be related to the eddies described in the previous chapters. Chapter 4 is where all the results from the previous three chapters are applied. It shows that the sediments resuspended by mesoscale features like the eddy described in chapter 2, can affect to the red shrimp (*Aristeus antennatus*) catches, presumably forcing the large individuals to displace to greater depths, where they cannot be fished [Amores et al., 2013b]. After the results explained in chapters 1, 2, 3 and 4, a discussion of their implications is developed. Then, the main conclusions of this thesis are listed. The last part of this document is focused on the possible future work that could be carried out based on the results of this thesis.*

Bibliography

Amores, A., and S. Monserrat (2014), **Hydrodynamic comparison between the north and south of Mallorca Island**, *J. Marine Systems*, doi: 10.1016/j.jmarsys.2014.01.005.

Amores, A., S. Monserrat, and M. Marcos (2013a), **Vertical structure and temporal evolution of an anticyclonic eddy in the Balearic Sea (western Mediterranean)**, *J. Geophys. Res. Oceans*, *118*, 2097–2106, doi: 10.1002/jgrc.20150.

Amores, A., L. Rueda, S. Monserrat, B. Guijarro, C. Pasqual, and E. Massutí (2013b), **Influence of the hydrodynamic conditions on the accessibility of Aristeus antennatus and other demersal species to the deep water trawl fishery off the Balearic Islands (western Mediterranean)**, *J. Marine Systems*, doi: 10.1016/j.jmarsys.2013.11.014.

Browman, H. I., and K. I. Stergiou (2004), Perspectives on ecosystem-based ap-

proaches to the management of marine resources, *Mar Ecol Prog Ser*, *274*, 269–303.

Carrère, L., and F. Lyard (2003), Modelling the barotropic response of the global ocean to atmospheric wind and pressure forcing Comparisons with observations, *Geophys. Res. Lett.*, *30*, doi: 10.1029/2002GL016473.

Cartes, J. E., V. Papiol, and B. Guijarro (2008), The feeding and diet of the deep-sea shrimp Aristeus antennatus off the Balearic Islands (Western Mediterranean): Influence of environmental factors and relationship with the biological cycle, *Progress in Oceanography*, *79*, 37–54, doi: 10.1016/j.pocean.2008.07.003.

Cartes, J. E., M. Hidalgo, V. Papiol, E. Massutí, and J. Moranta (2009), Changes in the diet and feeding of the hake Merluccius merluccius at the shelf-break of the Balearic Islands: Influence of the mesopelagic-boundary community, *Deep Sea Research Part I: Oceanographic Research Papers*, *56*(3), 344 – 365, doi: 10.1016/j.dsr.2008.09.009.

Cook, R. M., A. Sinclair, and G. Stefansson (1997), Potential collapse of North Sea cod stocks, *Nature*, *385*, 521–522, doi: 10.1038/385521a0.

Font, J., J. Salat, and J. Tintoré (1988), Permanent features in the general circulation of the Catalan Sea, *Oceanol. Acta*, *9*, 51–57.

García, E., J. Tintoré, J. M. Pinot, J. Font, and M. Manriquez (1994), Surface Circulation and Dynamics of the Balearic Sea, *Coastal Estuarine Stud.*, *46*, 73–91, doi: 10.1029/CE046p0073.

Guijarro, B., E. Massutí, J. Moranta, and P. Díaz (2008), Population dynamics of the red shrimp Aristeus antennatus in the Balearic Islands (western Mediterranean): Short spatio-temporal differences and influence of environmental factors, *Journal of Marine Systems*, *71 (3-4)*, 385–402, doi: 10.1016/j.jmarsys.2007.04.003.

Hidalgo, M., E. Massutí, J. Moranta, J. Cartes, J. Lloret, P. Oliver, and B. Morales-Nin (2008a), Seasonal and short spatial patterns in European hake (Merluccius merluccius L.) recruitment process at the Balearic Islands (western Mediterranean): The role of environment on distribution and condition, *Journal of Marine Systems*, *71*(34), 367 – 384, doi: 10.1016/j.jmarsys.2007.03.005.

Hidalgo, M., J. Tomás, H. Høie, B. Morales-Nin, and U. S. Ninnemann (2008b), Environmental influences on the recruitment process inferred from otolith stable isotopes in Merluccius merluccius off the Balearic Islands, *Aquat Biol*, *3(3)*, 195 – 207, doi: 10.3354/ab00081.

López-Jurado, J. L., M. Marcos, and S. Monserrat (2008), Hydrographic conditions affecting two fishing grounds of Mallorca island (Western Mediterranean): during the IDEA Project (20032004), *Journal of Marine Systems*, *71*, 303–315, doi: 10.1016/j.jmarsys.2007.03.007.

Massutí, E., M. Olivar, S. Monserrat, L. Rueda, and P. Oliver (2014), Towards understanding the influence of environmental conditions on demersal resources and ecosystems in the western Mediterranean: Motivations, aims and methods of the IDEADOS project, *Journal of Marine Systems*, doi: 10.1016/j.jmarsys.2014.01.013.

Mertens, C., and F. Schott (1998), Interannual variability of deep-water formation in the northwestern Mediterranean, *J. Phys. Oceanogr.*, *28*, 1410–1424, doi: 10.1175/1520-0485(1998)028⟨1410:IVODWF⟩2.0.CO;2.

Millot, C. (1999), Circulation in the Western Mediterranean Sea, *Journal of Marine Systems*, *20*, 423–442, doi: 10.1016/S0924-7963(98)00078-5.

Monserrat, S., J. L. López-Jurado, and M. Marcos (2008), A mesoscale index to describe the regional circulation around the Balearic Islands, *J. Mar. Syst.*, *71*, 413–420, doi: 10.1016/j.jmarsys.2006.11.012.

Pascual, A., B. B. Nardelli, G. Lanicol, M. Emelianov, and D. Gomis (2002), A case of an intense anticyclonic eddy in the Balearic Sea (western Mediterranean), *J. Geophys. Res.*, *107(C11)*, 3183, doi: 10.1029/2001JC000913.

Pasqual, C., A. Amores, M. Flexas, S. Monserrat, and A. Calafat (2013), **Environmental factors controlling particulate mass fluxes on the Mallorca continental slope (Western Mediterranean Sea)**, *Accepted in J. Marine Systems*, *XXX*, XXX, doi: XXX.

Pinot, J. M., J. L. López-Jurado, and M. Riera (2002), The canales experiment (19961998): interannual, seasonal, and mesoscale variability of the circulation in the Balearic Channels, *Prog. Oceanogr.*, *55(3-4)*, 335–370, doi: 10.1016/S0079-6611(02)00139-8.

Puillat, I., I. Taupier-Letage, and C. Millot (2002), Algerian Eddies lifetime can near 3 years, *Journal of Marine Systems*, *31*(4), 245 – 259, doi: http://dx.doi.org/10.1016/S0924-7963(01)00056-2.

Rio, M.-H., P.-H. Poulain, A. Pascual, E. Mauri, G. Larnicol, and R. Santoleri (2007), A mean dynamic topography of the mediterranean sea computed from altimetric data, in-situ measurements and a general circulation model, *J. Mar. Syst.*, *65*, 484–508, doi: 10.1016/j.jmarsys.2005.02.006.

Violette, P. E. L., J. Tintoré, and J. Font (1990), The surface circulation of the Balearic Sea, *J. Geophys. Res.*, *95*, 1559–1568, doi: 10.1029/JC095ic02p01559.

Volkov, D. L., G. Larnicol, and J. Dorandeu (2007), Improving the quality of satellite altimetry data over continental shelves, *J. Geophys. Res.*, *112*, C06,020, doi: 10.1029/2006JC003765.

Chapter 1

Hydrodynamic comparison between the north and south of Mallorca Island

La ciencia se compone de errores, que a su vez, son los pasos hacia la verdad.

Julio Verne (1828-1905)

This chapter has been published in:

- Amores, A. and S. Monserrat. Hydrodynamic comparison between the north and south of Mallorca Island. *J. Marine Systems*, 2014. doi: 10.1016/j.jmarsys.2014.01.005.

Abstract

A hydrodynamic comparison between two zones of fishing interest, one located to the north and the other to the south of Mallorca Island (Balearic Islands, Western Mediterranean) was done. The comparison was conducted using the data from two moorings, one placed in the middle of the Balearic Current, in the Balearic subbasin (herein, Sóller) and the other in the Mallorca Channel, near the Algerian subbasin (called Cabrera). The instruments moored, continuously recorded the temperature, salinity and currents at different depths, for over 15 months. The data analysis suggests that Sóller is hydrodynamically more active than Cabrera, at least during the time of recording the measurements. The mean currents were higher at Sóller than at Cabrera at all depths, also showing greater maximum speeds and variability. In addition, the presence of more mesoscale eddies in Sóller became evident from the altimetry data. These eddies were not only significantly more energetic near the surface, they also generally

reached to greater depths, affecting the velocities of the seabed currents. Subsequent to each significant eddy episode, strong changes in temperature and/or salinity were observed, along the entire water column. Spectral analysis revealed the presence of high frequency oscillations with periods of a few hours. One energy peak, with a period around 3.7h, was observed at both locations, probably related to trapped waves around Mallorca or the Balearic Islands, while others (3h and 2h) were reflected only in Sóller, suggesting they could be associated with some standing resonance waves between the Iberian Peninsula and Mallorca.

1.1 Introduction

The Balearic Islands, located in the Western Mediterranean, are the natural limit between the Balearic and the Algerian subbasins (Fig. 1.1). These two areas are connected via channels between the islands. The Ibiza Channel (80 km wide, with a maximum depth of 800 m) is located between Cape La Nao (Iberian Peninsula) and Ibiza Island; the channel between Ibiza and Mallorca is known as the Mallorca Channel (80 km wide and 600 m deep); meanwhile the Menorca Channel, the shallowest (100 m deep) and narrowest (35 km wide) is located between the Mallorca and Menorca Islands [*García et al.*, 1994].

The mean circulation in the Balearic subbasin, situated north of the archipelago up to the Iberian Peninsula, is driven by a density gradient between the fresher coastal water and the relatively saltier water in the center of the subbasin. Due to this density gradient, the Northern Current (NC) flows southward along the Iberian Peninsula slope, following the isobaths. When the NC reaches the Ibiza Channel, two different behaviors are possible, depending on the mesoscale situation [*Pinot et al.*, 2002]. Normally, a portion of the NC may leave the Balearic subbasin via the Ibiza and Mallorca Channels while the rest gets reflected northward to form the Balearic Current (BC) which flows along the Islands' northern slope. The resident water between 200 m and 700 m, is mostly the Levantine Intermediate Waters (LIW). When the previous winter was particularly cold, the Western Mediterranean Intermediate Waters (WIW) generated in the Gulf of Lion and normally located between 100 m and 300 m, could have displaced the LIW forming the resident water at the intermediate depths [*Mertens and Schott*, 1998; *Millot*, 1999; *Pinot et al.*, 2002]. When these WIW reach the Balearic Channels in late spring, the NC most often gets blocked and a different configuration of flow through the channels is observed. Most of the NC reflects northwards, reinforcing the BC, and the southward flow through the channels is reduced [*Monserrat et al.*, 2008]. The Western Mediterranean Deep Waters (WMDW) are located in the deeper part of the water column, below 700 m (refer *Massutí et al.* [2014]; *Millot* [1999]; *Pinot et al.* [2002] for a better description of the circulation and

the properties of these water masses).

The Algerian subbasin, the zone between the Balearic Islands and the north of Africa, is controlled by a completely different dynamics. The circulation of the Algerian subbasin is driven by the Algerian current which interacts with the Alboran sea eddies and spreads the Atlantic water towards the Balearic Islands. The northern part of the subbasin has no clear steady current, although its circulation is affected by the changes in the mesoscale structures in the southern part of the subbasin and the entrance of Mediterranean water coming in from the Balearic subbasin via the channels.

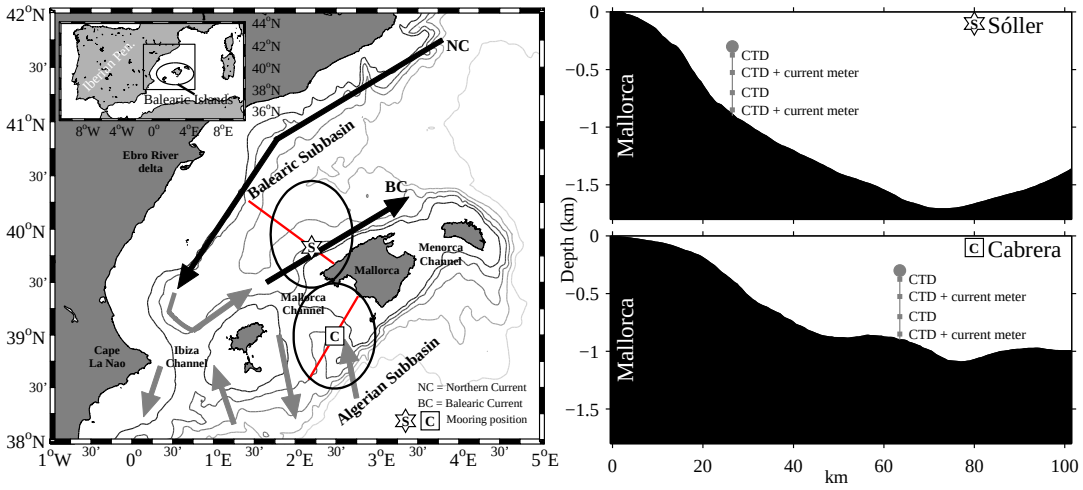

Figure 1.1: Map showing the main characteristics of the ocean circulation in the Balearic subbasin. The positions of the moorings are marked with an S inside a star for Sóller mooring and a C inside a square for Cabrera mooring. Isobaths are plotted between 500 m and 2500 m with a step of 500 m. Black arrows indicate the permanent currents, while the grey ones indicate the temporal features. The enclosed areas are 0.5° radius circles where the occurrence of eddies is checked (they seem to appear as ellipsoids due to the map projection). The bathymetric profiles correspond to the red lines indicated in the map.

The main objective of this study, which is included in the IDEADOS project [*Massutí et al.*, 2014], is to analyze the similarities and differences in the hydrodynamic conditions between two zones of fishing interest, one situated in the Balearic subbasin, to the north of Mallorca Island and the other in the northern part of the Algerian subbasin, to the south of Mallorca. The results found are to be of significance for IDEADOS when assessing the manner in which the variability of the fishery resources in both areas might be driven by a different hydrodynamic frame. With this objective in mind, a mooring line was deployed in each zone to retrieve a set of hydrodynamic data to facilitate a comparison. One instrument line was located in the Balearic subbasin, near Sóller, while a

second one was placed in the Mallorca Channel, in the northern part of the Algerian subbasin, close to Cabrera Island. The terms Sóller and Cabrera are used to identify these two regions throughout the manuscript (Fig. 1.1).

In this work, we first present the mooring lines, instrumentation and the data set measured. Then, the methodology used is described and the most interesting results are shown. A detailed comparison between the two zones is elaborated. The last section includes the summary and conclusions drawn.

1.2 Data Sets and Methodology

Hydrodynamic data were acquired using two identical mooring lines. The line from Sóller was placed on the northwest side of Mallorca Island (39°49.682 N - 2°12.778 E) and the line from Cabrera was located on the southwest side of the island, into the Mallorca Channel (38°59.484 N - 2°28.907 E) (Fig. 1.1).

The moorings were deployed at about 900 m depth to a height of 600 m above the seabed. Each mooring consisted of four CTD (Conductivity, Temperature and Depth) Seabird 37 sensors placed at fixed depths at around 300 m, 500 m, 700 m and 900 m. In addition, two Nortek Aquadopp current meters were installed in the middle levels (at about 500 m) and near the bottom (around 900 m depth). A sediment trap (not used in this study) was placed 30 m above the bottom. Observations of the thermohaline properties and currents were collected at sampling rates of 10 min for the CTD and 30 min for the current meters.

The moorings were continually recording data from mid-November 2009 until mid-February 2011. During this period, two maintenances were required because of the selected sampling rate for the sediment traps. These maintenances took place in mid-March and in mid-September 2010. The depth where the instruments were located did not change significantly after the maintenances. The instruments encountered no significant problems during the whole period. The only exceptions were the CTDs at 500m and 900m in Sóller and the one at 300m in Cabrera which ran out of batteries around January 2011, about one month prior to the end of the experiment.

Simultaneous surface information was obtained from the AVISO service available at http://www.aviso.oceanobs.com, which provides gridded Sea Surface Height (SSH) fields with a map sampling of $1/8° \times 1/8°$. The absolute dynamic topography is obtained as the sum of the sea level anomalies provided, measured by the altimetry satellites and the mean dynamic topography based on seven years of observations (1993-1999) [*Rio et al.*, 2007]. The regional sea level anomalies for the Mediterranean Sea are a multi-mission product with up to 4 satellites at a given time, spanning the period from 1992 to the present. The data provided are corrected to include all standard geophysical corrections, including Dynamic At-

mospheric Correction (DAC). This latter correction combines the high frequency of the Mog2D model [*Carrère and Lyard*, 2003] with the low frequency of the classical inverted barometer correction.

The formation and evolution of the eddies in the region of interest have been studied by applying an automated eddy detection scheme [*Nencioli et al.*, 2010]. This scheme is a flow geometry based scheme. The method fixes the center of the eddy as the local velocity minimum into an area with rotating flow, and the eddy boundaries are defined as the outermost closed streamline around the center, for which the velocity continues to still radially increase.

In order to improve the algorithm performance of the automatic method of detecting the eddies, the AVISO velocity fields are linearly interpolated from the $1/8^\circ \times 1/8^\circ$ grid to $1/16^\circ \times 1/16^\circ$ as performed by *Liu et al.* [2012]. The number of grid points from a reference one from which the increase in the magnitude of the velocity is checked, has been fixed to 3 (parameter a of the algorithm) and the number of grid points of the area used to find the velocity local minimum has been selected to be 2 (parameter b of the algorithm).

The equivalent radius of each eddy located has been calculated as the radius of the circumference with the same area while the circulation is the vorticity integral within the eddy area.

The computed spectra have been performed with a half-overlapping Kaiser-Bessel window of 2048 points, the initial number of degrees of freedom being 14. These spectra have also been smoothed, averaging per frequency bands, which permitted an increase in the degrees of freedom towards the high frequencies. Wavelets used Morlet as the mother function.

1.3 Results

The temperature and salinity time series measured by the moorings during the time of deployment are shown in Figs. 1.2 and 1.3. The first column shows the results from the Sóller mooring, whereas the second column lists the measurements from Cabrera. Each row is assigned to a particular depth in increasing order (300 m, 500 m, 700 m and 900 m). The time series colors denote time, starting with the purple color and moving linearly to blue. This time color scale enables us to identify the time of the relevant features in the TS and PVD diagrams shown later on. This color scheme is followed throughout the manuscript.

A visual inspection of the temperature and salinity time series shows greater amplitude oscillations in Sóller. This observation is quantified in Fig. 1.4 where the ratios between the standard deviations of the series measured at the Sóller and Cabrera locations are shown. All the instruments (the only exception being salinity at 900 m) presented standard deviations significantly greater in Sóller

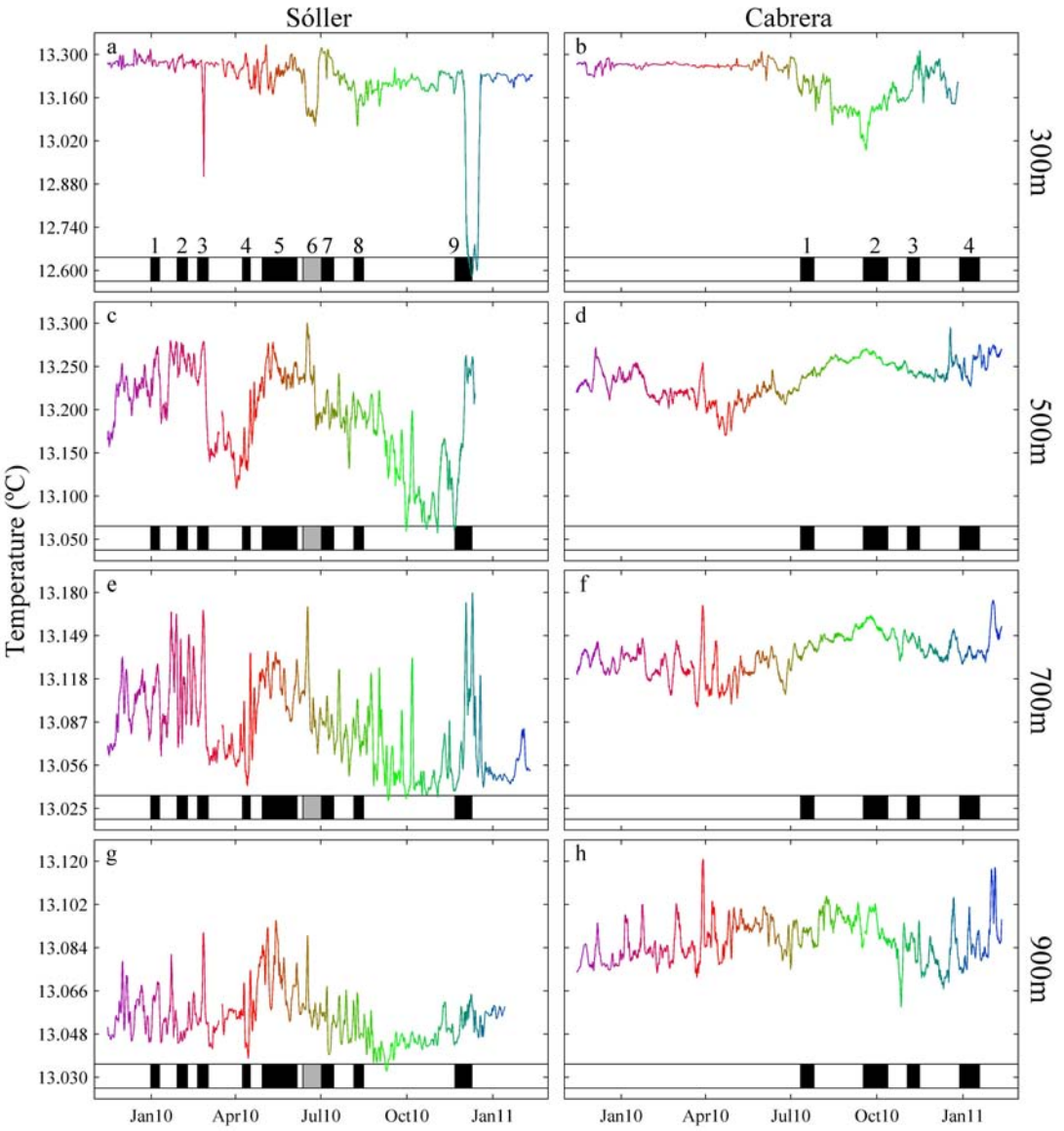

Figure 1.2: Temperature time series after been filtered with a 24h low pass running average filter. The first column shows the measurements from the Sóller mooring and the second column shows the data registered at Cabrera. Each row corresponds to an increasing depth (300 m, 500 m, 700 m and 900 m). Colors indicate the time evolution to facilitate the comparison with other diagrams. Black patches indicate when an eddy was detected. The grey patch in the Sóller time series indicates the presence of two eddies at the same time.

than in Cabrera, with the maximum value at 500 m depth. This result suggests that Sóller is a region with greater variability than Cabrera.

Only eddies meeting the selection criteria as detected by the automated scheme

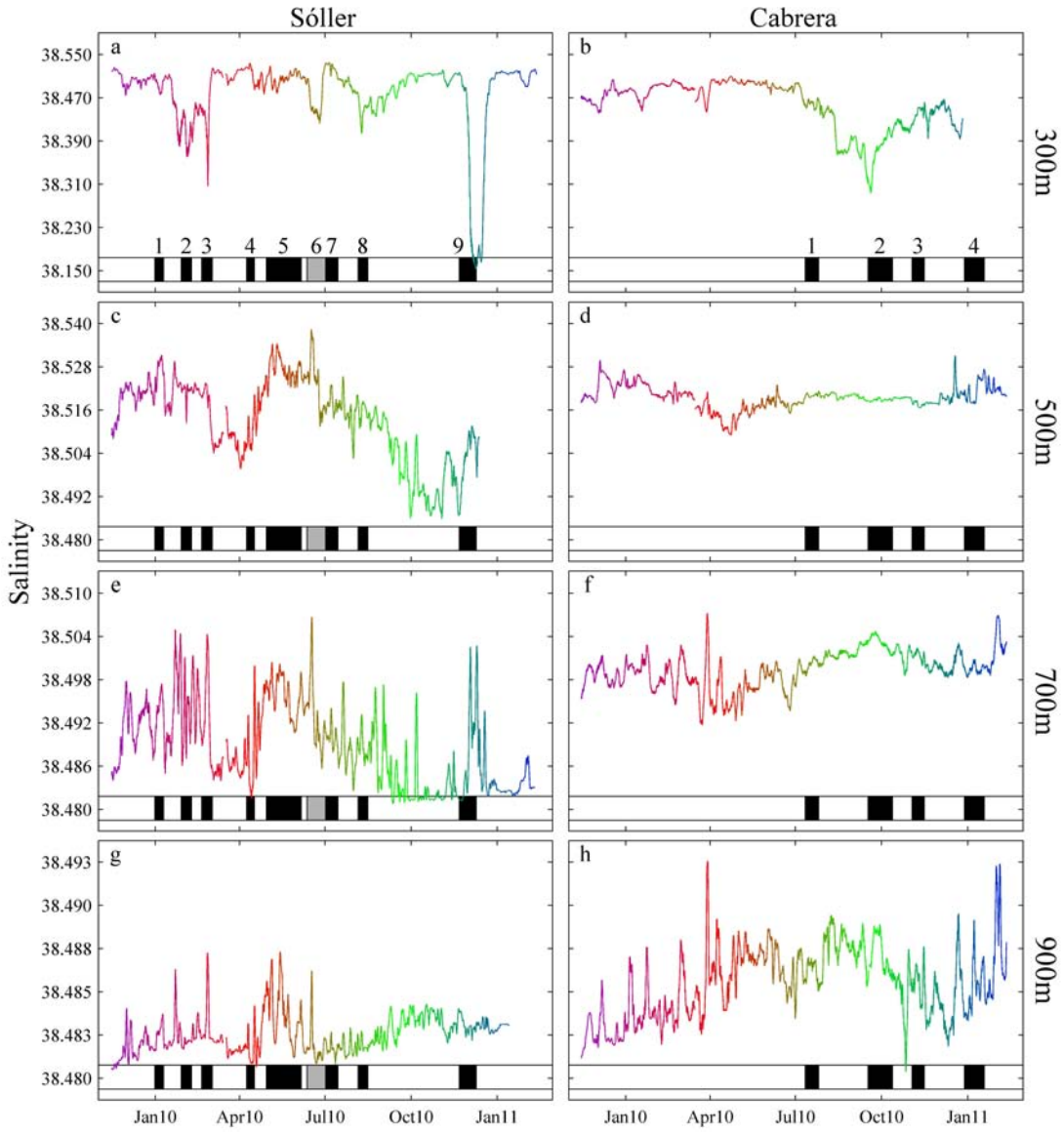

Figure 1.3: Similar to Fig. 1.2 but for the salinity time series.

[*Nencioli et al.*, 2010], are shown in Fig. 1.5. The detection requirements specify that eddies have a lifespan of more than 10 days and their centers remain for at least one whole day in the selected area (ellipsoids in Fig. 1.1), similar to the criteria applied by Amores et al. (2013a). The presence of the eddies is also shown in Figs. 1.2 and 1.3, using black patches in the lower parts of the frames. The eddies are also numbered.

The total number of eddies detected is around twice the number in Sóller

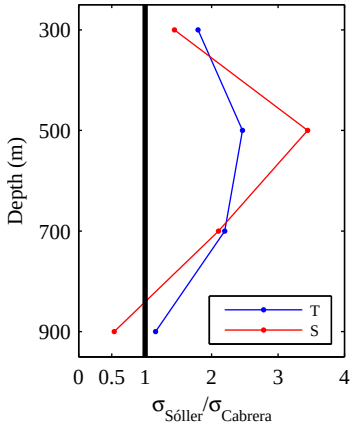

Figure 1.4: Ratios between the Sóller and Cabrera standard deviations at different depths. Temperature standard deviation ratios are shown in blue and the salinity standard deviation ratios in red.

(9) than in Cabrera (4) and almost all of them are anticyclonic. The mean of the absolute value of the circulation of the total number of eddies (being the circulation sum of the vorticity inside the eddy area during its entire lifetime) is around 1.5 times greater in Sóller than in Cabrera. The duration of the eddies remains almost the same in both areas ($\sim$ 19 days), although the mean equivalent radius is 5 km greater in Cabrera than in Sóller.

Observation of the temperature and salinity time series (Figs. 1.2 and 1.3) recorded when the eddies remained in each area, clearly reveals that the eddies in Sóller generally extend their effects down to the deeper levels than the eddies detected in Cabrera. One example of this fact is the significant drop in the temperature and salinity registered in Sóller at 300m between November and December 2010, coinciding with the last eddy detected in this region (No. 9). This decrease at 300 m changed into an increase of both the variables with depth, down to 900 m, which ensured the stability of the water column (refer *Amores et al.* [2013] for more details). The same effect, although of smaller magnitude, has also been observed in Sóller, at least during the third and sixth eddies. Conversely, this behavior has never been observed in the Cabrera time series of temperature and salinity, where the eddy effects were not noticeable below 500 m.

The TS diagrams for the entire period of study are shown in Fig. 1.6. The Sóller measurements spread out across a wider area than for Cabrera, which again reveals the greater variability present at Sóller.

The eddy episodes mentioned above are clearly reflected in Sóller at 300 m. The dark green portion, moving from the Levantine Intermediate Waters (LIW, the resident water at this depth) to the Western Mediterranean Intermediate

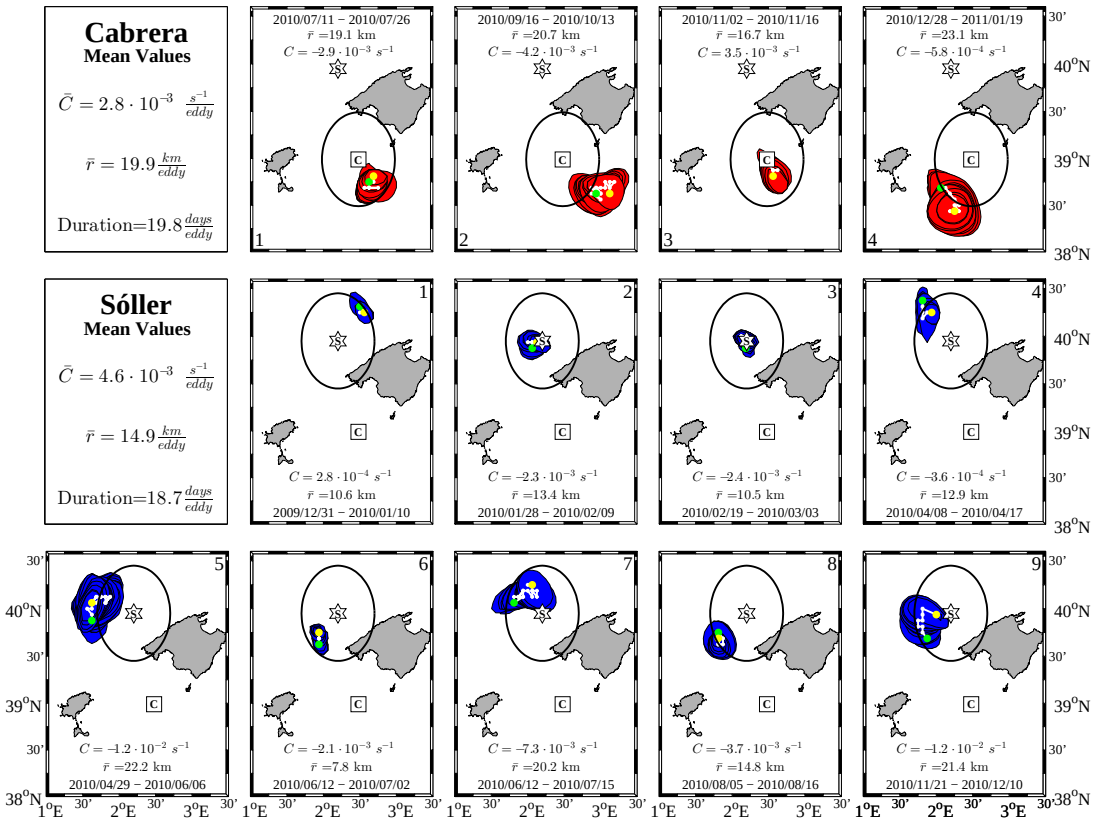

Figure 1.5: The first two panels show the mean features (circulation, radius and duration) of all the eddies detected in each zone. Each following frame shows the features of every individual eddy for Cabrera (in red) and Sóller (in blue) with the same numbering as from Figs. 1.2 and 1.3. The trajectory from the starting point in green to the ending point in yellow is also indicated. The enclosed areas are the zones where the occurrence of eddies has been checked. Note that the sixth and seventh eddies in Sóller were simultaneous for some time but they have been plotted in different frames.

Waters (WIW) correspond to the eddy described in *Amores et al.* [2013]. The red-pink area, which indicates two different eddies (Nos. 2 and 3), are clearly separated into two parts. The first part, which reveals a change in the salinity, however, maintaining the temperature more or less unchanged, corresponds to the entrance of waters revealing Atlantic features. The second part, when changes in both salinity and temperature are seen, is related to the WIW.

Moving downwards in depth, from 500 m to 900 m, the characteristics of the water change gradually from LIW to Deep Waters (DW), a normal response for the resident waters of this area [*Balbín et al.*, 2012; *Pinot et al.*, 2002].

On the other hand, the Cabrera 300 m TS diagram reveals that the characteristics of the waters in this region were confined to a smaller area (when compared

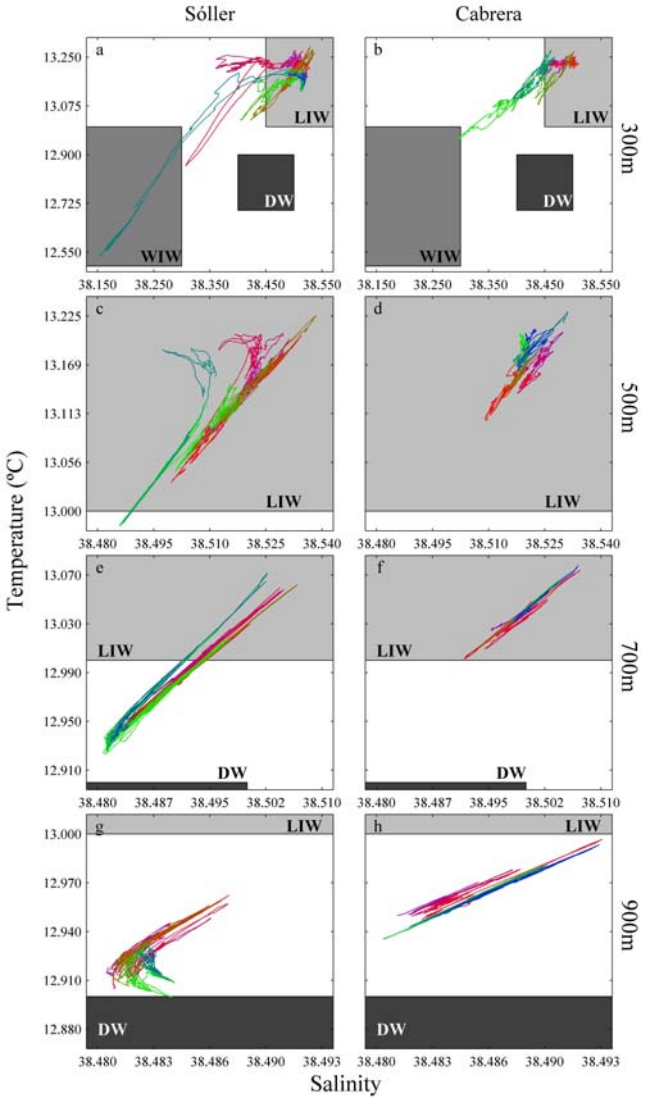

Figure 1.6: Temperature Salinity (TS) diagrams. Data have been smoothed by using a 24h low pass running average filter. The colors are the same than those used in Figs. 1.2 and 1.3 and they indicate the time evolution.

with Sóller). Water properties deviated from the normal LIW (the resident water) to WIW only in the green portion, which corresponds to the presence of some eddies in this region. When moving to the deeper levels, a slight displacement from LIW to DW is observed. However, the water properties do not get as close to DW as they do for the Sóller region.

A comparison of the Progressive Vector Diagrams (PVD) and the speed for each depth in which a current meter was deployed (500 m and 900 m) is presented

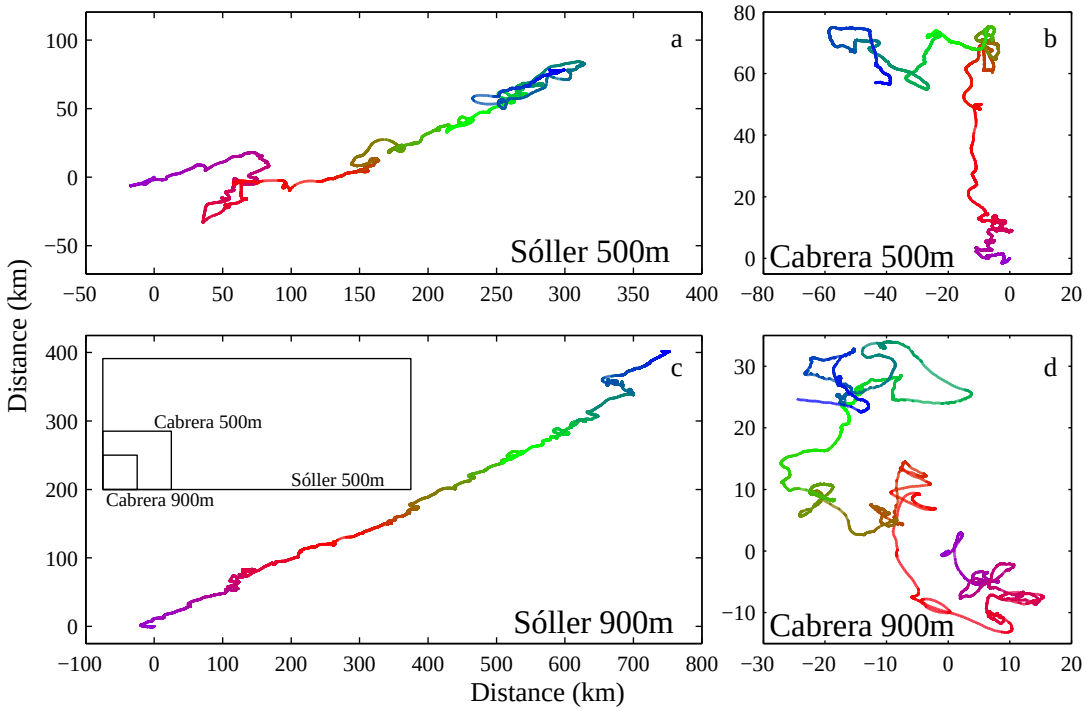

Figure 1.7: Progressive Vector Diagrams (PVD) for the current meters of both moorings. Data have been smoothed by using a 24h low pass running average filter. The scale relationship between the PVD scales is visible inside the Sóller 900 m PVD. The colors are the same than those used in Figs. 1.2 and 1.3 and indicate the time evolution.

in Figs. 1.7 and 1.8, respectively.

The current mean values are greater at Sóller (3.9 cm/s at 500 m and 5.2 cm/s at 900 m) than they are at Cabrera (2.3 cm/s at 500 m and 2.2 cm/s at 900 m). Significantly greater speeds have been recorded at 900 m than at 500 m in the Sóller region. Otherwise, at Cabrera, the speeds are observed to be similar at both depths. Greater speeds in the water column have been previously observed close to the bottom [*Millot*, 1994] although the exact reason for this phenomenon still remains unclear [*Pinot et al.*, 2002]. A possible explanation for these measurements could be attributed to the fact that the Sóller mooring has been deployed along a very steep slope, whereas the Cabrera mooring is located in a relatively flat area (Fig. 1.1). The placement of the Sóller mooring, the steep slope, and the fact that the Balearic Current flows in from the Northern Current, after experiencing a significant gyre just before the Ibiza Channel, could explain the greater velocities measured near the bottom.

The PVDs at Sóller (Figs. 1.7a and c) clearly reflect the steady Balearic Current, flowing northeast along the islands slope. The dominant current is

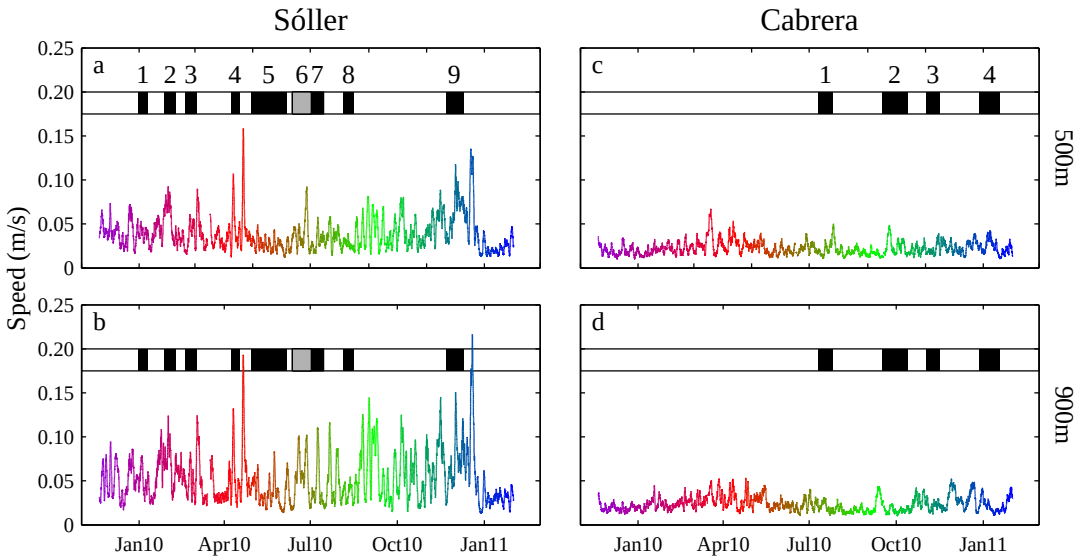

Figure 1.8: Speed time series for the current meters of both moorings (panel a *and* c *are from 500m depth and* b *and* d *are from 900m depth). Data have been smoothed by using a 24h low pass running average filter. The colors are the same as those used in Figs. 1.2 and 1.3 and indicate the time evolution. Black patches reveal when an eddy is detected. The grey patch in the Sóller time series indicates the presence of two eddies at the same time.*

only disturbed by the presence of successive eddies which trigger a change in the direction of the current (Fig. 1.7) as well as an increase in the speed values in almost all the cases (Fig. 1.8). These gyres, associated with the eddies, are stronger at 500 m but still noticeable at 900 m, at least for the third and ninth eddies. It should be stated that the dimensions of the Sóller PVD frame at 900 m are twice the size of the 500 m frame. This fact, which implies larger displacements at 900 m than at 500 m, takes into account two different effects: first, the direction of the current is more constant at 900 m than at 500 m; and second, the speed at 900 m is also generally greater than at 500 m. The same results are also observed in Fig. 1.8.

The PVDs from Cabrera, however, do not show a clear dominant direction for the currents, which is an intrinsic feature of the deployment area, due to the significant effect of the mesoscale events in this region on the distribution of the currents [*Pinot et al.*, 2002]. Only a dominant northwards current is observed at 500 m during the initial period. Also, neither the PVDs (Fig. 1.7) nor the speed time series (Fig. 1.8) present a clear signal of the eddies observed in this region on the surface data. Conversely to Sóller, the PVD frame from 500 m is double the size of the 900 m PVD frame, although in this case it is due only to the previously mentioned dominant northwards direction of the current during the

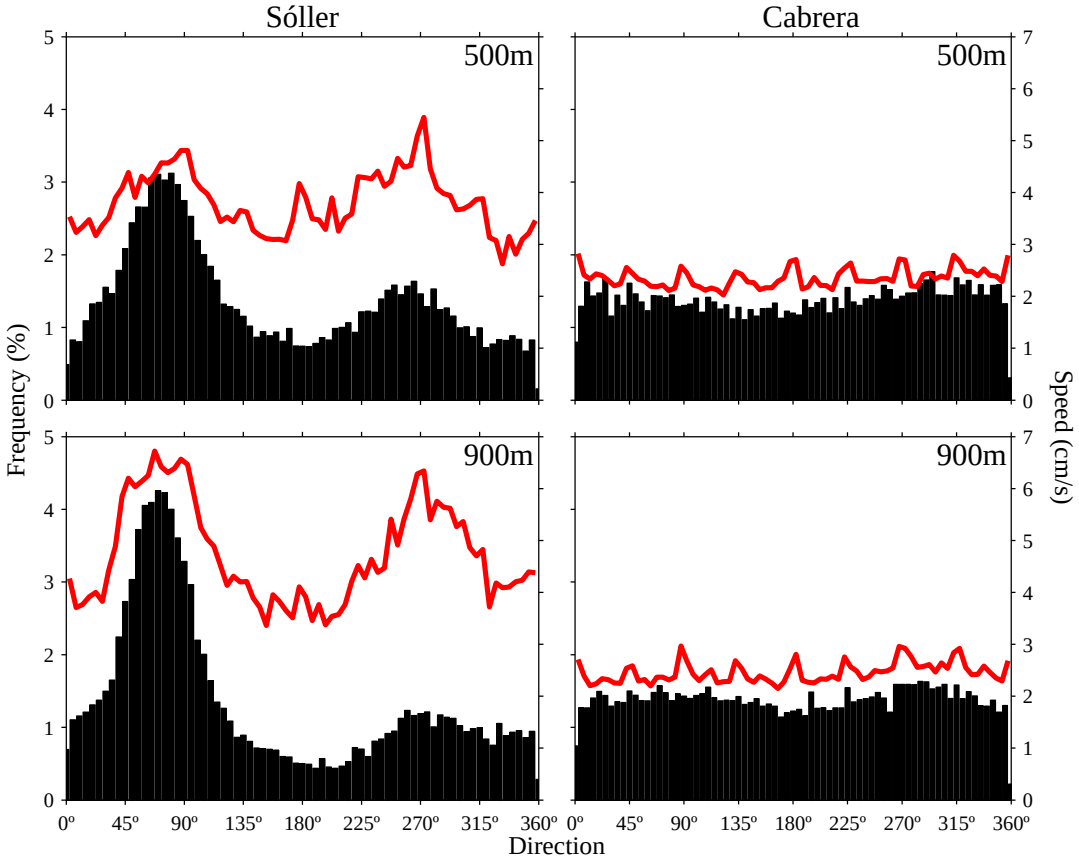

Figure 1.9: The number of times that a direction was measured (black histogram) and the corresponding mean speed for this orientation (red line) for each location and depth.

first part of the measurements, as the speeds show similar values at both depths.

Finally, a comparison between the Sóller and Cabrera PVDs frames sizes reveals, once more, that the current speeds are significantly greater in Sóller, and also that a more constant current direction is present, which is related to the steady Balearic Current.

The differences between the current distributions in both zones become even clearer on analyzing the number of times a given direction is measured and the mean speed for this orientation (Fig. 1.9). In Sóller, there is a predominant direction, around 70°(taking the zero at the north and increasing clockwise) at both the 500 m and 900 m depths. This direction coincides with the orientation of the slope of the island and, consequently, with the path of the Balearic Current. This predominant direction shows a higher frequency at 900 m than at 500 m, which indicates a greater variability in the upper layers. Moreover, there is a second maximum in the opposite direction (250°-260°) which takes into account the re-

versal of the currents during the eddy events. Regarding the velocity distribution, the same two maximums have been observed for the very same orientations, with almost the same mean speed values (between 5-6 cm/s at 500 m and 6-7 cm/s at 900 m).

The distribution of the speeds and directions is totally different at Cabrera. There is no predominant direction and the mean speed is almost the same in all directions. Values are also similar at both depths (between 2 and 3 cm/s).

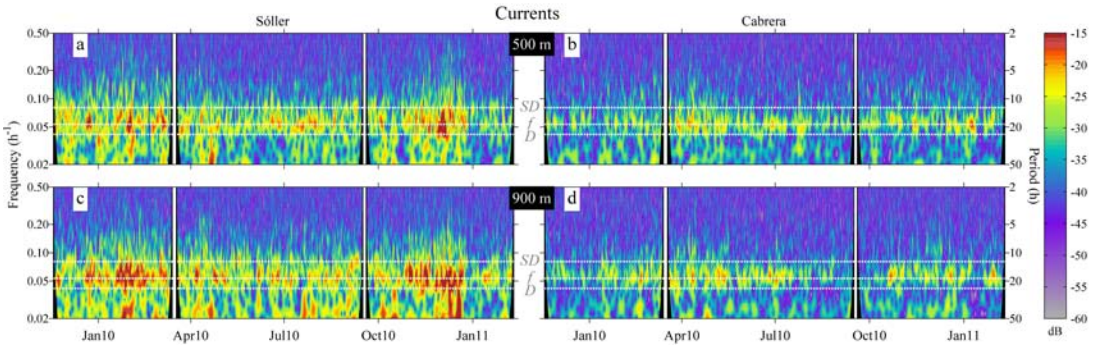

Figure 1.10: Velocity wavelets from Sóller at 500 m (a) and 900 m (c) and for Cabrera at 500 m (b) and 900 m (d) during the entire recording period. The vertical strips correspond to the mooring maintenances. The mother function used in wavelet computations is Morlet.

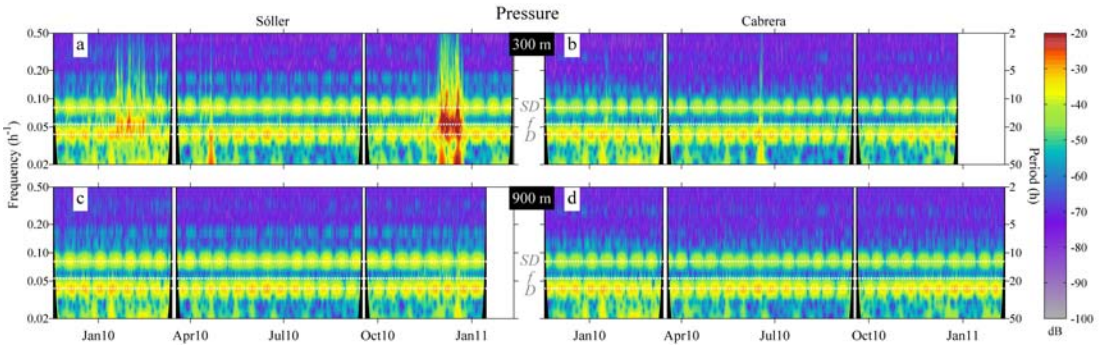

Figure 1.11: Pressure wavelets from Sóller at 300 m (a) and 900 m (c) and for Cabrera at 300 m (b) and 900 m (d) during the entire recording period. The vertical strips correspond to the mooring maintenances. The mother function used in wavelet computations is Morlet.

The frequency variability has been studied through wavelets and spectral analysis.

Wavelets for the velocity modulus and the whole set of available data are shown in Fig. 1.10. The inertial frequency (f $\sim 0.0534 h^{-1} \sim 18.74$ h) is the more energetic component during the whole period, being always more energetic in Sóller than in Cabrera. Moreover, sudden energy spurts are observed in Sóller

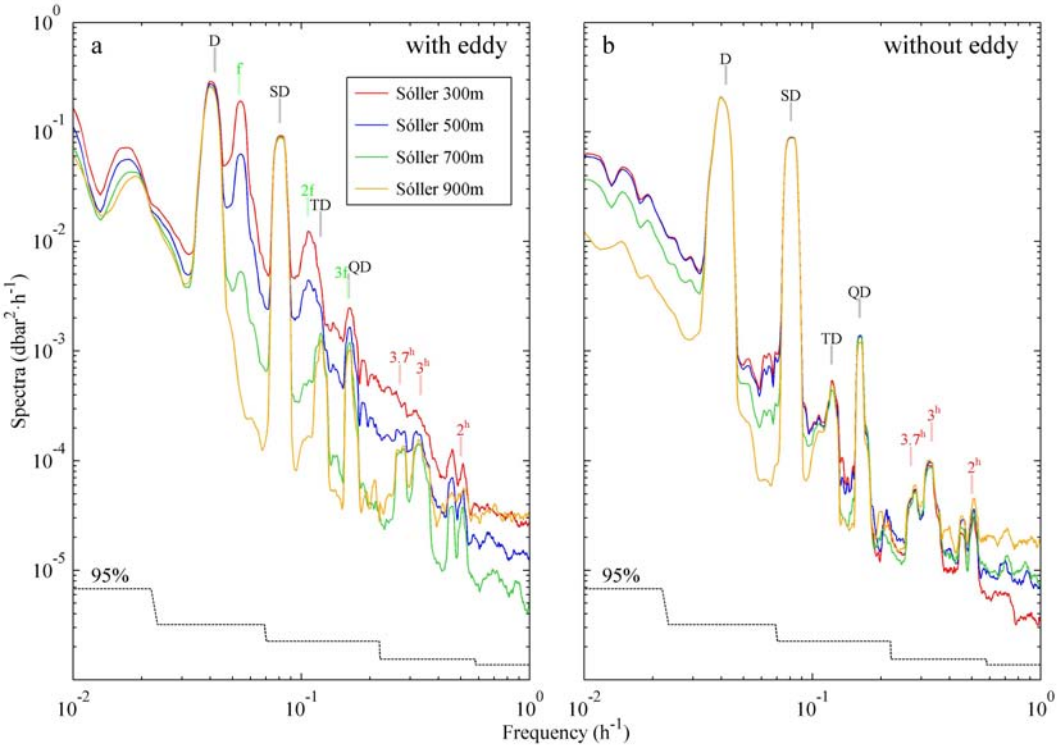

Figure 1.12: Pressure spectra for Sóller, at all available depths, for a period when an eddy was present in the area exerting a significant influence on the mooring (a) (from 18/11/2009 to 14/3/2010) and when no eddy was observed in the zone (b) (from 1/4/2010 to 26/7/2010). The main tide components are indicated in grey; the peaks with a possible resonant origin are indicated in red; the peaks related with the inertial frequency are indicated in green.

wavelets during the time when most of the eddies have been detected. At these times, the energy appears to spread outwards affecting the lower frequencies, these frequencies being related to the characteristics of the eddies.

These energy spurts in the speed wavelets are also reflected in the pressure wavelets (Fig. 1.10). A clear energetic increase at the inertial frequency is observed during the most energetic eddies (third and ninth). These energy increases are related to the depressions of the instruments due to the tilting of the mooring associated with the strong currents. This effect can be better visualized by performing a spectral analysis of two different periods of time: the first period (from November 18, 2009 to March 14, 2010) includes the presence of two intense eddies in Sóller (eddies 2 and 3) (Fig. 1.12a); meanwhile, the second period (from April 1 to July 26, 2010), does not show any particular feature, either in Sóller or Cabrera (Fig. 1.12b). Thus, to correctly interpret the pressure spectra in Sóller, it must be assumed that the currents associated with the eddies is strong

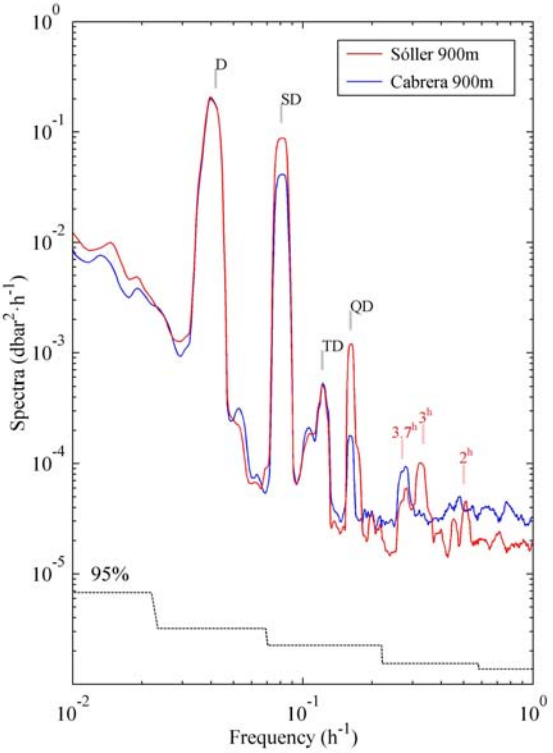

Figure 1.13: Comparison between the 900 m depth pressure spectra from Sóller (red) and Cabrera (blue) during the period between April 1 and July 26, 2010. The main tide components are indicated in grey; the peaks with a possible resonant origin are indicated in red.

enough to significantly tilt the mooring. Therefore, the inertial frequency and its harmonics present in the velocity field (Fig. 1.10), also become apparent in the pressure spectra (Fig. 1.12a). The energy observed at the inertial frequency and harmonics decreases as the depth of the instruments location increases (i.e. as the instrument gets closer to the sea bottom). This occurs because as the vertical distance to the bottom decreases, the vertical displacement due to the tilting becomes less. The inertial frequency peaks almost disappear in the instrument located near the bottom (900 m). These depressions occur only at some specific moments with a maximum value of around 4 m (see Fig. 7f in *Amores et al.* [2013]), which ensures that the water properties (i.e. salinity and temperature) measurements are not significantly affected by these depressions. On analyzing a period without eddies, (Fig. 1.12b) no significant differences are observed in the pressure spectra for the four available depths, as expected. Besides the tidal components, three high frequency peaks can also be identified (3.7h, 3h and 2h). The origin of the high frequency peaks observed may be better interpreted when the Sóller and Cabrera spectra are plotted together. Spectra for the selected

period with no eddy and for the instrument located at 900 m are shown in Fig. 1.13. Similar results (not shown) are obtained at different depths.

Although a suitable analysis should be performed using a harmonic analysis, the computed spectra suggests that the tidal components are similar, although not identical, in the two zones. Semi-diurnal (SD) and quarter-diurnal (QD) components are clearly more energetic in Sóller; however, the diurnal (D) and third-diurnal (TD) tidal components have the same energy content in both regions.

Regarding the high frequency energy contents, the peak at 3.7 h appears in both the Cabrera and Sóller spectra. This has always been observed when other time periods are analyzed. Therefore, this surely corresponds to some trapped wave surrounding Mallorca Island or the whole Balearic archipelago. A numerical computation could help to confirm or discard this hypothesis.

The peaks at 3h and 2h appear only in the Sóller spectrum, indicating they are probably related to some resonance between the Balearic Islands and the Iberian Peninsula. Again a numerical model could help to assess this hypothesis; however, by simply analytically solving the 1D shallow water equations we can see that the resonant modes between Mallorca and the Iberian Peninsula are expected to be of this order. Results for the 800 m constant depth and the 200 km length profile (which are the mean dimensions of the zone between Mallorca Island and the Iberian Peninsula), the fundamental period of resonance is found to be around 1.25 h. A better approximation, obtained numerically solving the shallow water equations in one dimension using the real bathymetry of the zone (Fig. 1.1), gives as a result that the first mode of resonance is around 2.18 h. This result shows that the 3 h and 2 h peaks found in the Sóller spectrum are of the same order that the expected resonance modes between the Balearic Islands and the Iberian Peninsula. However this result is, at this stage, only speculative, and additional data and the use of numerical computations would be needed in order to confirm the source of the peaks observed.

1.4 Summary and Conclusions

Two mooring lines were deployed, one to the north and the other to the south of Mallorca Island for over a year (November 2009 - February 2011) in order to study the hydrodynamic similarities and differences between the two zones of fishing interest.

The Sóller mooring was deployed in the middle of a steep slope, dominated by the Balearic Current and located within the Balearic subbasin. The Cabrera mooring, however, was installed in a flatter zone, near the Mallorca Channel, in the northern part of the Algerian subbasin.

On analyzing the daily SSH images over the period that the moorings were deployed, several mesoscale eddies were identified, crossing both regions. The total number of eddies in Sóller was found to be more than twice the number of eddies detected in Cabrera. The fact that the Sóller mooring was deployed in the middle of the Balearic Current could explain this difference, as the instabilities of the Balearic Current appeared to be the common source generating the eddies [*Amores et al.*, 2013].

This resulted in the greater number of eddies being detected in Sóller, as there were more intrusions of waters with properties very different from that of the resident waters (LIW). Depending on the eddy intensity, these water intrusions revealed different ranges in depth, affecting only the surface layers on some occasions, but clearly present down to the bottom during the more intense episodes. Conversely, the eddies in Cabrera appeared to affect the depths from the surface to only around 300 m depth, as the effects of the eddies detected at the surface and having some signal at 300 m did not disturb the measurements at 500 m.

Data showed that the Sóller area was hydrodynamically much more active than the Cabrera region at least during the time of deployment of the moorings. The velocities observed were considerably higher, with greater variability. This higher variability was also observed in the temperature and salinity time series. Moreover, a greater number of eddies was also detected in the Sóller area. Although the currents in the Cabrera region changed direction continuously, their speed oscillations were lower than those in Sóller.

The constant direction of the currents in Sóller, and the non-near-zero mean values of the currents, makes it difficult to fix a lower limit to the Balearic Current. Although it is true that the Balearic Front is located from the surface up to 200 m [*Ruiz et al.*, 2009] or 300 m [*Font et al.*, 1988], its effects on the currents appear to extend deeper, down to the bottom. This fact becomes significant in two different aspects. When calculating the dynamic height in this area, a reference level of zero velocity at about 500 m is usually taken. However, our observations show that this approach is not adequate, as the mean velocities around 4.5 cm/s have been measured from 500 m to 900 m. The non-zero speed values at the intermediate and deep layers are also important while computing the transport in the Balearic Current. The transport is usually calculated by taking an area 35-50 km in width and 200-250 m in depth (coinciding with the Balearic Front) and giving them transport values ranging from 0.3 Sv up to 0.9 Sv [*Font et al.*, 1988; *García-Ladona et al.*, 1995; *Pinot et al.*, 2002; *Ruiz et al.*, 2009]. However, when computing the transport from 300 m to 900 m, with a width half of the width used in the upper layers (17.5-25 km, trying to take into consideration the presence of the slope) and 4.5 cm/s as the mean velocity, values from 0.48 Sv to 0.68 Sv are obtained. These transport values obtained for the intermediate and

deep layers are comparable to the transport in the upper layers and they should possibly be taken into account for the following computations of the Balearic subbasin transport.

Differences in the frequency response in both zones were also found. As the eddies observed in Sóller were more intense than those in Cabrera, the associated strong currents during at least two episodes clearly caused the tilting of the mooring. The changes in the depth of the instruments related to this tilt introduced the inertial frequency in the pressure spectrum. Some differences between the TD and QD tidal components were also found, showing Sóller having greater energy than Cabrera. Finally, high frequency peaks were found in both sites, which could be related to some kind of resonance in the subbasins. One peak (3.7 h) observed in both locations appears to be related to some trapped wave surrounding Mallorca Island or the whole Balearic archipelago. The other two (3 h and 2 h) observed only at Sóller probably reflect resonance modes between the mainland and the island. More conclusive results could arise from a simulation of the 2D shallow water equations or after the use of a numerical model in the region.

Acknowledgments

This research has been partially sponsored by the IDEADOS project (CMT2008-04489-C03-01 and 03). The work of A. Amores has been funded by a JAE-PreDoc grant from Consejo Superior de Investigaciones Científicas (CSIC) and co-funded by Programa Operativo FSE 2007-2013. The authors also wish to express their gratitude to the IDEADOS team for their collaboration in the data acquisition process and the crews of the R/V Odón de Buen and F/V Punta des Vent for their valuable assistance during the mooring deployments.

Bibliography

Amores, A., S. Monserrat, and M. Marcos (2013), **Vertical structure and temporal evolution of an anticyclonic eddy in the Balearic Sea (western Mediterranean)**, *J. Geophys. Res. Oceans*, *118*, 2097–2106, doi: 10.1002/jgrc.20150.

Balbín, R., M. M. Flexas, J. L. López-Jurado, M. Peña, A. Amores, and F. Alemany (2012), **Vertical velocities and biological consequences at a front detected at the Balearic Sea**, *Cont. Shelf Res.*, *47*, 28–41, doi: 10.1016/j.csr.2012.06.008.

Carrère, L., and F. Lyard (2003), Modelling the barotropic response of the global ocean to atmospheric wind and pressure forcing Comparisons with observations, *Geophys. Res. Lett.*, *30*, doi: 10.1029/2002GL016473.

Font, J., J. Salat, and J. Tintoré (1988), Permanent features in the general circulation of the Catalan Sea, *Oceanol. Acta*, *9*, 51–57.

García, E., J. Tintoré, J. M. Pinot, J. Font, and M. Manriquez (1994), Surface Circulation and Dynamics of the Balearic Sea, *Coastal Estuarine Stud.*, *46*, 73–91, doi: 10.1029/CE046p0073.

García-Ladona, E., A. Castellón, J. Font, and J. Tintoré (1995), The Balearic current and volume transports in the Balearic basin, *Oceanologica Acta*, *19*, 489–497.

Liu, Y., C. Dong, Y. Guan, D. Chen, J. McWilliams, and F. Nencioli (2012), Eddy analysis in the subtropical zonal band of the North Pacific Ocean, *Deep Sea Res., Part I 68*, 54–67, doi: 10.1016/j.dsr.2012.06.001.

Massutí, E., M. Olivar, S. Monserrat, L. Rueda, and P. Oliver (2014), Towards understanding the influence of environmental conditions on demersal resources and ecosystems in the western Mediterranean: Motivations, aims and methods of the IDEADOS project, *Journal of Marine Systems*, doi: 10.1016/j.jmarsys.2014.01.013.

Mertens, C., and F. Schott (1998), Interannual variability of deep-water formation in the northwestern Mediterranean, *J. Phys. Oceanogr.*, *28*, 1410–1424, doi: 10.1175/1520-0485(1998)028⟨1410:IVODWF⟩2.0.CO;2.

Millot, C. (1994), *Models and data: A synergetic approach in the western Mediterranean Sea*, Kluwer Acad., Dordrecht, Netherlands, pp. 407425.

Millot, C. (1999), Circulation in the Western Mediterranean Sea, *Journal of Marine Systems*, *20*, 423–442, doi: 10.1016/S0924-7963(98)00078-5.

Monserrat, S., J. L. López-Jurado, and M. Marcos (2008), A mesoscale index to describe the regional circulation around the Balearic Islands, *J. Mar. Syst.*, *71*, 413–420, doi: 10.1016/j.jmarsys.2006.11.012.

Nencioli, F., C. Dong, T. Dickey, L. Washburn, and J. C. McWilliams (2010), A vector geometry-based eddy detection algorithm and its application to a high-resolution numerical model product and high-frequency radar surface velocities in the southern California bight, *J. Atmos. Oceanic Technol.*, *27*, 564–579, doi: 10.1175/2009JTECHO725.1.

Pinot, J. M., J. L. López-Jurado, and M. Riera (2002), The canales experiment (19961998): interannual, seasonal, and mesoscale variability of the circulation in the Balearic Channels, *Prog. Oceanogr.*, *55(3-4)*, 335–370, doi: 10.1016/S0079-6611(02)00139-8.

Rio, M.-H., P.-H. Poulain, A. Pascual, E. Mauri, G. Larnicol, and R. Santoleri (2007), A mean dynamic topography of the mediterranean sea computed from altimetric data, in-situ measurements and a general circulation model, *J. Mar. Syst.*, *65*, 484–508, doi: 10.1016/j.jmarsys.2005.02.006.

Ruiz, S., A. Pascual, B. Garau, F. Yannice, A. Álvarez, and J. Tintoré (2009), Mesoscale dynamics of the Balearic Front, integrating glider, ship and satellite data, *J. Mar. Syst.*, *78*, S3S16, doi: 10.1016/j.jmarsys.2009.01.007.

Chapter 2

Vertical structure and temporal evolution of an anticyclonic eddy in the Balearic Sea (western Mediterranean)

La verdadera ciencia enseña, por encima de todo, a dudar y a ser ignorante.

Miguel de Unamuno (1864-1936)

This chapter has been published in:

- Amores, A., S. Monserrat, and M. Marcos. Vertical structure and temporal evolution of an anticyclonic eddy in the Balearic Sea (western Mediterranean). *J. Geophys. Res. Oceans*, 118:2097–2106, 2013a. doi: 10.1002 /jgrc.20150.

Abstract

An anticyclonic eddy in the Balearic Sea (western Mediterranean) was described using data from a mooring line deployed at the northern slope of Mallorca Island at about 900mdeep. Its surface signature was investigated using sea surface height and sea surface temperature images. The eddy, which lasted around 1 month, modified the thermohaline characteristics and the currents of the entire water column. Levantine Intermediate Waters, usually resident in the region, were displaced by colder and fresher Western Mediterranean Intermediate Waters associated with the eddy. Along-slope main currents (toward NE) were completely reversed at 500 m and significantly deviated at 900 m. Interestingly, near-bottom velocities were found to be systematically larger

than those at intermediate depths. Furthermore, during the eddy, velocities reached values up to 26 $cm \cdot s^{-1}$ at the bottom, 5 times larger than the bottom average speed. The recurrence of the phenomenon was explored with an eddy detection tool applied to satellite observations. Results indicated that anticyclonic eddies are common structures in the Balearic Current.

2.1 Introduction

The Balearic Sea, located in the western Mediterranean, is the subbasin confined between the Iberian Peninsula and the Balearic Islands, covering the area from 38° 45' N to 42° 30' N and 0° 20' W to 4° 00' E (Figure 2.1). On the continental side, the shelf is relatively narrow (15-30 km), with the exception of the Ebro River delta southward, where it becomes wider up to 6070 km. The slope is very steep, with depth increasing from 200 m to over 1000 m in only a few kilometers. On the islands side, the shelf is even narrower (5-20 km), and the slope becomes steeper and discontinuous due to the channels between the islands. Between Cape La Nao (Iberian Peninsula) and Ibiza Island, there is the so-called Ibiza Channel with 80 km width and a maximum depth of 800 m. The Mallorca Channel is located between Ibiza and Mallorca Islands, with approximately 80 km width and a maximum depth of 600 m. The Menorca Channel is placed between Mallorca and Menorca Islands, and it is the narrowest (35 km width) and shallowest (100 m depth). Further details about the topographic characteristics of the region can be found, for example, in *García et al.* [1994].

The oceanic mean circulation in the Balearic subbasin is generally cyclonic. Along the continental slope, the Catalan Front [*Font et al.*, 1988; *Violette et al.*, 1990] separates the fresher waters near the coast from saltier waters in the deeper basin. Its associated current, known as Northern Current (NC), flows southward along the continental slope and transports Atlantic Water from the Gulf of Lions toward the Balearic Channels (Figure 2.1). A bimodal behavior has been identified for the NC when it reaches the channels. In a normal situation, when the NC reaches the Ibiza Channel, it splits into two different branches. One branch flows through the channel, leaving the Balearic subbasin toward the Algerian subbasin. The other branch is cyclonically reflected and flows northward along the Balearic slope, forming the so-called Balearic Current (BC) with its associated Balearic Front (Figure 2.1). Simultaneously, other secondary currents flow northward into the Balearic subbasin from the Algerian subbasin through the channels. These currents transport fresher and warmer waters which join the BC. However, some of the inflow through the Ibiza Channel may be anticyclonically recirculated to the Algerian subbasin via the Mallorca Channel [*Pinot et al.*, 2002].

After winters colder than the average, the NC changes its usual path when it

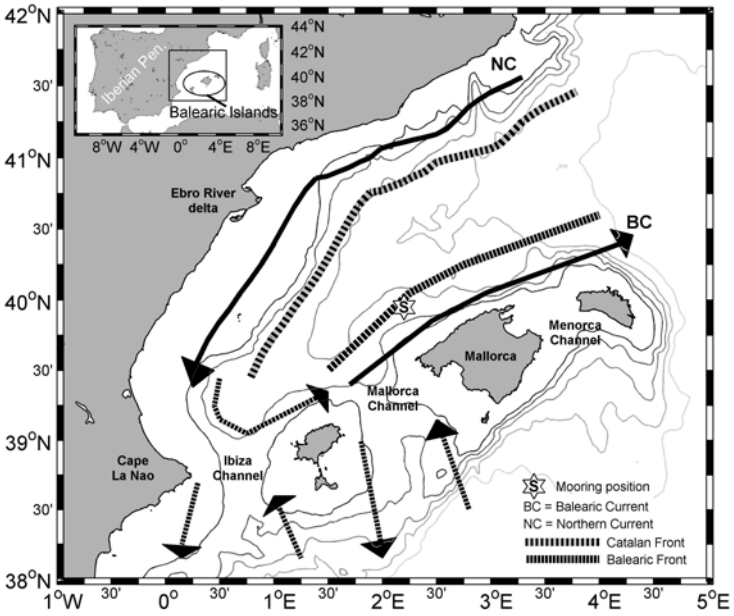

Figure 2.1: Map of the characteristics of the ocean circulation in the Balearic subbasin. The position of the mooring is marked with an S inside a star. Isobaths are plotted between 500 and 2500 m with a step of 500 m. Solid arrows indicate permanent currents, while dashed arrows are temporal features.

reaches the Ibiza Channel. Western Mediterranean Intermediate Waters (WIW) are formed in the Gulf of Lions during the winter season [*Mertens and Schott*, 1998; *Millot*, 1999; *Pinot et al.*, 2002]. During cold winters, an additional amount of WIW, normally located between 100 and 300 m, are formed, reaching the Balearic Channels later in spring [*Pinot et al.*, 2002].When this occurs, the branch which flows toward the Algerian subbasin may be blocked by the presence of mesoscale structures in the Ibiza Channel, so that the Balearic Current is then reinforced. The hydrodynamic characteristics of the subbasins and channels are strongly influenced then by the presence of WIW, which is basically controlled by the atmospheric conditions in the northwestern Mediterranean during winter. *Monserrat et al.* [2008] defined a climatic index (the IDEA index), based on near-surface air temperature at the Gulf of Lions during winter months (from December to March), capable of successfully predicting the presence of WIW at the channels the following spring.

The importance of the mesoscale variability of the Balearic Front has been largely underestimated because this front was thought to be more stable than the Catalan Front [*Violette et al.*, 1990]. This general point of view changed when *López-García et al.* [1994] observed significant mesoscale activity at the Balearic

Front, with a large number of eddies and filaments. They concluded that the Balearic Front is the northward extension of the eddy-dominated regime of the Algerian subbasin, which is well known for its strong mesoscale activity [*Millot et al.*, 1997]. Many works have shown afterward the existence of these structures in the Balearic Current using satellite data, drifting buoys, oceanographic cruises, gliders, and/or modeling tools [*Álvarez et al.*, 1996; *Balbín et al.*, 2012; *Bouffard et al.*, 2012; *Pinot et al.*, 1994; *Rubio et al.*, 2009; *Ruiz et al.*, 2009; *Tintoré et al.*, 1990]. In particular, *Pascual et al.* [2002] described, with satellite and in situ data, the origin, develop- ment, and decay of an intense anticyclonic eddy which survived during 6 months, moving into the Balearic Sea and even producing a reversal of the cyclonic circulation of the subbasin. *Balbín et al.* [2012] used conductivity- temperature-depth (CTD) measurements, satellite data, and mooring data to study a front present at the north of Mallorca Island in December 2009. This structure evolved into an eddy which was later on measured by the mooring presented in this work. Most of the mesoscale structures in the region have been identified and described using the time evolution of surface data or by a 3-D spatial snapshot obtained from cruise hydrographic data. However, very scarce information exists so far on the temporal evolution of mesoscale structures for deeper levels.

Mesoscale eddies are common structures in the ocean. They may have a topographic origin, when a bottom flow encounters a seamount, or atmospheric, when wind-driven currents, convergent or divergent, may result in the formation of such structures. Another well-known eddy formation mechanism consists of the intensification of an ocean current, which can lead to the development of a meander. Such meander may finally pinch off relatively warm or cool waters acting as the seed of an eddy. These eddies are sometimes referred to as rings.

In this work, we describe the formation, development, and disappearance, as well as the hydrodynamic characteristics, of a mesoscale anticyclonic eddy recorded by a mooring line placed at the north of Mallorca Island, in the path of the Balearic Current. The eddy lasted in the region around 1 month, between November and December 2010. This is the first time that it has been possible to describe the complete temporal evolution for deeper levels of a mesoscale eddy in the Balearic Sea.

This study is organized as follows: First, the data set and methodology are presented in 2.2. In 2.3, the hydrodynamic conditions of the eddy are shown, describing the surface situation and its vertical structure. Finally, in 2.4, the conclusions are presented.

2.2 Data Sets and Methodology

Two different data sets were used in this study. The vertical structure was determined by means of observations from a mooring line, while the horizontal surface characteristics were studied using satellite data.

The mooring line was deployed north of Mallorca Island (39°49.682'N − 2° 12.778'E) from November 2009 until February 2011. It was placed at 900 m depth in the Mallorca's slope of the Balearic subbasin. The line consisted of four CTD Seabird 37 (at 300, 500, 700, and 900 m deep), two current meters Nortek Aquadopp (at 500 and 900 m deep), and a sediment trap at the bottom. Observations of thermohaline properties and currents were collected at sampling rates of 10 min for the CTD and 30 min for the current meters. Two maintenance surveys were carried out during the deployment period in order to recover the data stored in the instruments and to change batteries in December 2009 and July 2010. All instruments operated correctly during the entire period, except for the 500 and 900 m CTDs, which ran out of batteries in mid-December 2010 and mid-January 2011, respectively.

Current meter observations were analyzed using wavelets [*Liu and Miller*, 1996], a standard tool widely used for the analysis of non stationary data sets, including oceanographic observations [*Emery and Thomson*, 1998]. The time series from 1 November 2010 to 31 January 2011 were used in order to visualize the most energetic frequency bands before, during, and after the development of the eddy.

Daily gridded absolute dynamic topography fields with a map spacing of $1/8° \times 1/8°$ were obtained from the merged satellite Archiving, Validation, and Interpretation of Satellite Oceanographic data (AVISO) products available at `www.aviso.oceanobs.com`. The absolute dynamic topography is calculated as the sum of the sea level anomalies and the mean dynamic topography [*Rio et al.*, 2007]. The regional sea level anomalies for the Mediterranean Sea available at the AVISO server are a multimission product with up to four satellites at a given time, spanning the period from 1992 to present. All standard geophysical corrections were applied, including the so-called Dynamic Atmospheric Correction, produced by CLS. This correction combines the high frequency (H−F) of the Mog2D model [*Carrère and Lyard*, 2003] and the low frequency of the classical inverted barometer correction. These model outputs were used to correct the newly released altimeter data sets, therefore reducing the aliasing effects of H−F signals [*Volkov et al.*, 2007]. The regional mean dynamic topography covers the Mediterranean Sea, and it is based on 7 years of observations (1993−1999). Despite its good performance in the open ocean and the wide range of applications, the altimetric products, both gridded and along track, fail when approaching the coast, mostly due to the land contamination in the signal. Several efforts are

currently devoted to the recovery and improvement of near-coastal altimetry observations. However, this new generation of observations is not fully developed for the global coastal ocean yet, not even for the Mediterranean Sea.

Daily sea surface temperature (SST) data were collected from MyOcean database (`http://www.myocean.eu`). The regional gridded product for the Mediterranean Sea is a high-resolution SST anomaly, computed using the CNR MED analysis at $1/16° \times 1/16°$ horizontal resolution and starting in December 2010.

The time evolution of the eddy features was explored using the vector geometry-based eddy detection algorithm [*Nencioli et al.*, 2010]. This scheme is a flow geometry-based method. The center of the eddy is determined by a local velocity minimum into an area where rotating flow has been detected. The eddy boundaries are defined as the outermost closed streamline around the center, across which velocity is still radially increasing.

In order to improve the algorithm performance, the AVISO velocity fields were linearly interpolated from a $1/8° \times 1/8°$ grid to a $1/16° \times 1/16°$ grid, as it was performed in Liu et al. [2012]. Finally, the method was applied to the resultant fields with parameters $a = 3$ and $b = 2$. Parameter a defines the amount of grid points away from a given point, in which the increases in magnitude of the velocity component v along the EW axes and velocity component u along the NS axes are checked, and b is the dimension in grid points of the area used to define the velocity local minimum.

Once the boundaries and the center of the eddy were established, its main features could be derived. The equivalent radius was calculated as the radius of a circumference with the same area than the area of the eddy; the circulation was the sum of the vorticity in all points inside the eddy area; and the SSH maximum was the maximum value of the SSH inside the limits of the eddy.

2.3 Results and Discussion

During the operational time of the mooring, several mesoscale structures were identified in the Balearic Sea using satellite images. In the present work, we concentrated on an anticyclonic eddy observed between mid-November and mid-December 2010. Among all structures observed, this eddy generated the largest variations of the hydrodynamic characteristics of the intermediate and deep waters. In the following, the eddy is described from surface remote sensing observations and from moored in situ data.

2.3.1 Surface Description of the Eddy

Figure 2.2 shows the temporal evolution of sea surface height (SSH) before, during, and after the eddy formation provided by the altimetry data. Prior to the eddy formation, SSH depicted the usual nonperturbed situation with the NC flowing southward along the mainland coast and the BC flowing northward along the islands' slope (BC) (Figure 2.2a). However, a small meander is observed in the Balearic Current starting to develop in front of the Mallorca Channel (Figure 2b) and strengthening (Figure 2.2c). The first day on which the automatic eddy detection scheme [*Nencioli et al.*, 2010] detected the eddy (not shown) that remained almost stationary in the zone was on 21 November. Figures 2.2d−2.2j show the eddy boundaries of the fully developed anticyclonic structure which was detected with the method during 19 days. This anticyclonic structure partially blocked the surface circulation of the NC and forced the branch flowing along the shelf of the Islands to leave the Balearic subbasin through the Mallorca Channel.

The evolution of the main features of the eddy is shown in Figure 2.3. The equivalent radius was confined between 4 and 28 km with an average value of 21.4 km. Taking its mean radius and a mean velocity of 20 cm/s at this point, the rotation period of the eddy rises around 8 days. The circulation varied between $-1.5 \times 10^{-4} s^{-1}$ and its minimum value $-6.8 \times 10^{-4} s^{-1}$, which coincided in time with the maximum SSH value (18.4 cm). The eddy was almost stationary (map in Figure 2.3), although, in the last part of its life, it shifted toward the mooring position.

The last day in which the eddy was detected by the automatic scheme was on 10 December 2010. Nevertheless, a structure moving toward the mooring was still present in the subsequent images. Although the scheme did not detect the eddy, its existence cannot be ruled out due to the well-known troubles of satellite measurements near the coast. The structure weakened and disappeared (Figures 2.2m−2.2o), becoming first a meander of the current similar to Figure 2.2b.

Changes in the sea surface temperature anomalies were also explored for the same period of time (Figure 2.4). Before the eddy formation (around 3 November 2010; not shown), the strongest feature was a very large SST gradient located between longitudes 2.75° E−6.50° E and latitudes 41° N−42° N (2.5° C in around 20 km). This gradient, found at the north of the Balearic Sea, was previously identified as the North Balearic Front [*López-García et al.*, 1994; *Millot*, 1999]. The footprint of this gradient is still visible in Figure 2.4a, with a negative temperature anomaly around 1.8° C. At the same time, there was a core of warmer water growing southwest of the mooring position (Figures 2.4a−2.4c) having as a result the formation of the eddy. The maximum temperature anomaly (∼1° C) was observed on 28 November, with the eddy being fully developed. This region with warmer water surrounded by colder water disappeared in Figure 2.4j and

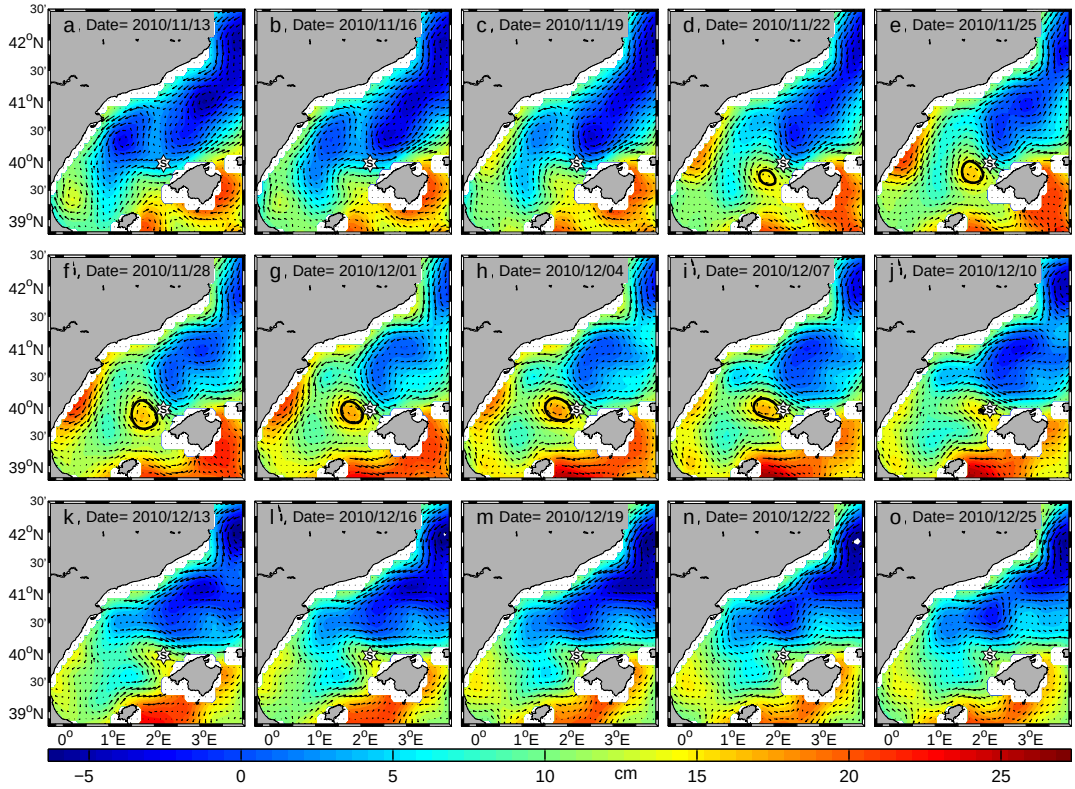

Figure 2.2: Sea surface height (SSH) images of the formation, development, and subsequent disappearance of the eddy. Colors indicate SSH (in cm); vectors are the direction and modulus of the geostrophic currents associated to the SSH field; and the star with an S inside shows the mooring position. The dark enclosed area delimits the perimeter of the eddy following the criteria in Nencioli et al. [2010] (see text).

subsequent images.

2.3.2 Vertical Structure of the Eddy

The eddy development was recorded at different depths by the moored array of instruments.

Figures 2.5a and 2.5b show the progressive vector diagrams (PVDs) of the currents measured at 500 and 900 m, respectively, between 10 November 2010 and 5 January 2011. The black part represents the normal situation for the currents in the zone: flowing northeastward along the slope (see Figure 2.1). Between 20 November and 19 December, a complete reversal of the current was measured at 500m (grey part Figure 2.5a), which also had its footprint at 900m (grey part Figure 2.5b). In the latter, the flow was not completely reversed but changed its direction in about 90° becoming across slope.

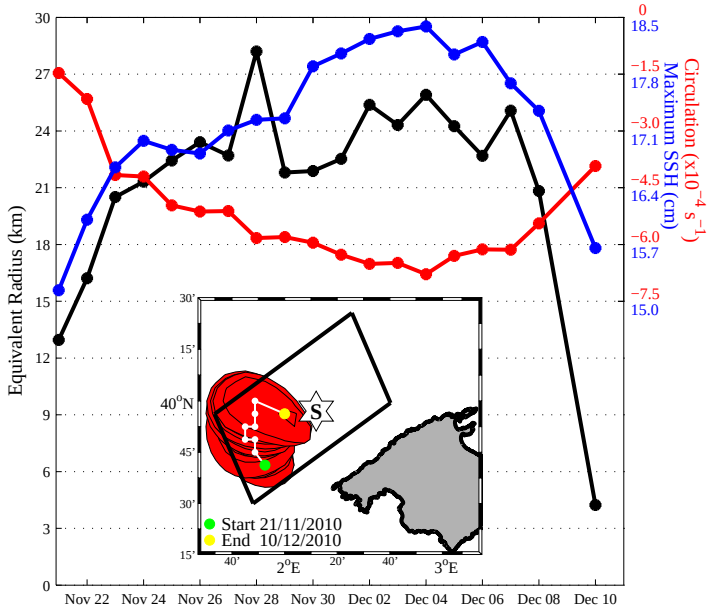

Figure 2.3: Main features of the eddy: the equivalent radius (black), the maximum SSH value (blue), and the circulation (red). In the inset map, the white line shows the trajectory of the eddy, and the red enclosed area shows the evolution of its surface location. The mooring position is marked with a star with an S inside. The thick black rectangle delimits the area used for the study of the recurrence of the phenomenon (see text for details).

The current values for the same time period and depths are shown in Figure 6, decomposed in along-slope (Figures 2.6a and 2.6c) and across-slope (Figures 2.6b and 2.6d) components. Low-pass-filtered time series (with a cutoff frequency of 48h) are also plotted in red. The currents reached their maximum velocities during the episode. The mean current speed during the episode doubled the mean velocity values (from 2 to 4 cm/s at 500 m and from 3 to 7 cm/s at 900 m) with maximum speeds of 19 and 26 cm/s at 500 and 900 m, respectively. It is worth mentioning that measured velocities, during the episode and in the normal situation, were constantly greater at 900 m depth than at 500 m. The nonfiltered data also revealed that inertial oscillations of velocity were amplified during the episode.

The changes in T and S associated to the presence of the eddy are plotted in Figure 2.7, together with their low-pass-filtered time series. During the episode, a significant decrease of salinity (0.35, Figure 2.7a) and temperature (0.6° C,Figure 2.7b) at 300 m was observed. A reduction in salinity (at constant T) produces a reduction of density; likewise, a temperature drop (at constant S) is translated in an increase of density. Therefore, in terms of density, salinity reduction domi-

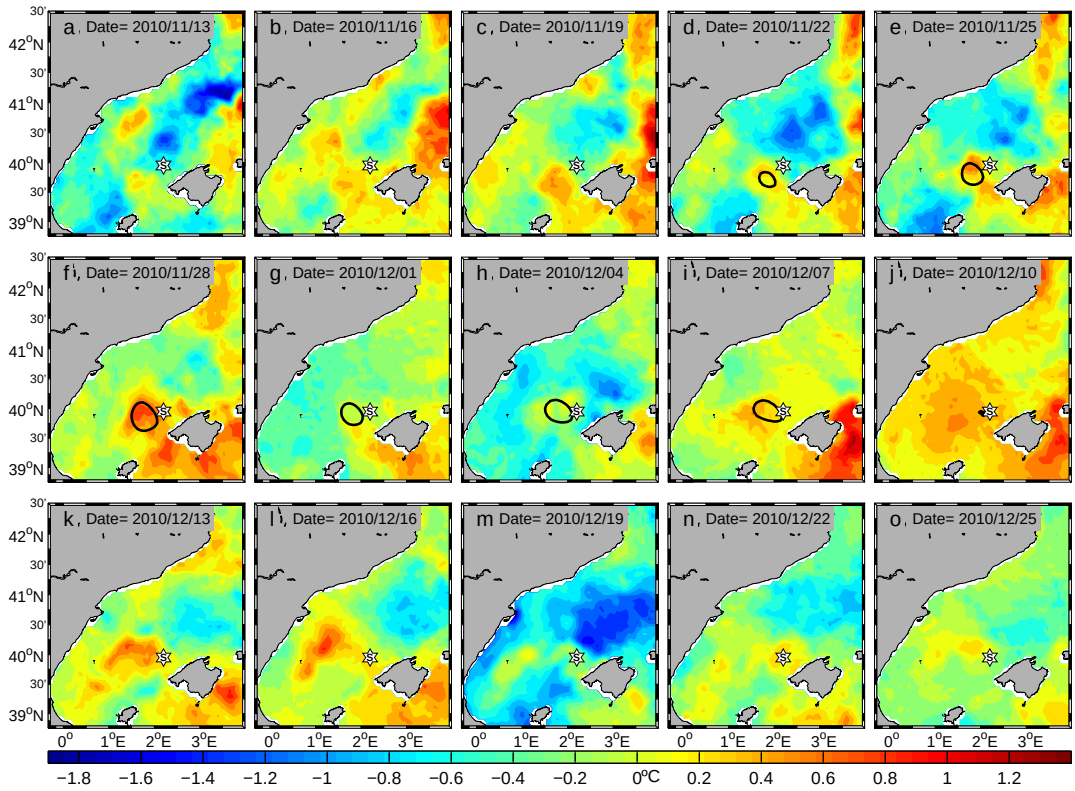

Figure 2.4: SST images of the same moments of the first four SSH images. Colors indicate the temperature of the sea surface; and the star with an S inside represents the mooring position. The dark enclosed area delimits the perimeter of the eddy following the criteria in Nencioli et al. [2010]

nated over temperature cooling, thus decreasing density drastically at these levels (Figure 2.7e). At 700 m, an increase of temperature and salinity was observed (0.02 and 0.15°C, respectively; Figures 2.7c and 2.7d). However, at this depth, salinity and temperature exchanged their roles, and temperature changes dominated and induced a decrease of density (Figure 2.7g). The combination of both effects guaranteed the stability of the water column. As for the velocity, it is noteworthy that inertial oscillations were amplified during the episode.

The pressure record showed significant oscillations (Figures 2.7f and 2.7g) with decreasing magnitude in depth. The origin of these oscillations was not related to density changes or different heights of the water column since both variations tend to geostrophically compensate each other. Observed pressure changes were clearly linked to the increase of currents associated with the eddy, tilting the mooring up to 7° and sinking the instruments below their usual depth. For the CTD deployed at 300 m, the mooring tilt increased the pressure up to 4 dbar.

Changes in water mass properties during the episode were explored through

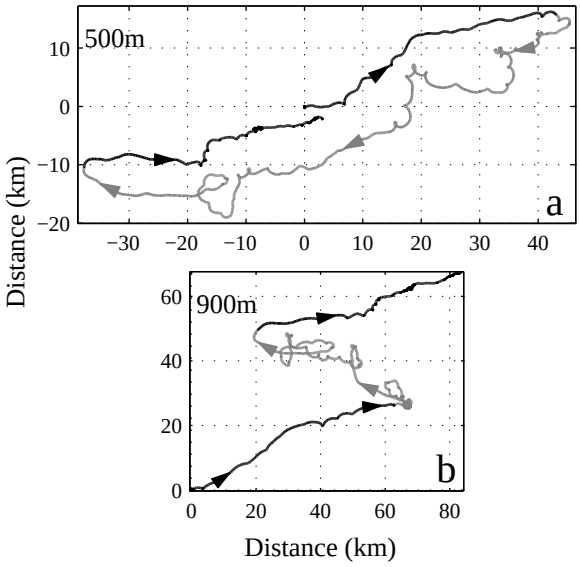

Figure 2.5: Progressive vector diagram (PVD) of the current meters at (a) 500 m and (b) 900 m depth from 10 November 2010 to 5 January 2011.

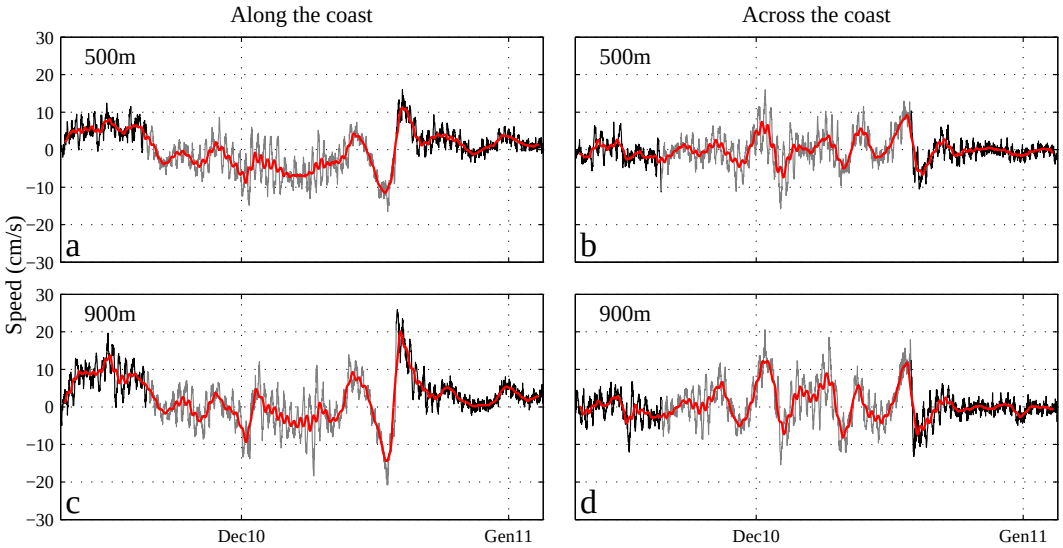

Figure 2.6: Currents measured in (a and b) 500 m and (c and d) 900 m decomposed along (see Figures 2.6a and 2.6c) and across (see Figures 2.6b and 2.6d) the coast components. The original record is presented in black and grey, and the 2 day low-pass-filtered series is presented in red.

TS diagrams (Figure 2.8). At 300 m, the drastic drop in temperature and salinity changed the properties of the resident water of the zone, Levantine Intermediate Water (LIW), to those of Western Mediterranean Intermediate Water (WIW),

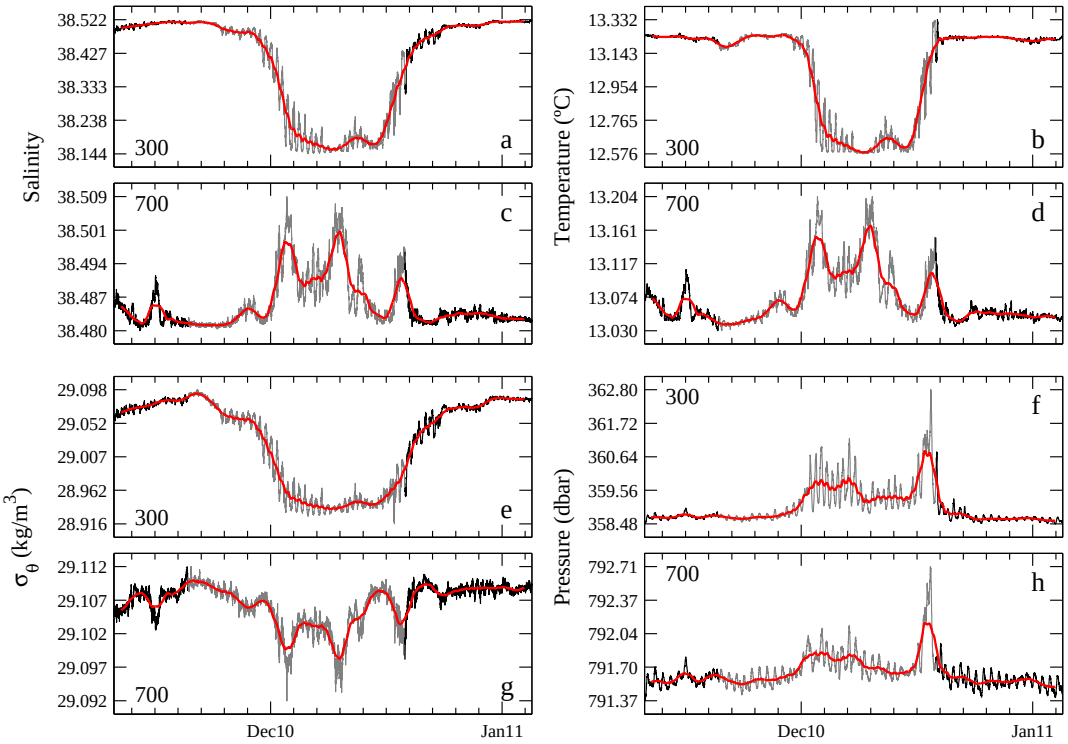

Figure 2.7: Time series of (a) salinity, (b) temperature, (c) potential density, and (d) pressure recorded by the Seabird37 at (1) 300 m and (2) 700 m from 10 November 2010 to 5 January 2011. The original record is presented in black and grey, and the 2 day low-pass-filtered series is presented in red.

which is less saline, cooler, and lighter. This evidence suggests that the eddy at this depth was formed by WIW. These waters are generated in the Gulf of Lions during the winter season, transported by the NC southward reaching the Ibiza Channel typically in spring and may remain in the region until late autumn or early winter. Therefore, given the presence of WIW in the eddy at intermediate depths, it is hypothesized that the meander, and later the eddy formed in the BC, transported WIW remaining in the Mallorca Channel to the mooring position. When the eddy disappeared, the water characteristics returned to LIW. At deeper levels (700 m in Figure 2.8), TS diagrams show how Western Mediterranean Deep Waters (WMDW) that usually occupy these levels were displaced by LIW during the episode.

Figure 2.9 depicts the temporal changes in density throughout the water column and during the presence of the eddy, as recorded by the instrumental array of CTDs. The values in depths were interpolated using splines, whereas a 1 week running average was applied to the temporal time series in order to remove the high-frequency signals. Time series (without mean value) are also provided for

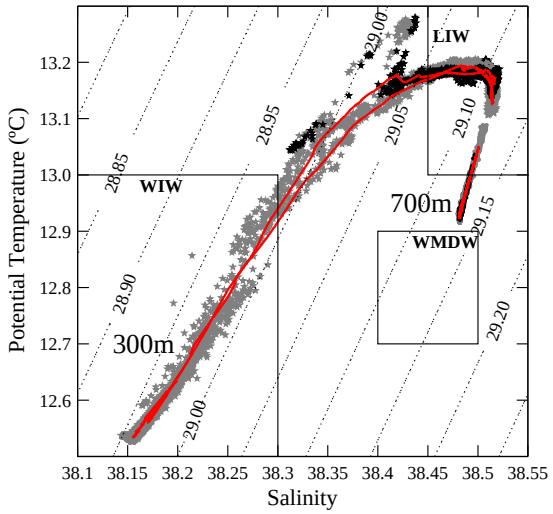

Figure 2.8: TS *diagram of 300m (series with stars) and 700m (dotted series) recorded from 10 November 2010 to 5 January 2011. The original record is presented in black and grey, and the 2 day low-pass-filtered series is presented in red.*

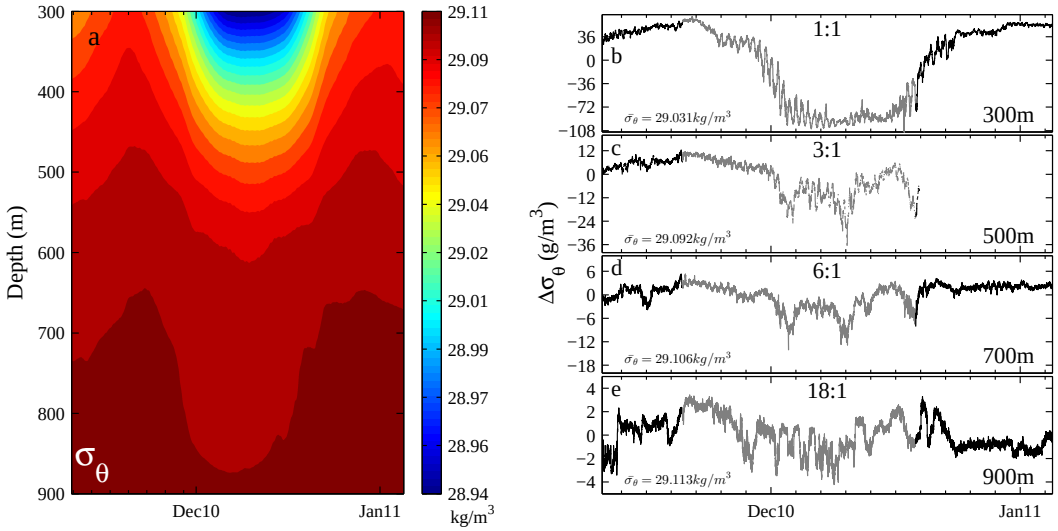

Figure 2.9: (a) Temporal evolution of the vertical structure of the density interpolating the values in depth using splines and density time series (without mean value) as measured for the moored instruments at (b) 300 m, (c) 500 m, (d) 700 m, and (e) 900 m.

comparison (note that vertical scales are proportional to the 300 m scale for the sake of comparison). The effects of the eddy were reflected in a deepening of the isopycnals and were substantial in the entire water column. In particular and compared with values at 300 m, the effect in 500 m is around 3 times weaker; in

700 m, it is 67 times smaller; and in 900 m, it has been attenuated by more than 18 times.

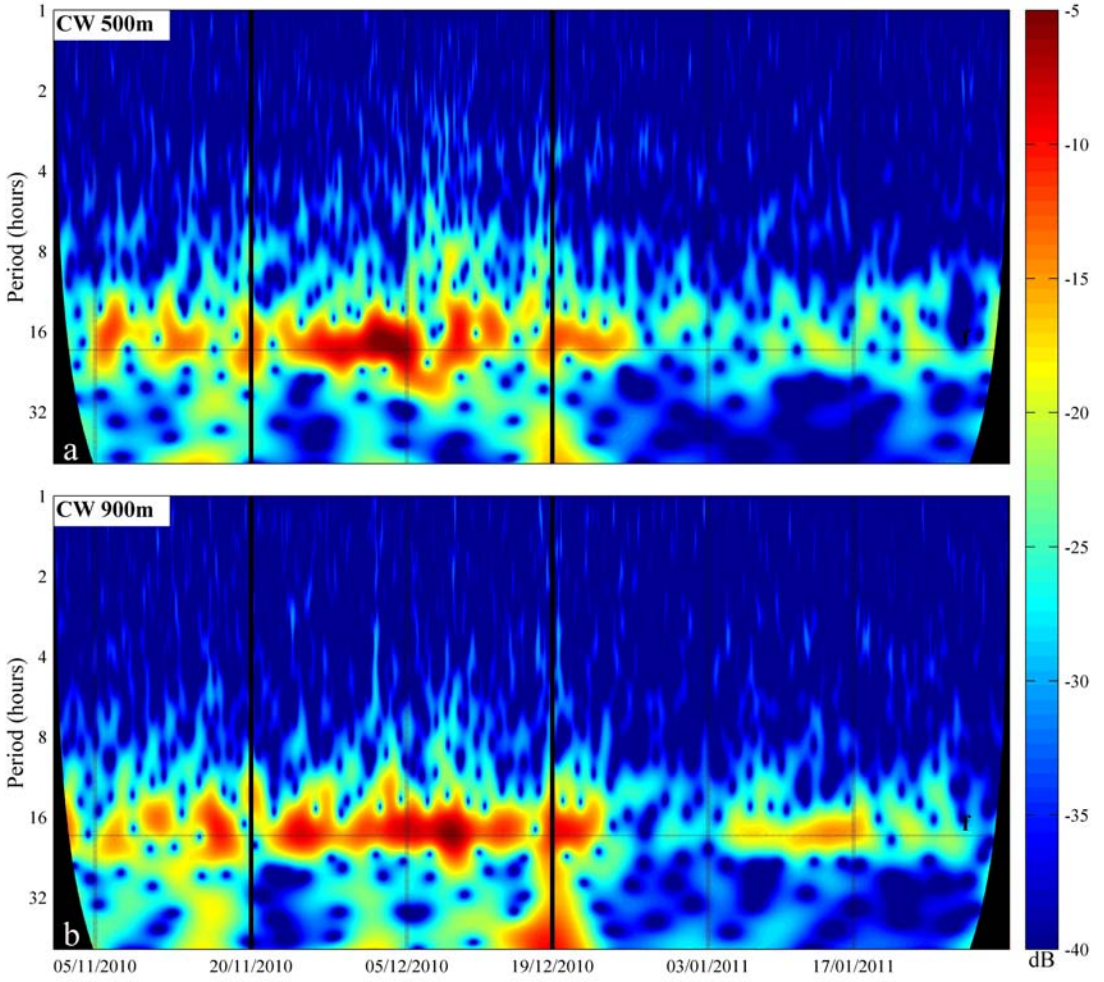

Figure 2.10: Clockwise wavelet of currents at (a) 500 m and (b) 900 m. f *is the inertial frequency (18.73 h). Units are dB.*

Changes in the frequency domain of the current records were explored using wavelets. The length of the time series used is 92 days (from 1 November to 31 January) with a sampling interval of 30 min. As the eddy is anticyclonic, only the clockwise components of the currents were explored [*Liu and Miller*, 1996]. Highest energies were found at periods of a few days, associated with the rotation of the eddy itself and with synoptic-scale atmospheric forcing. However, anticyclonic eddies trap inertial waves, being their effective period inside the eddy larger than outside due to the sum of the relative vorticity of the eddy [e.g., *D'Asaro*, 1995]. Therefore, only periods between 1 and 50 h were explored.

The clockwise wavelets of the currents at 500 and 900mfor such period bands are represented in Figure 2.10. Two thick vertical lines denote the time in which the reversal of the currents was detected. At both depths, higher energy levels were concentrated around the inertial frequency f ($\lambda = 39.83°$, $T_f = 18.7$ h, indicated in the plot as a horizontal line). This observation is in agreement with the fact that inertial oscillations appeared amplified in the velocity, temperature, and salinity time series (Figures 2.6 and 2.7). According to Figure 2.2, the eddy did not cross the mooring position, except tangentially at the end of its life. Therefore, the increase of energy at the inertial frequency corresponds to the detection of a meander circulating around the eddy periphery. However, around 19 December, there was a significant increase of the energy at periods between 30 and 40 h, suggesting an inertial wave trapping caused by the eddy. The fact that the inertial energy increased in the clockwise wavelet and not in the counter-clockwise (not shown) is in agreement with the anticyclonic character of the eddy.

It is also noteworthy that the energy content was higher, clearer, and more constant at 900 m than at 500 m during the eddy life, which indicates once again that the eddy signal reached higher depths and that it had an important effect even near the bottom.

2.3.3 Recurrence of the Phenomenon

It has been shown above that the presence of an anticyclonic eddy in the path of the BC can seriously distort the current regime in the Balearic Sea and have an impact on the entire water column. Thus, the frequency at which these phenomena take place may have implications for the hydrodynamics of the area. With the aim of determining the repeatability of this episode, the automatic eddy detection tool from *Nencioli et al.* [2010] was used in the same region where the mooring was deployed (rectangle of $1° \times 0.5°$ in the map in Figure 2.3) for the period 19922011. The episodes were chosen to satisfy two criteria: first, the total time in which the eddy was detected by the method (referred to as duration hereinafter) must be at least 10 days, a value which corresponds to half of the duration of our target eddy; and second, the center of the eddy must remain at least 1 day inside the area. These criteria are subjective, and the final number of episodes would change if the area or the duration were modified. Our goal was not to perform a detailed statistical analysis but only to compare the studied eddy with a regular situation in the region affected by the Balearic Current.

Table 2.1 lists the starting and ending dates, the duration (in days), the total circulation, the relative circulation compared with our eddy, and its mean radius of the 37 episodes that fulfill all the criteria, sorted by decreasing circulation. The circulation is calculated as the sum of the vorticity over the whole eddy area and for all days of its duration.

	Start	End	Duration (days)	Circulation ($10^{-3}s^{-1}$)	Percentage (Circ/Circ Our)	Radius (km)
	13/03/1999	14/04/1999	33	-13.11	181.7	14.63
	22/04/1999	04/05/1999	13	-10.02	138.9	10.83
	10/11/1995	25/11/1995	16	-10.01	138.8	9.80
	04/01/2009	24/01/2009	19	-9.10	126.2	13.70
	29/12/1995	09/01/1996	12	-7.38	102.3	8.69
★	**21/11/2010**	**10/12/2010**	**19**	**-7.21**	**100.0**	**21.40**
	05/12/2001	29/12/2001	25	7.17	99.4	21.90
	15/07/2001	03/08/2001	20	6.31	87.5	13.81
■	28/01/2010	09/02/2010	13	-6.10	84.6	13.43
	03/06/2001	04/07/2001	32	5.96	82.6	19.90
	27/07/1998	18/08/1998	22	5.93	82.3	16.60
	16/11/2008	04/12/2008	18	5.43	75.4	25.39
■	19/02/2010	03/03/2010	13	-5.01	69.5	10.49
	21/08/2007	03/09/2007	14	3.77	52.3	18.05
	20/06/2009	09/07/2009	20	-3.72	51.6	15.01
	09/07/1999	22/07/1999	13	-3.57	49.5	15.79
	05/08/2010	16/08/2010	12	-3.46	47.9	14.84
	30/05/2002	15/06/2002	17	-3.45	47.9	17.06
	27/05/2005	06/06/2005	11	-2.81	39.0	21.81
	26/05/1996	11/06/1996	17	-2.66	36.9	10.59
	20/08/2008	26/10/2008	66	-2.44	33.9	18.88
●	12/06/2010	15/07/2010	34	-2.38	32.9	7.75
	19/10/1998	30/10/1998	12	2.28	31.6	14.50
	30/10/2008	27/12/2008	59	2.00	27.7	12.77
	05/09/1994	01/10/1994	27	1.68	23.3	13.26
	03/08/1994	25/08/1994	22	1.68	23.3	11.98
	06/04/1993	15/04/1993	10	1.50	20.8	11.89
	01/04/1995	17/04/1995	17	1.45	20.1	16.84
	23/04/2008	13/05/2008	19	1.40	19.4	12.28
	12/06/2010	02/07/2010	18	-1.39	19.3	20.22
	29/04/2010	06/06/2010	39	1.29	17.9	22.16
	07/03/2005	16/03/2005	10	0.75	10.4	16.04
	04/11/2005	16/11/2005	13	-0.58	8.0	23.41
	07/01/2008	23/01/2008	17	0.43	6.0	21.69
	08/05/2002	20/05/2002	12	-0.36	5.0	21.63
	09/07/1995	22/07/1995	14	0.30	4.1	18.06
	21/07/2002	13/08/2002	24	-0.12	1.6	17.35

Table 2.1: List of events that fulfill the selection criteria from 1992 to 2011

The eddy of the longest duration took place in August 2008 with 66 days. The mean duration of the selected eddies was 21 days with a standard deviation of 12 days. The mean radius was 16 km with a standard deviation of 4.5 km. Although most of the episodes (23) took place during warmer months, from April to September, the most intense eddies in terms of circulation occurred in colder months (October−March). More precisely, 9 of the 13 most intense eddies occurred during winter time. This fact is related to the intensification of the Northern Current during the winter season, which also affects the Balearic Current [*Pinot et al.*, 2002]. Moreover, 17 of the 22 most intensive eddies were anticyclonic.

The eddy studied in this paper is the 6th most intense of all the eddies fulfilling the selection criteria (star with an S inside, see Table 2.1) and the 8th in terms of the length of the radius (21.40 km), although it is only the 16th longest.

During 2010, there were a total of three episodes similar to our eddy measured

by the mooring. The first episode, described in *Balbín et al.* [2012], corresponds to the two eddies marked with a square in Table 1. The second eddy is marked with a circle in Table 2.1. The eddy described in this paper is the most intense measured by the mooring in terms of circulation and the only one which presents a clear footprint at the bottom and the largest changes in temperature and salinity.

2.4 Summary and Conclusions

A mooring line deployed at the northern slope of Mallorca Island (western Mediterranean) during more than 1 year measured the effects of a strong anticyclonic eddy (the 6th with higher total circulation and the 8th with bigger radius) that modified the hydrodynamic properties in the whole water column (∼1000 m). The eddy remained in the area about 1 month (November−December 2010) and caused a complete reversal of the current direction at 500 m and a change of 90°in 900 m with respect to the along-slope main direction under unperturbed conditions. CTD observations indicated that the core of the eddy was formed by Western Mediterranean Intermediate Waters (WIW) at depths between 300 and 700 m, while Levantine Intermediate Waters (LIW) were found at deeper levels (700900 m). It is suggested, based on satellite altimetry observations, that the eddy was formed as a consequence of a meander in the Balearic Current which transported WIW northward from the Mallorca Channel. As WIW present lower temperatures and salinity than the resident LIW, its presence during the eddy episode was clearly detected through TS diagrams.

It has been shown that the presence of the eddy affected the entire water column. This finding is in agreement with *Pinot et al.* [2002], who showed the presence of an eddy down to 500 m, and contrasts with other reported mesoscale structures in the western Mediterranean which did not extend deeper than 300 m [*Font et al.*, 1988; *Pinot et al.*, 1994]. In our area of study, however, all eddies measured during the time in which the mooring was deployed have a clear footprint at 500 m and a weaker one at 900 m (not shown).

Interestingly, the comparison of current meter and CTD measurements revealed a 10 day time lag between the beginning of the observed current reversal at 500 m and the later appearance of WIW. This lag is consistent with an eddy formed by a core of WIW generated west from the observation site and shifted toward the mooring position, as shown by SSH and SST images. In this case, currents associated with the external part of the eddy affect the area before the entrance of the core.

The same time lag was also observed when the eddy disappeared. The currents returned to its usual direction before the hydrodynamic properties recovered their usual values. As also suggested by satellite images, this fact was a consequence

of the extinction of the eddy over the observation area. The currents recovered their unperturbed direction, and the WIW core waters were then swept out of the area.

Current meter observations revealed that velocities were higher at 900 m than at 500 m during the entire period of observation. In particular, averaged values of velocity were 4 cm/s at 500 m and 7 cm/s at 900 m and reached peak values up to 26 cm/s at 900 m. This effect is not new and was also reported in other places in the western Mediterranean [*Millot*, 1994], but it still remains unclear [*Pinot et al.*, 2002]. Since velocities measured at the surface by altimetry were larger than at intermediate depths (and probably the near-surface velocities, too), it is suggested that the velocity reaches its minimum at some unknown intermediate depth. More current meter observations at additional depths would be needed to estimate the complete vertical velocity profile of the Balearic Current, paying special attention from surface up to 300 m where data were not acquired. The 90° turn in the bottom currents at 900 m, which caused a change in its main direction from along slope to cross slope, could be related to turbidity currents generated by the eddy resuspending sediments from the seabed. This turbid water would become heavier than the water below, and it would fall downslope. Previous studies suggested that a small amount of resuspended material could give rise to significant downslope velocities [*Thomson et al.*, 2010]. This suggestion is supported by the fact that the total flux mass recorded by the sediment trap during the eddy life is around 2 times larger (595 $mg \cdot m^2 \cdot d^{-1}$) than its average for the entire deployment period (313 $mg \cdot m^2 \cdot d^{-1}$).

A reference level of zero velocity at about 500 m has been usually taken in the computation of the dynamic height from hydrographic observations in the region of study. Our observations indicated that this approximation does not hold, as significant average velocities of 4 cm/s at 500 m were found. It is advisable therefore to account for this effect in the computation of dynamic heights.

Acknowledgments

This research was partially sponsored by the IDEADOS project (proyecto del Plan Nacional CMT2008-04489-C03-03). The work of A. A. was funded by a JAE-PreDoc grant from Consejo Superior de Investigaciones Científicas (CSIC) and cofunded by Programa Operativo FSE 20072013. M. M. acknowledges a Ramon y Cajal contract funded by the Spanish Ministry of Economy and Competitiveness. The authors are grateful to Richard Thomson, D. Gomis, G. Jordà, and M. Flexas for useful discussions on the paper. The authors are deeply grateful to all the IDEADOS team for their collaboration in the data acquisition process. We also wish to thank three anonymous reviewers for their valuable comments on the manuscript and N. Oliver for helping with the English. A. A. wants to thank

Maiman Oliver for their invaluable help in the interpretation of the results found.

Bibliography

Álvarez, A., J. Tintoré, and A. Sabatés (1996), Flow modification and shelf-slope exchange induced by a submarine canyon off the northeast Spanish coast, *J. Geophys. Res.*, *101*, 12,043–12,055, doi: 10.1029/95JC03554.

Balbín, R., M. M. Flexas, J. L. López-Jurado, M. Peña, A. Amores, and F. Alemany (2012), **Vertical velocities and biological consequences at a front detected at the Balearic Sea**, *Cont. Shelf Res.*, *47*, 28–41, doi: 10.1016/j.csr.2012.06.008.

Bouffard, J., L. Renault, S. Ruiz, A. Pascual, C. Dufau, and J. Tintoré (2012), Sub-surface small-scale eddy dynamics from multi-sensor observations and modeling, *Prog. Oceanogr.*, *106*, 62–79, doi: 10.1016/j.pocean.2012.06.007.

Carrère, L., and F. Lyard (2003), Modelling the barotropic response of the global ocean to atmospheric wind and pressure forcing Comparisons with observations, *Geophys. Res. Lett.*, *30*, doi: 10.1029/2002GL016473.

D'Asaro, E. A. (1995), Upper-ocean inertial currents forced by a strong storm. Part III: Interaction of inertial currents and mesoscale eddies, *J. Phys. Oceanogr.*, *25*, 2953–2958.

Emery, W. J., and R. E. Thomson (1998), *Data Analysis Methods in Physical Oceanography*, Pergamon, Netherlands, pp. 500509.

Font, J., J. Salat, and J. Tintoré (1988), Permanent features in the general circulation of the Catalan Sea, *Oceanol. Acta*, *9*, 51–57.

García, E., J. Tintoré, J. M. Pinot, J. Font, and M. Manriquez (1994), Surface Circulation and Dynamics of the Balearic Sea, *Coastal Estuarine Stud.*, *46*, 73–91, doi: 10.1029/CE046p0073.

Liu, P. C., and G. S. Miller (1996), Wavelet transforms and ocean current data analysis, *J. Atmos. Oceanic Technol.*, *13*, 1090–1099.

López-García, M. J., C. Millot, J. Font, and E. García-Ladona (1994), Surface circulation variability in the Balearic Basin, *J. Geophys. Res.*, *99(C2)*, 3285–3296, doi: 10.1029/93JC02114.

Mertens, C., and F. Schott (1998), Interannual variability of deep-water formation in the northwestern Mediterranean, *J. Phys. Oceanogr.*, *28*, 1410–1424, doi: 10.1175/1520-0485(1998)028⟨1410:IVODWF⟩2.0.CO;2.

Millot, C. (1994), *Models and data: A synergetic approach in the western Mediterranean Sea*, Kluwer Acad., Dordrecht, Netherlands, pp. 407425.

Millot, C. (1999), Circulation in the Western Mediterranean Sea, *Journal of Marine Systems*, *20*, 423–442, doi: 10.1016/S0924-7963(98)00078-5.

Millot, C., M. Benzohra, and I. Taupier-Letage (1997), Circulation off Algeria inferred from the Mediprod-5 current meters, *Deep Sea Research Part I: Oceanographic Research Papers*, *44*, 1467–1495, doi: 10.1016/S0967-0637(97)00016-2.

Monserrat, S., J. L. López-Jurado, and M. Marcos (2008), A mesoscale index to describe the regional circulation around the Balearic Islands, *J. Mar. Syst.*, *71*, 413–420, doi: 10.1016/j.jmarsys.2006.11.012.

Nencioli, F., C. Dong, T. Dickey, L. Washburn, and J. C. McWilliams (2010), A vector geometry-based eddy detection algorithm and its application to a high-resolution numerical model product and high-frequency radar surface velocities in the southern California bight, *J. Atmos. Oceanic Technol.*, *27*, 564–579, doi: 10.1175/2009JTECHO725.1.

Pascual, A., B. B. Nardelli, G. Lanicol, M. Emelianov, and D. Gomis (2002), A case of an intense anticyclonic eddy in the Balearic Sea (western Mediterranean), *J. Geophys. Res.*, *107(C11)*, 3183, doi: 10.1029/2001JC000913.

Pinot, J. M., J. Tintoré, and D. Gomis (1994), Quasi-synoptic mesoscale variability in the Balearic Sea, *Deep Sea Research Part I: Oceanographic Research Papers*, *41 (5-6)*, 897–914, doi: 10.1016/0967-0637(94)90082-5.

Pinot, J. M., J. L. López-Jurado, and M. Riera (2002), The canales experiment (19961998): interannual, seasonal, and mesoscale variability of the circulation in the Balearic Channels, *Prog. Oceanogr.*, *55(3-4)*, 335–370, doi: 10.1016/S0079-6611(02)00139-8.

Rio, M.-H., P.-H. Poulain, A. Pascual, E. Mauri, G. Larnicol, and R. Santoleri (2007), A mean dynamic topography of the mediterranean sea computed from altimetric data, in-situ measurements and a general circulation model, *J. Mar. Syst.*, *65*, 484–508, doi: 10.1016/j.jmarsys.2005.02.006.

Rubio, A., B. Barnier, M. E. G. Jordà, and P. Marsaleix (2009), Origin and dynamics of mesoscale eddies in the Catalan Sea (NWMediterranean): Insight

from a numerical model study, *J. Geophys. Res.*, *114*, C06,009, doi: 10.1029/2007JC004245.

Ruiz, S., A. Pascual, B. Garau, F. Yannice, A. Álvarez, and J. Tintoré (2009), Mesoscale dynamics of the Balearic Front, integrating glider, ship and satellite data, *J. Mar. Syst.*, *78*, S3S16, doi: 10.1016/j.jmarsys.2009.01.007.

Thomson, R. E., E. E. Davis, M. Heesemann, and H. Villinger (2010), Observations of long-duration episodic bottom currents in the Middle America Trench: Evidence for tidally initiated turbidity flow, *J. Geophys. Res.*, *115*, C10,020, doi: 10.1029/2010JC006166.

Tintoré, J., D.-P. Wang, and P. E. L. Violette (1990), Eddies and thermohaline intrusions of the shelf-slope front off Northeast Spain, *J. Geophys. Res.: Oceans*, *95*, 1627–1633, doi: 10.1029/JC095iC02p01627.

Violette, P. E. L., J. Tintoré, and J. Font (1990), The surface circulation of the Balearic Sea, *J. Geophys. Res.*, *95*, 1559–1568, doi: 10.1029/JC095ic02p01559.

Volkov, D. L., G. Larnicol, and J. Dorandeu (2007), Improving the quality of satellite altimetry data over continental shelves, *J. Geophys. Res.*, *112*, C06,020, doi: 10.1029/2006JC003765.

Chapter 3

Environmental factors controlling particulate mass fluxes on the Mallorca continental slope (Western Mediterranean Sea)

Un sutil pensamiento erróneo puede dar lugar a una indagación fructífera que revela verdades de gran valor.

Isaac Asimov (1920-1992)

This chapter has been accepted to be published in *J. Marine Systems*:

- Pasqual, C., A. Amores, M. M. Flexas, S. Monserrat and A. Calafat. Environmental factors controlling particulate mass fluxes on the Mallorca continental slope (Western Mediterranean Sea). Accepted in *J. Marine Systems*, 2014.

Abstract

Settled material recorded by two near bottom sediment traps deployed from November 2009 to February 2011 at northern (Sóller) and southern (Cabrera) slopes of Mallorca Island (Western Mediterranean) is studied with the aim of discerning their possible origin. The total settled particulate mass fluxes (TMF) at Sóller station were found to be, on average, 2.8 times greater than at Cabrera location during the deployment period, although both time series had a similar temporal evolution. It is suggested that wind episodes affecting the entire area were the common forcing, causing a primary production enhancement and being responsible of the similar temporal behavior. The greater sediment amounts collected in Sóller are explained on the basis of two physical

mechanisms: 1) a number of successive eddies generated by instabilities of the Balearic Current that are regularly observed on satellite images, some of which have been reported to reach the seabed, thus increasing near bottom velocities and causing sediment resuspension. And 2) bottom trapped waves that are evidenced from a wavelet analysis in Sóller which could affect the TFM by enhancing sediment resuspension or advecting material from the surrounding areas.

3.1 Introduction

The Balearic Islands, an archipelago located on the Western Mediterranean, are the natural boundary separating the Balearic and the Algerian sub-basins of the Mediterranean Sea (Fig. 3.1). These two sub-basins are connected via the channels between the islands. The northernmost channel, located between Menorca and Mallorca Islands (known as Menorca Channel) is the shallowest (100 m depth) and narrowest (35 km). Between Mallorca and Ibiza Islands, there is the Mallorca channel. This connection is around 80 km width and with a maximum depth of 600 m. The deepest channel ($\backsim$800 m) is the Ibiza channel, located between Ibiza Island and cape La Nao, in the Iberian Peninsula. The continental shelf of the archipelago in the Balearic sea side is relatively narrow (5-20 km) finishing with a steep slope. In the Algerian subbasin side, the width of the shelf is similar but the slope is even steeper, changing in a few km from 500 m to more than 2500 m depth. Further details on the topographic characteristics of the region can be found, for example, in *García et al.* [1994] or *Massutí et al.* [2014].

Two density fronts define the mean currents in the Balearic Sea. The Northern Current (NC) flows southwards from the Gulf of Lyons down to the Ibiza Channel where partially diverts cyclonically joining the Balearic Current (BC), which flows northeastward along the Islands slope (Fig. 1). Depending on the mesoscale situation, the flow between the channels presents different configurations, with most of the NC leaving the Balearic sub-basin through the Ibiza Channel or being reflected and becoming part of the BC [*Pinot et al.*, 2002]. On the contrary, the part of the Algerian subbasin affecting the Balearic Islands does not have a clear current pattern and its hydrodynamics is completely dominated by mesoscale processes such as eddies.

Two different processes mainly contribute to the presence of particles in the water column in the studied area: the primary production (PP) and the resuspended material from the seabed.

PP takes place in the uppermost layers of the ocean, where light and nutrients are available for primary producers to transform CO_2 into organic carbon. The limiting factors to PP are the nutrients availability such as N, Si, P and Fe. Surface chlorophyll concentrations obtained from ocean color satellite-derived mea-

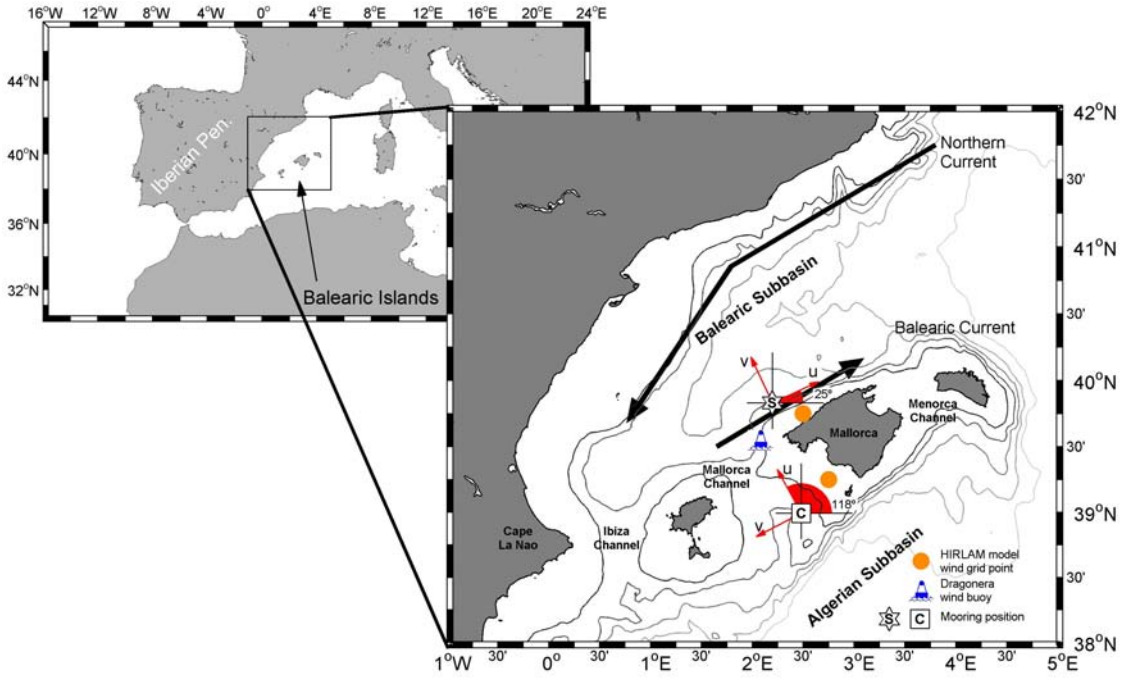

Figure 3.1: Map of the zone of interest. Black arrows show the permanent currents of the zone. Sóller and Cabrera moorings are marked with an S surrounded by a star and with a C surrounded by a square. The decomposition in along- and across-slope components is indicated on the mooring position. The position of the Dragonera wind buoy is shown by a blue buoy. Orange dots mark the location of the HIRLAM model wind points used. Isobaths are plotted between 500 m and 2500 m with a step of 500 m.

surements (Chl-a) is considered a quantification of phytoplankton biomass and becomes an indicator of the photosynthetic fixation of C [*Falkowski et al.*, 2000]. The process by which the particulate organic carbon is removed from the euphotic zone and transported to the oceanic interiors is known as the biological pump. This process operates ubiquitously in the pelagic ocean [*Honjo et al.*, 2008] and is driven by bio-physical processes that enhance the particle production and settling into the water column.

In the classic work by *Gage and Tyler* [1991], it was considered that deep ecosystems were generally food-limited ecosystems, where the main entrance of organic matter corresponded to the contributions from the photic zone of the water column. However, in recent years different studies [*Danovaro et al.*, 2001; *Pusceddu et al.*, 2010] have shown that certain parts of the deep basins operate as zones of accumulation of organic matter due to their hydrodynamic, climate or physiographic conditions [*Lopez-Fernandez et al.*, 2013]. Among the various proposed mechanisms that would generate resuspension of sediments of the continental slope and the deep basin in the NW Mediterranean Sea are: in-

teraction between geostrophic currents and bathymetry [*Puig et al.*, 2001], the open-sea convection [*Martín et al.*, 2010; *Stabholz et al.*, 2013], cascading of dense shelf waters [*Canals et al.*, 2006; *Pasqual et al.*, 2010] and coastal severe storms [*Sanchez-Vidal et al.*, 2012]. These events play an important role in the oceanic carbon cycle and in the maintenance of the nektobenthic deep communities, as for example in the reproductive and recruitment processes of crustacean decapods [*Company et al.*, 2003] and mitigating the general trend of overfishing [*Company et al.*, 2008].

One main feature that distinguishes the Balearic Islands is the absence of fluvial contributions and geomorphologic structures such as submarine canyons. The lack of these characteristics hinders the particle transference from the upper near coast layers to the deeper interior-basin layers, having as a result an oligotrophic environment.

The aim of this work is to identify the environmental factors that take part in the particle fluxes in the Balearic Islands deep slope through the data recorded from two mooring lines each one located in an area of fishing interest [*Massutí et al.*, 2014]. The isolation from strong lateral continental sediment sources (i.e., river inputs and submarine canyons) allows delimiting the role of atmospheric factors and local dynamics on the particle flux settling. This will be assessed by performing an analysis of the environmental factors and by studying their relation with settled mass particles recovered from sediment traps during more than one year.

The paper is structured as follows: the methodology and the data sets used are described in section 3.2. In section 3.3 some hypothesis are raised about the origin of the measured sediment fluxes as deduced from their variability and composition. Ecological implications are indicated in section 3.4 and some conclusions are presented in the last section.

3.2 Data Sets and Methodology

Two mooring lines were deployed over the northern and southern slopes of Mallorca Island (Fig. 3.1). One mooring was located at the gentle part of continental slope at the Balearic sub-basin (Sóller station, 39° 49.682 N − 02° 12.778 E) and the second one was placed in the eastern side of the Central Depression [*Acosta et al.*, 2003], between the Cabrera Island and the Emile Baudot seamount (Cabrera station, 38° 59.484' N − 02° 28.907' E).

Both lines, deployed at a depth around 900 m, were structurally identical, with 600 m height over the seafloor. They had 4 SeaBird 37 CTD (300 m, 500 m, 700 m and 900 m depth), 2 current meters Nortek Aquadopp (500 m and 900 m) and a PPS3 Technicap sequential sampling sediment trap (12 collecting cups, 0.125

m^2 opening and 2.5 height/diameter aspect ratio for the cylindrical part) located at 30 m above the bottom, paired with one of the Nortek Aquadopp current meter and a SeaBird 37 CTD. A complete description of the hydrodynamic data recorded may be found in *Amores and Monserrat* [2014].

The mooring lines were continuously recording data from mid-November 2009 to mid-February 2011. During this time, the instruments operated correctly, although the sediment trap records presented some gaps. Data gaps in March 2010 (10/3 to 18/3) were due to mooring maintenances; the longer gaps from 5th July to 21th September 2010 were due to ship availability. Data gap at Cabrera during the second sampling period (18th March to 5th July 2010) was due to the malfunctioning of the sediment trap.

Original sampling rates were 10 minutes for the CTD, 30 minutes for the current meters and 4 to 11 days for the sediment traps. All variables were resampled to the sediment trap time interval for the sake of comparison. To do so, the average was computed as the mean value during the time that each sediment trap cup was open. For a sediment trap sampling rate of 10 days, for instance, a total of 480 current meter points were used for each resampled point.

Some magnitudes derived from the hydrodynamic data, namely kinetic energy and buoyancy, are used throughout this manuscript. Kinetic Energy per unit mass (KE) has been computed at both locations as:

$$KE = \frac{1}{2} \cdot (u^2 + v^2) \tag{3.1}$$

where u and v are the longitudinal and latitudinal components of the currents. Along- (uKE) and across-slope (vKE) components were also computed. The angles for this decomposition, taken from east and counterclockwise, were 25° for Sóller and 118° for Cabrera (Fig. 3.1).

An estimation of the Brunt-Väisälä (buoyancy) frequency, N, was obtained from the 500 m and 900 m depth Sea Bird 37 CTDs as:

$$N = \sqrt{-\frac{g}{\rho} \cdot \frac{\Delta\rho}{\Delta z}} \tag{3.2}$$

where g is gravity acceleration, ρ is potential density and z is depth.

Sediment trap samples were wet-sieved through a 1 mm nylon mesh in order to retain the largest organisms. Swimmers smaller than 1 mm were manually removed under a dissecting microscope using fine tweezers. Finally, the samples were freeze-dried and weighted to calculate the Total Mass Flux (TMF). Total and organic carbon, contents were measured using an elemental analyzer (EA Flash series 1112 and NA 2100). Samples for organic carbon analysis were first decarbonatated using repeated additions of 100 μl 25% HCl with 60° C drying

steps in between until no effervescence occurred. Organic matter (OM) content has been estimated as twice the total organic carbon content, and carbonate content was calculated assuming all inorganic carbon is contained within the calcium carbonate ($CaCO_3$) fraction, thus using the molecular mass ratio 100/12. Biogenic Si was analyzed using a two-step extraction with 0.5MNa2 CO_3 (2.5 h each) separated after filtration of the leachate. Inductive Coupled Plasma Atomic Emission Spectroscopy (ICP-AES) was used to analyze Si and Al contents in both leachates, and a correction of the Si of the first by the Si/Al relation of the second one was applied to obtain the opaline Si concentration [*Fabres et al.*, 2002]. Corrected Si concentrations were transformed to opal after multiplying by a factor of 2.4 [*Mortlock and Froelich*, 1989]. Analytical precision of opal measurements was 4.5%. The lithogenic fraction was calculated assuming % lithogenic = 100 - (% OM + % $CaCO_3$ + % opal). Analyses of chlorophyll-a (Chl-a) and phaeopigments (Phaeo) were carried out according to *Pusceddu et al.* [1999]. Phytopigments were calculated as the sum of the Chl-a and phaeopigments [*Pusceddu et al.*, 2010]. As some analyses were carried out when small amount of sediments remained, the time series present some additional gaps when the material was not enough for the estimation. This was the case of phytopigments, for example.

Sediment fluxes were compared with some atmospheric variables. Near surface hourly wind speeds (10 m-height) for each area were obtained from the closest points to the mooring positions in HIRLAM model, provided by the Spanish meteorology agency (AEMET) (orange points in Fig. 3.1). This numerical model is a mesoscalar, hydrostatic model with a mean spatial resolution of 15 km. Although there is a wind buoy in the area, the Direccional Met-Oce Dragonera Buoy (blue buoy in Fig. 3.1), located at 2.10°E − 39.56°N (Red Exterior de Boyas (REDEXT), of Puertos del Estado, Ministerio de Fomento, Spanish Government) we decided to use the model data because the buoy time series had some long gaps. However, we visually compared the model outputs with the buoy data and no significant differences were detected.

Chl-a concentration data for the mooring locations were computed from satellite data obtained from Giovanni Ocean Color Radiometry 8-day Data Product Visualization web site (http://disc.sci.gsfc.nasa.gov/giovanni# maincontent).

3.3 On the origin of the measured sediment fluxes

The Total Mass Fluxes (TMF) measured in Sóller and in Cabrera are shown in Fig. 3.2. Both records oscillate in a similar way, with two main common peaks highlighted by grey bands (grey band #1, between February-March 2010 and grey band #2, between November 2010 January 2011). This similar behavior

was suggestive of a common general forcing acting at both sites. Provided that both sites are located in different hydrographic environments [*Amores and Monserrat*, 2014], it seemed likely that the common forcing was of atmospheric origin. Modeled wind (Fig. 3.2c) showed a very similar behavior at both zones, with two peaks coinciding with the TFM peaks indicated above. The reason is that wind episodes create turbulence and mixing of the upper layers that in turn lead to an enhancement of primary production (see for example *Simpson and Sharples* [2012]). This mechanism was supported by the Chl-a time series (Fig. 3.2d), which showed two peaks very well correlated with the wind (a correlation factor of 0.68 in Cabrera and 0.69 in Sóller) and also coinciding with the TFM peaks. Wind forcing also enhanced the arrival of pelagic material to the deep benthic ecosystems of Sóller and Cabrera stations. The main source of organic matter to the nektobenthic communities is produced by phytoplankton photosynthetic processes (in form of Chl-a produced at surface waters and quickly degrating). A measure of pelagic components in settling particles is the phytopigments flux, being the phytopigment concentration an indicative of inputs of fresh marine organic matter [*Lee et al.*, 2004]. The correspondence of peaks in Chl-a concentration (Fig. 2d) with increases in phytopigments fluxes (Fig. 3.2e) indicated the possible pelagic nature of the particle flux input during February-March 2010 and December 2010 in both locations.

Besides wind forcing, other mechanisms have also been explored. For example, from mid-January to late-February 2010 (first grey band) a frontal structure was identified at the north of Mallorca producing some changes in the stationary Balearic Current. For several weeks the Balearic current hit perpendicularly to the coast of Mallorca and a fluorescence relative maximum was observed in coincidence with the location of the maximum upward velocities [*Balbín et al.*, 2012]. It is know that frontal dynamics increase PP due to the injection of nutrients to euphotic layers and become particularly important in the oligotrophic waters of the Western Mediterranean [*Estrada and Salat*, 1989; *Raimbault et al.*, 1993]. This suggests that vertical velocities could enhance phytoplankton production in the frontal area. Therefore, part of the increase in phytopigments (which are indicative of fresh phytoplanktonic organic matter) detected at Sóller station during February March 2010 could be also the result of the frontal structure affecting the area. There are evidences that this frontal structure could have been affecting the Sóller area since late autumn 2009 [*Balbín et al.*, 2012] so this mechanism could also be the responsible for the large amount of TFM observed in Sóller in November - December 2009 which seems not to be related to any wind increase in the area.

Despite their similar temporal variability, the TFM values recorded in Sóller are much larger than in Cabrera, being, on average, 2.8 times greater. The differences were almost entirely due to the lithogenic fraction as the amounts of

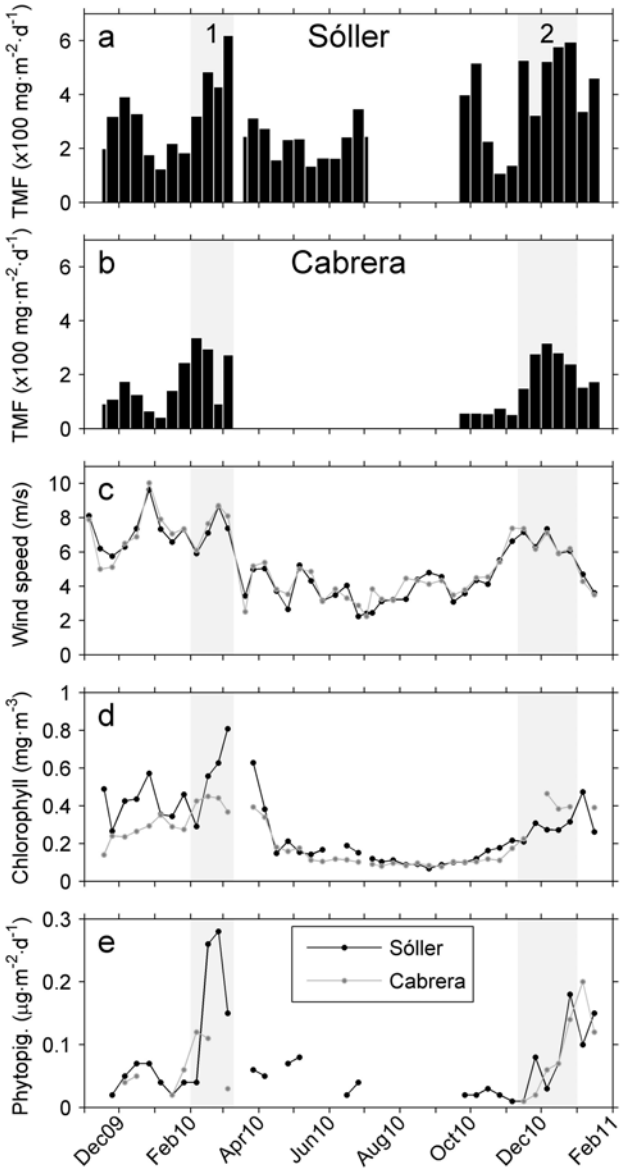

Figure 3.2: TMF recorded by the sediment trap at Sóller a), TMF collected by the trap at Cabrera b), Wind speed time series from the positions marked as orange dots in Fig. 3.1 c), Chl-a time series from satellite observations d) and Phytopigments recorded by the sediment traps e). Grey bands correspond to two selected intervals when large amounts of TFM were recorded.

biogenic components were similar at both sites. A comparison between lithogenic and biogenic matter (OM) fractions measured in Sóller and Cabrera is presented in Fig. 3.3. We have selected OM as a representative of the biogenic component

but results are similar when comparing other indicators as the biogenic-Si for instance.

The differences between lithogenic and OM fractions result from the different hydrodynamic scenarios in each zone: the mooring at Sóller, being located in the middle of a steady current, the Balearic Current; whereas the Cabrera line was in the Mallorca Channel where there is not a clear and steady current path. These differences imply that currents are generally much larger in Sóller than in Cabrera in the whole water column and in particular close to the seabed. Kinetic energy per unit mass (KE) derived from the current meters deployed at 500 and 900m were significantly larger in Sóller than in Cabrera (Fig. 3.3): KE from 500m and 900m depth were 3.7 and 6.5 times greater, respectively, in Sóller than in Cabrera. More details supporting the greater hydrodynamic activity of Sóller as compared with Cabrera can be found in *Amores and Monserrat* [2014].

In addition to these generally larger near bottom velocities, a number of eddies have been reported in Sóller during the deployment time of the sediment traps, some of them reaching down to the bottom and probably causing sediment resuspensions [*Amores and Monserrat*, 2014; *Amores et al.*, 2013a]. A clear across-slope kinetic energy increase (vKE) is observed at 900 m in Sóller, coinciding with the two episodes marked with grey bands (Fig. 3d) and suggesting that an additional mechanism related to large across-slope near bottom velocities could be responsible for the major peaks of lithogenic sediments found in Sóller TFM.

As mentioned above, from mid-January to late-February 2010 (first grey band) a frontal structure was identified at the north of Mallorca producing some changes in the stationary Balearic Current which for several weeks hit perpendicularly to the coast of Mallorca [*Balbín et al.*, 2012]. The increase of lithogenic flux coinciding with this first episode was likely related to this frontal structure and the presence of an associated eddy that clearly reached 500m and had a noticeable footprint at 900m [*Amores and Monserrat*, 2014].

On November 2010 (second grey band) the Balearic current hit again perpendicularly to the coast, forming a persistent and particularly energetic anticyclonic eddy that dissipated in late December [*Amores et al.*, 2013a]. The Sóller mooring station was located under the edge of the eddy during that period and the hydrodynamic properties, large values of uKE and vKE at both 500 and 900 m (Fig. 3.3c and d), indicated that this structure reached down to the bottom (900 m) generating a downslope current associated with the presence of the eddy. *Amores et al.* [2013a] reported that during this event, near-bottom currents reached up to 26 $cm \cdot s^{-1}$, velocities large enough to resuspend bottom sediments and increase the lithogenic material collected by the sediment trap [*Wainright*, 1990]. Several works on the impact of mesoscale activity on the deep sea carrying upper ocean material or resuspending bottom sediments support this hypothesis [*Fabres et al.*,

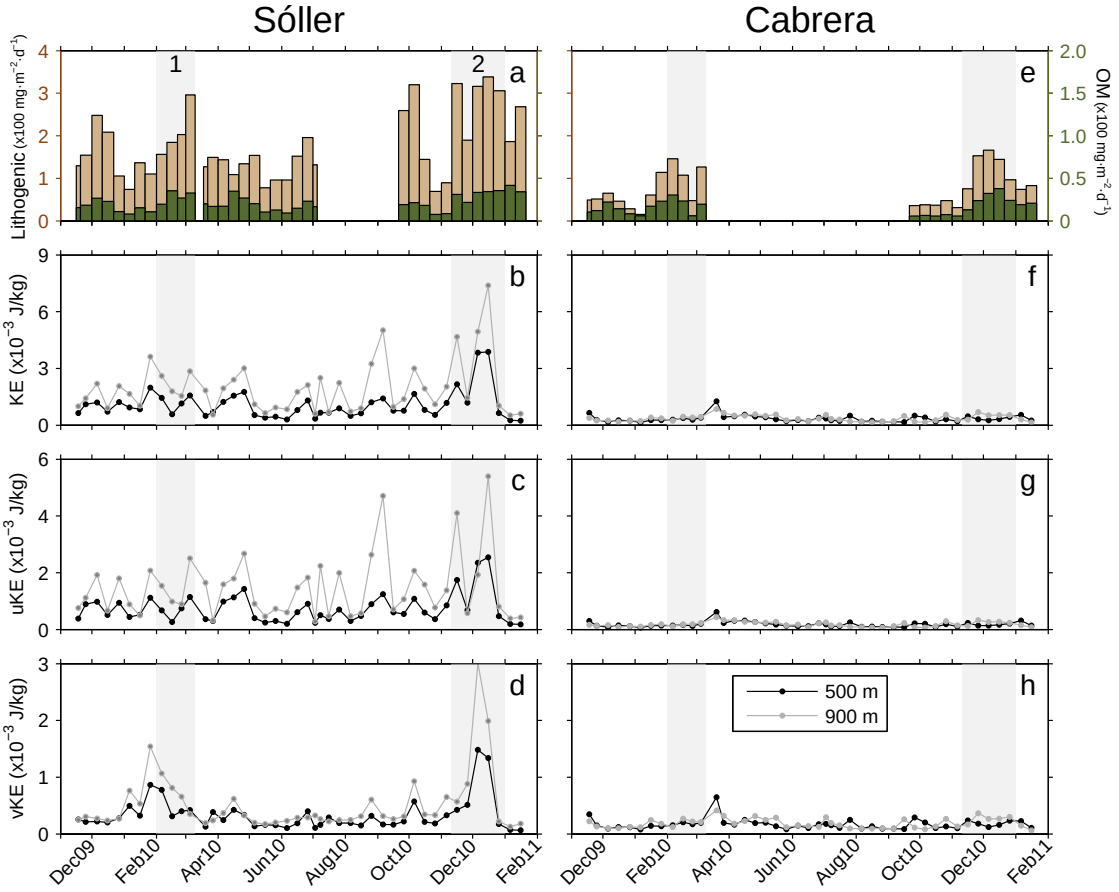

Figure 3.3: The lithogenic fraction (brown) and the organic matter (OM) fraction (green) recorded in Sóller a), the total kinetic energy (KE) computed for the current meters from 500 m (black line) and 900 m (grey line) b) and the along-slope KE (uKE) c) and across-slope KE (vKE) d) measured in Sóller. Panels e), f) g) and h) show the same magnitudes but as measured in Cabrera

2002; *Martín et al.*, 2010; *OBrien et al.*, 2013].

Besides these two major TFM peaks indicated with grey bands, other recurrent TFM increases were detected and easily associated with KE peaks at Sóller site (Fig. 3.3). For example, a mass flux maximum during early October (11/10/10) recorded 516.9 $mg \cdot m^{-2} \cdot d^{-1}$ and was associated with increases in both uKE and vKE at 500 and 900 m, with dominance of the along-slope component. During these energetic episodes, near-bottom currents (900 m) present a relative increase of their magnitude with respect to the mid-depth currents (500 m). This fact, together with the dominance of the along-slope component of KE over the across-slope component, suggested that KE increases could be the result

of intensifications of the along-slope current component (the Balearic Current) that could be in turn related to bottom-trapped topographic waves propagating along the Island's northern slope. Current speed wavelet at 900 m showed a wide mesoscale band at 5-30 days, with continuous structure at 6, 12, 15 and 30 days periods (Fig. 3.4). The clockwise and counter-clockwise wavelets at 900 m (not shown) indicated that the mesoscale peaks were present in both directions with a weak preference for the clockwise rotation.

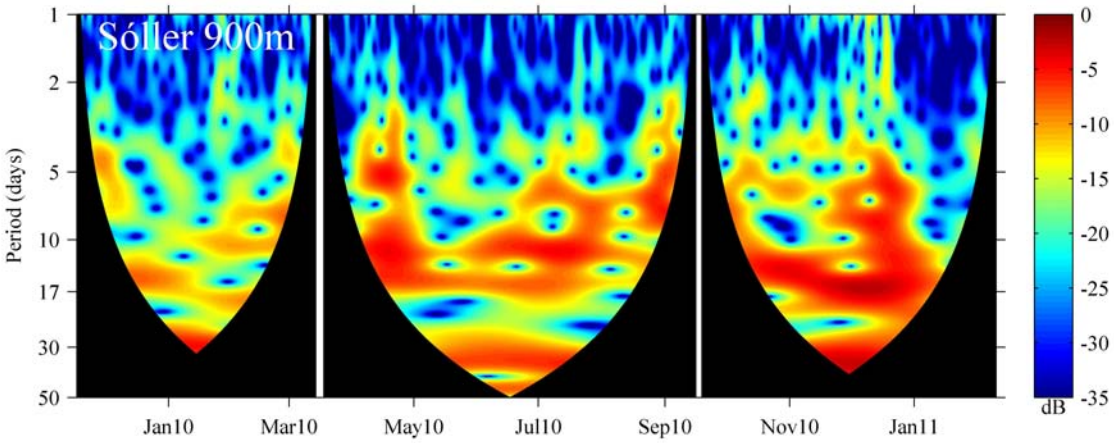

Figure 3.4: Velocity wavelets from the 900 m depth current meter at Sóller. The mother function is Morlet.

With the aim of explaining these energy periods in currents, the frequency of topographic Rossby waves was explored. The frequency range for topographic Rossby waves is given by:

$$\omega = \beta \cdot N \cdot \sin\theta \cdot \coth \frac{k \cdot N \cdot H}{f} \tag{3.3}$$

where β is the topographic slope, N is the BruntVäisälä frequency, θ is the wave propagation direction with respect to the slope, k is the wavenumber, H is the mean depth and f the Coriolis parameter [*Pedlosky*, 1979]. Waves with lower frequency than $\omega = \beta \cdot N$, which is the high frequency limit of Eq. 3.3, are bottom-trapped.

The average slope around the Sóller site is $\beta = 0.031 - 0.045$ and the buoyancy frequency range in the last 100 m of the water column is $N = 2.1 - 4.7 \cdot 10^{-4} s^{-1}$. Therefore, the threshold period ranges between 3.4 and 11.2 days, which means that the bottom-intensified current fluctuations of 12, 15 and 30 days period may correspond to propagating bottom-trapped topographic waves. The 6-day period fluctuations are more uncertain because they appear on either side of the high frequency limit. Previous works in the NW Mediterranean have reported bottom

topographic waves of 8-day [*Millot*, 1985], 2.5-day [*Sammari et al.*, 1995], and 7-day [*Flexas et al.*, 2002] period.

3.4 Ecological Implications

Massutí et al. [2014] indicates that the coupling between the pelagic and benthic domains in the Balearic Islands is relatively more important than in other areas of the western Mediterranean, such as along the coasts of the mainland, in which the continental contributions determine the hydrological and sedimentological dynamics and act as drivers of biological productivity in the deep water ecosystems. As a consequence of the general circulation of the Balearic Basin, the slope communities at the north of the Archipelago (i.e. Sóller station) receive a greater influence from the processes that take place on the continental margin of the Iberian Peninsula and Gulf of Lions. On the contrary, south of the Archipelago, (i.e. Cabrera) the pelagic system plays a more relevant role as a trophic resource for the species of the benthic slope ecosystems. Our results are in accordance with *Massutí et al.* [2014] hypothesis for Cabrera station. In Cabrera, TMF are mainly triggered by wind episodes that enhance primary production and thus the settling of pelagic sediment.

In contrast, in Sóller, besides the main wind forcing common at both sites, TMF are also influenced by the mesoscale variability of the Balearic current and bottom-trapped waves that enhance resuspension of material, potentially affecting the deep benthic ecosystem. Therefore, even though the northern Mallorca slope (Sóller) does not have geomorphologic structures such as submarine canyons that enhance the transference of continental shelf material [*Acosta et al.*, 2003], it is affected by bottom-intensified currents that can resuspend material and affect deep-ecosystem benthic populations as it is described in *Amores et al.* [2013b]. They reported a good agreement between the surface vorticity of the surrounding area and the *Aristeus antennatus* adult individual catches, showing that surface vorticity, related to the presence of eddies, would affect *Aristeus antennatus* by causing sediment resuspensions when these eddies are persistent and energetic enough to reach down to the seabed.

3.5 Summary and Conclusions

In this work, temporal evolution of TFM at two sites around Mallorca Island has been analyzed and different possible generating mechanisms have been explored.

Wind forcing was identified as a common factor governing the behavior at both sites due to an enhancement of PP, also observed in the chlorophyll, phytopigments and OM time series. The TFM at Sóller was found to be significantly

greater than the TFM at Cabrera. The fact that Sóller sediment trap was in the middle of the steady Balearic Current, with higher velocities than Cabrera area could partially explain this difference. Moreover, Sóller slope is affected by anticyclonic eddies and bottom-trapped topographic waves that could induce bottom sediments resuspension (as the eddy described in *Amores et al.* [2013a]) increasing total mass fluxes at 900 m water depth and affecting to the benthonic species [*Amores et al.*, 2013b].

This work points out the importance of multidisciplinary studies in order to correctly describe the interaction between physical, biological and geological factors that potentially control deep ecosystems.

Acknowledgments

We thank the chief scientists, participants and crews of R/V Sarmiento de Gamboa, R/V Odón de Buen and F/V Punta des Vent for their help and dedication during sample collection. We also thank Pilar López-Fernández, Monserrat Guart and Antonio Pusceddu for their help in sample processing at Universitat de Barcelona and Università Politecnica delle Marche (Ancona, Italy) and Marta Marcos (IMEDEA) for her valuable comments. This research has been supported by IDEADOS project (CMT2008-04489-C03-03). The work of A. Amores was funded by a JAE-PreDoc grant from Consejo Superior de Investigaciones Científicas (CSIC) and cofunded by Programa Operativo FSE 20072013. A. C. was also supported by GRACCIE (CSD2007-00067, Consolider-Ingenio Program) research projects, a Generalitat de Catalunya Grups de Recerca Consolidats grant (2009 SGR-1305).

Bibliography

Acosta, J., M. Canals, J. López-Martínez, A. Muñoz, P. Herranz, R. Urgeles, C. Palomo, and J. L. Casamor (2003), The Balearic Promontory geomorphology (western Mediterranean): morphostructure and active processes, *Geomorphology*, *49*(34), 177 – 204, doi: 10.1016/S0169-555X(02)00168-X.

Amores, A., and S. Monserrat (2014), **Hydrodynamic comparison between the north and south of Mallorca Island**, *J. Marine Systems*, doi: 10.1016/j.jmarsys.2014.01.005.

Amores, A., S. Monserrat, and M. Marcos (2013a), **Vertical structure and temporal evolution of an anticyclonic eddy in the Balearic Sea (western Mediterranean)**, *J. Geophys. Res. Oceans*, *118*, 2097–2106, doi: 10.1002/jgrc.20150.

Amores, A., L. Rueda, S. Monserrat, B. Guijarro, C. Pasqual, and E. Massutí (2013b), **Influence of the hydrodynamic conditions on the accessibility of Aristeus antennatus and other demersal species to the deep water trawl fishery off the Balearic Islands (western Mediterranean)**, *J. Marine Systems*, doi: 10.1016/j.jmarsys.2013.11.014.

Balbín, R., M. M. Flexas, J. L. López-Jurado, M. Peña, A. Amores, and F. Alemany (2012), **Vertical velocities and biological consequences at a front detected at the Balearic Sea**, *Cont. Shelf Res.*, *47*, 28–41, doi: 10.1016/j.csr.2012.06.008.

Canals, M., P. Puig, X. D. de Madron, S. Heussner, A. Palanques, and J. Fabres (2006), Flushing submarine canyons, *Nature*, *444 (7117)*, 354–357, doi: 10.1038/nature05271.

Company, J. B., F. Sardà, P. Puig, J. E. Cartes, and A. Palanques (2003), Duration and timing of reproduction in decapod crustaceans of the NW Mediterranean continental margin: is there a general pattern?, *Marine Ecology Progress Series*, *261*, 201–216.

Company, J. B., P. Puig, F. Sardà, A. Palanques, M. Latasa, and R. Scharek (2008), Climate influence on deep sea populations, *PLoS ONE*, *3*, e1431, doi: 10.1371/journal.pone.0001431.

Danovaro, R., A. Dell'Anno, M. Fabiano, A. Pusceddu, and A. Tselepides (2001), Deep-sea ecosystem response to climate changes: the eastern Mediterranean case study, *Trends in Ecology & Evolution*, *16*(9), 505 – 510, doi: 10.1016/S0169-5347(01)02215-7.

Estrada, M., and J. Salat (1989), Phytoplankton assemblages of deep and surface water layers in a Mediterranean frontal zone, *Scientia Marina*, *53 (2-3)*, 203–214.

Fabres, J., A. Calafat, A. Sanchez-Vidal, M. Canals, and S. Heussner (2002), Composition and spatio-temporal variability of particle fluxes in the Western Alboran Gyre, Mediterranean Sea, *Journal of Marine Systems*, *33-34*, 431–456, doi: 10.1016/S0924-7963(02)00070-2.

Falkowski, P., R. J. Scholes, E. Boyle, J. Canadell, D. Canfield, J. Elser, N. Gruber, K. Hibbard, P. Högberg, S. Linder, F. T. Mackenzie, B. I. Moore, T. Pedersen, Y. Rosenthal, S. Seitzinger, V. Smetacek, and W. Steffen (2000), The global carbon cycle: a test of our knowledge of earth as a system, *Science*, *290*, 291–6.

Flexas, M., X. D. de Madron, M. A. Garcia, M. Canals, and P. Arnau (2002), Flow variability in the Gulf of Lions during the MATER HFF experiment (MarchMay 1997), *Journal of Marine Systems*, *33-34*, 197–214, doi: 10.1016/S0924-7963(02)00059-3.

Gage, J. D., and P. A. Tyler (1991), *Deep-Sea Biology: A Natural History of Organisms at the Deep-Sea Floor*, p. 504, Cambridge University Press, London.

García, E., J. Tintoré, J. M. Pinot, J. Font, and M. Manriquez (1994), Surface Circulation and Dynamics of the Balearic Sea, *Coastal Estuarine Stud.*, *46*, 73–91, doi: 10.1029/CE046p0073.

Honjo, S., S. J. Manganini, R. A. Krishfield, and R. Francois (2008), Particulate organic carbon fluxes to the ocean interior and factors controlling the biological pump: A synthesis of global sediment trap programs since 1983, *Progress in Oceanography*, *76*, 217–285, doi: 10.1016/j.pocean.2007.11.003.

Lee, C., S. Wakeham, and C. Arnosti (2004), Particulate Organic Matter in the Sea: The Composition Conundrum, *AMBIO: A Journal of the Human Environment*, *33*, 565–575, doi: 10.1579/0044-7447-33.8.565.

Lopez-Fernandez, P., S. Bianchelli, A. Pusceddu, A. Calafat, R. Danovaro, and M. Canals (2013), Bioavailable compounds in sinking particulate organic matter, Blanes Canyon, NW Mediterranean Sea: Effects of a large storm and sea surface biological processes, *Progress in Oceanography*, *118*(0), 108 – 121, doi: 10.1016/j.pocean.2013.07.022.

Martín, J., J.-C. Miquel, and A. Khripounoff (2010), Impact of open sea deep convection on sediment remobilization in the western Mediterranean, *Geophysical Research Letters*, *37*, 13,60413,610, doi: 10.1029/2010GL043704.

Massutí, E., M. Olivar, S. Monserrat, L. Rueda, and P. Oliver (2014), Towards understanding the influence of environmental conditions on demersal resources and ecosystems in the western Mediterranean: Motivations, aims and methods of the IDEADOS project, *Journal of Marine Systems*, doi: 10.1016/j.jmarsys.2014.01.013.

Millot, C. (1985), Evidence of a several-day propagating wave, *Journal of Physical Oceanography*, *15*, 258–272.

Mortlock, R. A., and P. N. Froelich (1989), A simple method for the rapid determination of biogenic opal in pelagic marine sediments, *Deep Sea Research Part A. Oceanographic Research Papers*, *36*(9), 1415 – 1426, doi: 10.1016/0198-0149(89)90092-7.

OBrien, M. C., H. Melling, T. F. Pedersen, and R. W. Macdonald (2013), The role of eddies on particle flux in the Canada Basin of the Arctic Ocean, *Deep Sea Research Part I: Oceanographic Research Papers*, *71*, 1–20, doi: 10.1016/j.dsr.2012.10.004.

Pasqual, C., A. Sanchez-Vidal, D. Zúñiga, A. Calafat, M. Canals, X. D. de Madron, P. Puig, S. Heussner, A. Palanques, and N. Delsaut (2010), Flux and composition of settling particles across the continental margin of the Gulf of Lion: the role of dense shelf water cascading, *Biogeosciences*, *7*, 217–231, doi: 10.5194/bg-7-217-2010.

Pedlosky, J. (1979), *Geophysical fluid dynamics*, Springer-Verlag, New York and Berlin, pp. 624.

Pinot, J. M., J. L. López-Jurado, and M. Riera (2002), The canales experiment (19961998): interannual, seasonal, and mesoscale variability of the circulation in the Balearic Channels, *Prog. Oceanogr.*, *55(3-4)*, 335–370, doi: 10.1016/S0079-6611(02)00139-8.

Puig, P., J. B. Company, F. Sardà, and A. Palanques (2001), Responses of deep-water shrimp populations to intermediate nepheloid layer detachments on the Northwestern Mediterranean continental margin, *Deep Sea Research Part I: Oceanographic Research Papers*, *48*, 21952207, doi: 10.1016/S0967-0637(01)00016-4.

Pusceddu, A., G. Sarà, M. Armeni, M. Fabiano, and A. Mazzola (1999), Seasonal and spatial changes in the sediment organic matter of a semi-enclosed marine system (W-Mediterranean Sea), *Hydrobiologia*, *397*, 59–70, doi: 10.1023/A:1003690313842.

Pusceddu, A., S. Bianchelli, M. Canals, A. Sanchez-Vidal, X. D. D. Madron, S. Heussner, V. Lykousis, H. de Stigter, F. Trincardi, and R. Danovaro (2010), Organic matter in sediments of canyons and open slopes of the Portuguese, Catalan, Southern Adriatic and Cretan Sea margins, *Deep Sea Research Part I: Oceanographic Research Papers*, *57*(3), 441 – 457, doi: 10.1016/j.dsr.2009.11.008.

Raimbault, P., B. Coste, M. Boulhadid, and B. Boudjellal (1993), Origin of high phytoplankton concentration in deep chlorophyll maximum (DCM) in a frontal region of the Southwestern Mediterranean Sea (algerian current), *Deep Sea Research Part I: Oceanographic Research Papers*, *40 (4)*, 791–804, doi: 10.1016/0967-0637(93)90072-B.

Sammari, C., C. Millot, and L. Prieur (1995), Aspects of the seasonal and mesoscale variabilities of the Northern Current in the western Mediterranean Sea inferred from the PROLIG-2 and PROS-6 experiments, *Deep Sea Research Part I: Oceanographic Research Papers*, *42 (6)*, 893–917, doi: 10.1016/0967-0637(95)00031-Z.

Sanchez-Vidal, A., M. Canals, A. Calafat, G. Lastras, R. Pedrosa-Pàmies, M. Menéndez, R. Medina, J. B. Company, B. Hereu, J. Romero, and T. Alcoverro (2012), Impacts on the Deep-Sea Ecosystem by a Severe Coastal Storm, *PLoS ONE 7(1)*, *e30395*, doi: 10.1371/journal.pone.0030395.

Simpson, J. H., and J. Sharples (2012), *Introduction to the Physical and Biological Oceanography of Shelf Seas*, p. 424, Cambridge University Press, U.K.

Stabholz, M., X. D. D. Madron, M. Canals, A. Khripounoff, I. Taupier-Letage, P. Testor, S. Heussner, P. Kerhervé, N. Delsaut, L. Houpert, G. Lastras, and B. Dennielou (2013), Impact of open-ocean convection on particle fluxes and sediment dynamics in the deep margin of the Gulf of Lions, *Biogeosciences*, *10*(2), 1097–1116, doi: 10.5194/bg-10-1097-2013.

Wainright, S. C. (1990), Sediment-to-water fluxes of particulate material and microbes by resuspension and their contribution to the planktonic food web, *Marine ecology progress series*, *62 (3)*, 271–281.

Chapter 4

Influence of the hydrodynamic conditions on the accessibility of the demersal species to the deep water trawl fishery off the Balearic Islands (western Mediterranean)

La ignorancia afirma o niega rotundamente; la ciencia duda.

Voltaire (1694-1778)

This chapter has been published in:

- Amores, A., L. Rueda, S. Monserrat, B. Guijarro, C. Pasqual, and E. Massutí. Influence of the hydrodynamic conditions on the accessibility of Aristeus antennatus and other demersal species to the deep water trawl fishery off the Balearic Islands (western Mediterranean). *J. Marine Systems*, 2013b. doi: 10.1016/ j.jmarsys.2013.11.014.

Abstract

Monthly catches per unit of effort (CPUE) of adult red shrimp (*Aristeus antennatus*), reported in the deep water bottom trawl fishery developed on the Sóller fishing ground off northern Mallorca (Western Mediterranean), and the mean ocean surface vorticity in the surrounding areas are compared between 2000 and 2010. A good correlation is found between the rises in the surrounding surface vorticity and the drops in the CPUE

of the adult red shrimp. This correlation could be explained by assuming that most of the surface vorticity episodes could reach the bottom, increasing the seabed velocities and producing sediment resuspension, which could affect the near bottom water turbidity. *A. antennatus* would respond to this increased turbidity disappearing from the fishing grounds, probably moving downwards to the deeper waters. This massive displacement of red shrimp specimens away from the fishing grounds would consequently decrease their accessibility to fishing exploitation. Similar although more intense responses have been observed during the downslope shelf dense water current episodes that occurred in a submarine canyon, northeast of the Iberian peninsula. The proposed mechanism suggesting how the surface vorticity observed can affect the bottom sediments is investigated using a year-long moored near-bottom current meter and a sediment trap moored near the fishing grounds. The relationship between vorticity and catches is also explored for fish species (*Galeus melastomus*, *Micromesistius poutassou*, *Phycis blennoides*) and other crustacean (*Geryon longipes* and *Nephrops norvegicus*), considered as by-catch of the deep water fishery in the area. Results appear to support the suggestion that the water turbidity generated by the vorticity episodes is significant enough to affect the dynamics of the demersal species.

4.1 Introduction

The decapod crustacean red shrimp, *Aristeus antennatus* (Risso, 1816), a demersal species distributed throughout the Mediterranean and the north-eastern Atlantic, from Portugal to the Cabo Verde Islands [*Arrobas and Ribeiro-Cascalho*, 1987], mainly occurs in the muddy bottoms of the slope, between 400 and at least 3300 m [*Sardà et al.*, 2004]. This species is one of the most valuable deep-water fishing resources in the western and central basins of the Mediterranean, remaining at a low level of exploitation in the eastern basin [*Papaconstantinou and Kapiris*, 2001] and revealing important bathymetric migrations [*Relini et al.*, 2000]. However, despite its wide bathymetric distribution, it is mainly exploited between 400 and 800 m depth, and is the target species of the well-developed deep water bottom trawl fishery on the western basin slope [*Sardà et al.*, 2003].

The trawl fleet operating off the Balearic Islands (western Mediterranean) is characterized by its versatility, which is determined by the specific dynamics of the resources, among other factors (e.g. sea conditions and fish market). Bottom trawlers not only target different species, they also change the fishing location at a given time of the year, as well as the fishing tactics during the same fishing trip. *Palmer et al.* [2009] defined four fishing tactics in this fishery, related to the exploitation of different bathymetric strata and target species.

The annual catches of the red shrimp in the Balearic Islands are estimated to be around 100−200 t, which represents 10% of the landings and 40% of the

earnings in the trawl fishery [*Guijarro et al.*, 2012]. Sóller, one of the most important fishing grounds for red shrimp around the Balearic Islands, is situated North of Mallorca (solid black line area in Fig. 4.1), where an important part of the island fleet is concentrated during the summer months [*Moranta et al.*, 2008], when catches of large specimens occur. The red shrimp population in this fishing ground shows important seasonal variations throughout the year (such as the high abundance of juveniles recruiting to the fishing grounds in autumn-winter and the high abundance of large spawning females during the summer), compared with the other nearby fishing grounds, south of Mallorca [*Guijarro et al.*, 2008].

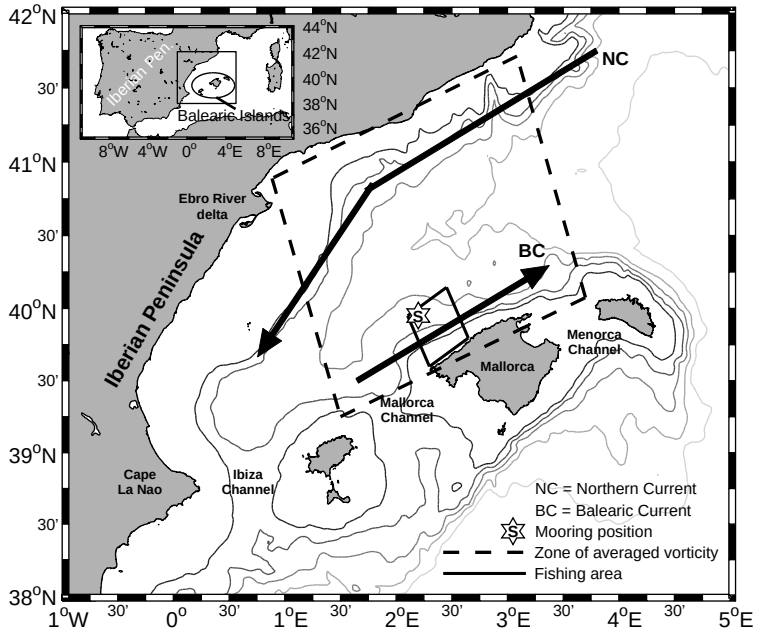

Figure 4.1: Map of the studied area in the western Mediterranean. The unbroken line encloses Sóller fishing grounds where Aristeus antennatus *is exploited and the broken line corresponds to the zone where the time series of vorticity has been calculated. Mooring location is indicated by a star.*

The Sóller fishing ground is located on the island slope, in a well known very active area, with numerous eddies normally generated by some instabilities of the Northern current or the Balearic current (Fig. 4.1), particularly more intense during winter (October-March; *Amores et al.* [2013]). These eddies, clearly visible on satellite images, have been known to reach the deeper waters, and their effects are usually felt down to the seabed, where their velocities may increase to several times those of the mean currents measured in the zone [*Amores et al.*, 2013]. These strong bottom currents of the order of 25 cm/s are known to produce sediment resuspension which, in turn, may generate additional cross slope

turbidity currents [*Thomson et al.*, 2010].

In the western Mediterranean, the red shrimp distribution, and its accessibility to fishing exploitation, has been shown to be mainly influenced by geomorphology [*Sardà et al.*, 1994, 1997] and hydrodynamics [*Bombace*, 1975; *Demestre and Martín*, 1993; *Ghidalia and Bourgois*, 1961; *Guijarro et al.*, 2008; *Relini and Relini*, 1987; *Sardà et al.*, 2009]. These last factors are probably linked to regional and large-scale climatic patterns [*Carbonell et al.*, 1999; *Massutí et al.*, 2008; *Maynou*, 2008]. In a recent study, *Company et al.* [2008] revealed that the downslope shelf dense water current events into submarine canyons, along the whole northern Catalan margin, strongly affected the red shrimp landings. This downslope shelf dense water current events is one of the main processes contributing to the shelf-deep ocean exchange [*Ivanov et al.*, 2004], enhancing organic-matter flux and deposition, increasing suspended particulate matter concentrations and transport of organic matter from coastal zones to the deep ocean [*Bosley et al.*, 2004; *Canals et al.*, 2006; *Company et al.*, 2008]. In the northern Catalan margin, it exerts a negative effect on the catches of red shrimp and a positive effect for recruitment, due to the transportation of the particulate organic matter. The increase of suspended particulate matter also appears to be related to the abundance of other crustacean species such as pandalids and penaeid [*Lin et al.*, 1992; *Puig et al.*, 2001] and to an enhance of benthic productivity and biodiversity inside canyon habitats [*Rowe et al.*, 1982; *Schlacher et al.*, 2007; *Vetter et al.*, 2010]. In addition to downslope shelf dense water current, mesoscale eddies have also been reported to be responsible of transport of shelf sediments to the deep ocean, resuspension of bottom sediments creating turbidity layers and formation of sediment plumes around their periphery [*Washburn et al.*, 1993]. The influence of vorticity (as indicator of eddy development) on catchability of marine species has been mostly addressed for pelagic organisms such as tuna fisheries [*Hyder et al.*, 2009; *Kai and Marsac*, 2010; *Ramos et al.*, 1996; *Zainuddin et al.*, 2006]. However, the effect of such physical processes has also been explored for benthic species, which are also linked to variables that describe water column properties and structures [*Beentjesa and Renwick*, 2001; *Palamara et al.*, 2012].

The objective of this work is to analyze the possible links between the presence of eddies (which will be quantified by their associated surface vorticity) affecting the Sóller fishing ground and the red shrimp yields of the deep water trawl fishery developed in the area. This relationship is also explored for other demersal species frequently caught by the deep water bottom trawl fishery developed in the area [*Guijarro and Massutí*, 2006], which consist of three fishes (*Galeus melastomus*, *Micromesistius poutassou* and *Phycis blennoides*) and two decapod crustaceans (*Geryon longipes* and *Nephrops norvegicus*), with the objective of discussing their different responses in relation to their living habits.

A year-long near-bottom current meter and a sediment trap moored near

the fishing grounds are used to infer the mechanism to explain how the surface vorticity observed can affect the bottom sediments and, in turn, the red shrimp yields.

4.2 Data and Methods

4.2.1 Catches

Daily time series of the landings from the bottom trawl fleet have been obtained from the official sale bills of OP Mallorca Mar, the fishery producer organization of Mallorca, between 2000 and 2010 (both years included). Each daily sale bill was assigned to one fishing tactic (FT) or a combination of them following the methodology described by *Palmer et al.* [2009]. Landings were standardized to CPUEs (catches per unit of effort), referred to as kilograms caught per day and boat. For *A. antennatus*, only catches obtained from the middle slope fishing tactic, developed between 600 and 800 m depth, have been considered, because this is the target species for this FT. Moreover, the daily sale bills distinguished red shrimp catches into two size categories (small and large) up to year 2004, and three categories (small, medium and large) from 2004 to the present day. According to *Guijarro et al.* [2008], two different categories were defined in order to homogenize the available data, small (including individuals with a carapace length $<$32mm) and medium-large (adults, with a carapace length $\geq$32mm). For this analysis, only those of the medium-large sized category, mainly adult females, were considered. Juveniles are not taken into account for two reasons:

1. The fishing fleet mainly targets large individuals (adults) due to their higher commercial value. This fact would surely provoke a bias when trying to relate juvenile catches with abundances

2. Adult and juvenile red shrimps present a clear different bathymetric distribution. Adult individuals are mainly located at the 500-800 m range, where the fishing fleet is developed. But the highest concentrations of juveniles are situated deeper than 1000 m *Sardà et al.* [2003], where the bottom trawl fishery is forbidden. So juvenile catches do not properly reflect the juvenile population abundances.

From the entire fleet that currently operates in Mallorca, only five boats regularly fish in the zone of interest (Sóller) throughout the year (other boats fishing in this area only in summer are not considered). Among these five boats, exclusively two devote most of their efforts to red shrimp fishery along the middle slope and they were the only ones finally considered for the analysis.

Finally, as a direct response to hydrodynamics changes in a daily basis is not expected, a monthly average was calculated according to the daily time series. We intentionally filtered out the high frequency variations in order to compute an integrated response in a longer time scale and take into account for the gaps in the data (that occurred, for example, on weekends or bad weather days).

Regarding the other species considered in this work (*G. melastomus*, *M. poutassou*, *P. blennoides*, *G. longipes* and *N. norvegicus*), all the boats and slope fishing tactics have been considered because, unlike *A. antennatus*, they are the by-catch species of the deep water trawl fishery, and therefore, their abundance in daily landings is not as frequent as that of the red shrimp. The final time series for each species were also averaged monthly as the CPUEs in terms of kg of catch per day per boat.

4.2.2 Hydrodynamic Data

4.2.2.1 Satellite images

We estimated the relative vorticity ζ (from now on referred to as only vorticity) from the daily Sea Surface Height (SSH) satellite images with a map spacing of $1/8° \times 1/8°$, obtained from the merged satellite AVISO products available at http://www.aviso.oceanobs.com. The vorticity is calculated as the curl of the velocity field, but we only retain the third component as it represents the vorticity of a horizontal field. By considering the hydrostatic and homogeneous fluid, the final expression of ζ is:

$$\zeta = \frac{g}{f} \cdot \bigtriangledown^2 SSH \tag{4.1}$$

where g is the gravity acceleration, f the Coriolis parameter and $\bigtriangledown^2$ the horizontal Laplacian.

After computing the daily vorticity fields, their absolute value was taken because both, cyclonic ($\zeta > 0$) and anticyclonic episodes ($\zeta < 0$), were expected to have the same effect on the seabed velocities and sediment resuspension. Next, we computed the spatial average in the dashed rectangle, as shown in Fig. 4.1. The choice of the area is somewhat arbitrary. The size should be significantly greater than the fishing ground dimension because the eddy sizes are significantly greater, and their horizontal influence is not known. The best results are found when the area is selected to be large enough to include the Northern and the Balearic currents, potentially the eddy generators. Finally, the daily time series was averaged on a monthly basis in order to have the same time step as the time series of the catches.

4.2.2.2 Moorings

A mooring was deployed north-west of Mallorca (39°49.682 N − 02°12.778 E; star in Fig. 4.1) between November 2009 and February 2011. Located around 900 m depth in the Mallorca slope, it had four CTD Seabird 37 (300, 500, 700 and 900 m) and two current meters Nortek Aquadopp (500 and 900 m). Moreover, the mooring had also a sediment trap placed 30 m above the bottom. The CTD sampling rate was 10 minutes, while the current meters recorded one value every 30 minutes. The sediment trap had a sampling interval of 10 days and it had 12 bottles. The combination of sampling rate and number of bottles made necessary a maintenance of the mooring every four months.

All the instruments operated perfectly during the entire period, except for the 500 and 900 m CTDs, which ran out of batteries in mid-December 2010 and mid-January 2011, respectively. The sediment trap worked well too, but the unavailability of boat lead to no recorded data between July 5 and September 21, 2010.

Sediment trap samples were wet-sieved through a 1 mm nylon mesh in order to retain the largest organisms. Swimmers smaller than 1 mm were manually removed under a dissecting microscope using fine tweezers. Finally, the sample was freeze-dried and weighed to calculate the Total Mass Flux (TMF).

Despite we did not have any direct measurement of turbidity, the Nortek Aquadopp current meters give us an estimation of it throughout the backscattering of the particles used to compute the velocity (as suggested by *Lohrmann* [2001]). Acoustic backscattering has been used as turbidity surrogate in different references such as *Thomson et al.* [2010].

4.2.3 Statistical Analysis

Quantification of the similarity between surface vorticity and time series of catches was performed with the correlation function. If we define V and C as the monthly anomalies (time series after subtracting the mean value) for vorticity and catches, respectively, the correlation between these two series is calculated as:

$$\rho_{VC}(lag) = \frac{1}{(N-1-|lag|)\cdot\sqrt{\sigma_{VV}\cdot\sigma_{CC}}} \begin{cases} \sum_{i=|lag|+1}^{N} V_i \cdot C_{i-|lag|} & \text{if } lag<0 \\ \sum_{i=|lag|+1}^{N} V_{i-|lag|} \cdot C_i & \text{if } lag\geq 0 \end{cases} \tag{4.2}$$

with N being the series length, σ_{VV} the covariance of V and σ_{CC} the covariance of C.

The significance level may be obtained with:

$$sig(lag) = \frac{T_q(0.99, N-|lag|-2)}{\sqrt{N-|lag|-2+[T_q(0.99, N-|lag|-2)]^2}} \tag{4.3}$$

where $T_q(0.99, D)$ is the t-student distribution with a significance of 99% and D degrees of freedom.

4.3 Results and Discussion

A visual inspection of the monthly average vorticity and *A. antennatus* CPUE time series appears to suggest that any increase in vorticity generally causes a decrease in the CPUEs, although a decrease in vorticity does not cause an increase in CPUEs (Fig. 4.2a). In fact, a negative correlation (i.e. both series are in antiphase) between time series has been found (Fig. 4.2b).

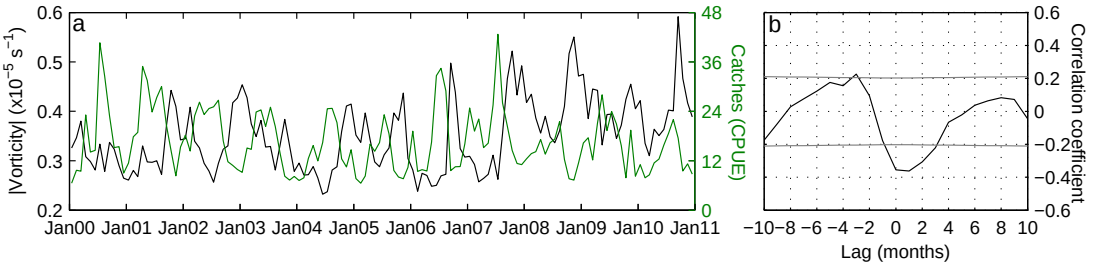

Figure 4.2: a) Monthly averaged time series of vorticity (black) and Aristeus antennatus *CPUEs (green). b) Correlation between these two series, showing the maximum correlation (-0.35) around lag 0. Black line represents the 95% confidence level.*

In the following we will give several evidences supporting the fact that surface vorticity affects red shrimp availability by modifying near bottom turbidity in the fishing grounds. If we assume that any increase in vorticity affects the CPUE of the red shrimp by producing a near bottom turbidity, which in turn would decrease the resource availability, we could not expect that the opposite, a decrease in vorticity, would immediately produce an increase in the CPUEs. Water turbidity would persist for some period of time in the area after the end of any vorticity episode and then the red shrimp response would be delayed. Therefore, the two series have been modified, trying to take into account the different, although expected, CPUE response to the increase and decrease in vorticity. Vorticity and CPUE time derivatives have been computed. As we want to highlight the part when the vorticity increases (positive derivative) and when de CPUE decreases (negative derivative), the negative vorticity and positive CPUE derivatives were artificially set at zero. Therefore, only the increases in vorticity and decreases in CPUE are considered. Furthermore, the sign of the CPUE derivatives has also been reversed for better visualization (Fig. 4.3a).

Vorticity and *A. antennatus* CPUEs derivative series show quite a similar pattern. The zones where the series have been forced to read zero coincide, and

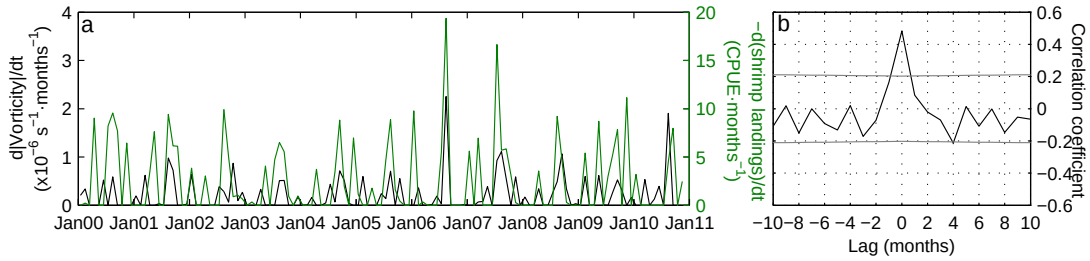

Figure 4.3: a) Derivative time series of vorticity (black) and Aristeus antennatus *CPUEs (green). In the series of the vorticity derivative, the negative values have been fixed at 0, while the positive values of the derivative CPUEs series have been set at 0. Notice that the last one has suffered a change of sign. b) Correlation between these two series show the maximum value (0.48) at lag 0. Black line represents the 95% confidence level.*

almost any increase in the vorticity derivative corresponds with an increase in the reversed catches derivative. The correlation between both series at lag zero, now positive due to the sign change in the CPUEs derivatives mentioned, is slightly larger than before, as expected, reaching a value of 0.48 (Fig. 4.3b). This result strongly supports a relationship between the increases in the surrounding absolute surface vorticity and decreases in the adult *A. antennatus* availability in the fishing grounds.

The suggested mechanism explaining the relationship observed is now supported analyzing some surface vorticity episodes recorded when the mooring was deployed in the area. During 2010, at least three of these episodes produced some footprint in the instruments deployed in the mooring line.

The increase in the absolute value of the surface vorticity is commonly caused by the presence of an eddy, such as the one shown in Fig. 4.4. This particular eddy remained in the area between mid-November and mid-December 2010 and was studied in detail by *Amores et al.* [2013]. This eddy was clearly reflected in the currents registered at 500 and 900 m depth. A significant velocity increase was measured at both depths (episode 3 in Fig. 4.5a and 4.5b). Velocities showed spikes reaching up to 26 cm/s at 900 m, where the mean current during the whole year was computed to be around 5 cm/s. This eddy also affected the current direction, causing a complete reversal in the currents at 500 m (Fig. 4.5c) and a down slope gyre at 900 m (Fig. 4.5d).

This particular eddy clearly reached down to the bottom, and the recorded gyres and velocity increases could easily have caused the material resuspension. This hypothesis is supported by three indirect measurements:

1. the increase in the total flux mass (TFM) recorded by the moored sediment trap at the time of the eddy (Fig. 4.6)

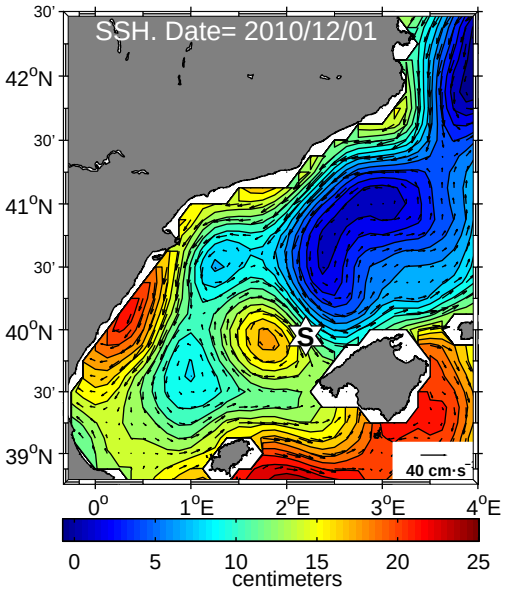

Figure 4.4: Sea Surface Height (SSH) image from December 1, 2010. It shows an eddy in the region analyzed. The star shows the mooring position.

2. the increase of the acoustic backscattering during the episode (Fig. 4.7a)

3. the clear down slope gyre at 900 m which could be related to a near bottom turbidity current (Fig 4.5d).

The eddy shown in Fig. 4.4 was not the only one recorded when the mooring was deployed. Another eddy, which occurred between mid-January and March 2010, was also measured by the mooring (episode 1 in Fig. 4.5). This eddy too reached the bottom, although with a weaker footprint in velocity. However, the TFM still reached similar values to those observed during the December 2010 eddy and an increase in backscattering is also observed.

Still another gyre was observed between June and July 2010; however, it was only noticeable at 500 m (episode 2 in Fig. 4.5). Its effect at 900 m was weak. Even so, a TFM peak was also measured by the sediment trap, although much weaker than during the other two eddies (Fig. 4.6). Backscattering did not show any significant increase during this episode. This could be explained by the steep slope of the area. Even if the eddy was not energetic enough to reach down to 900 m depth, where the mooring was deployed, it could still affect the bottom at shallower depths and the resuspension of material could have reached deeper waters, causing the increased TFM that is recorded in the sediment trap.

From the above described episodes, it has been observed that the surface eddies exert some degree of influence on the seabed dynamics and that might

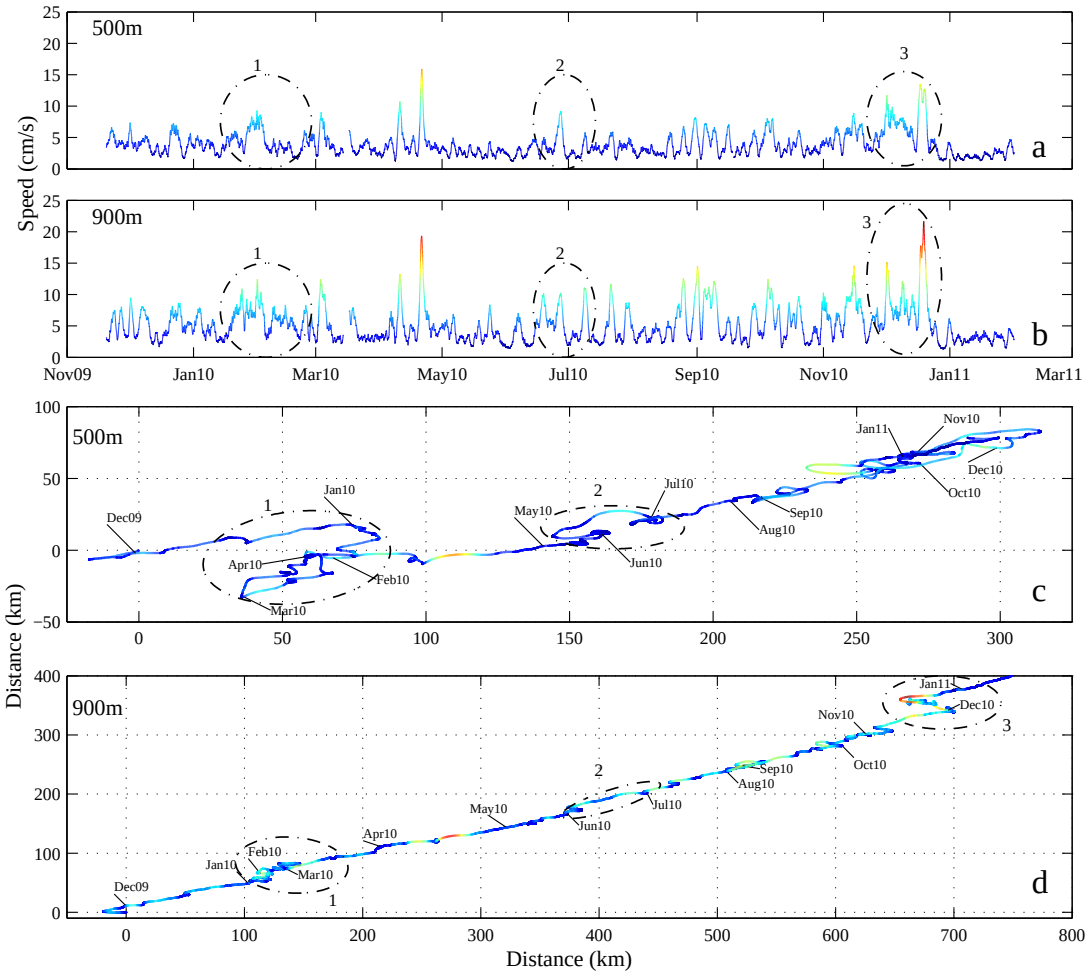

Figure 4.5: 24h low-pass filtered speed series of 500 (a) and 900 (b) m depth current meters of the mooring for the whole recorded period. Blue indicates the low speed values degrading to red, which indicates the high values. (c) and (d) are the progressive vector diagrams for 500 and 900 m depth, respectively. The different colors coincide temporally with the speed time series. Enclosed areas represent moments where an eddy is present in the zone. Ellipse number 1 highlight an eddy which is strongly present at 500 m depth, but weakly present at 900 m; number 2 ellipse shows an eddy which reached to 500 m depth, although not right up to 900 m; and number 3 ellipse illustrates an eddy which arrived strongly to the 500 and 900 m depths. Note that in the PVDs the ratio between the scales of x and y axis is 2:1.

increase the water turbidity near the bottom and affect the availability of *A. antennatus* in the fishing grounds. This mechanism can be better visualized by restricting the time interval to a shorter period of time of some of the data shown in Fig. 4.2, for the period, 2006-2010 (Fig. 4.8). During these years, the vorticity episodes are time spaced enough to allow an almost complete recovery towards a normal situation after any episode, before the arrival of the next one. The

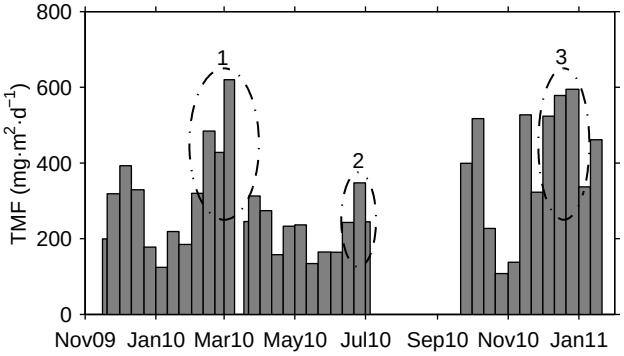

Figure 4.6: Total Flux Mass (TFM) collected by the sediment trap during the whole sampling time. The gap in the data is due to the unavailability of ship for carrying out the mooring maintenance. The dashed ellipses show the increment of TFM due to the eddies reported in Fig. 4.5.

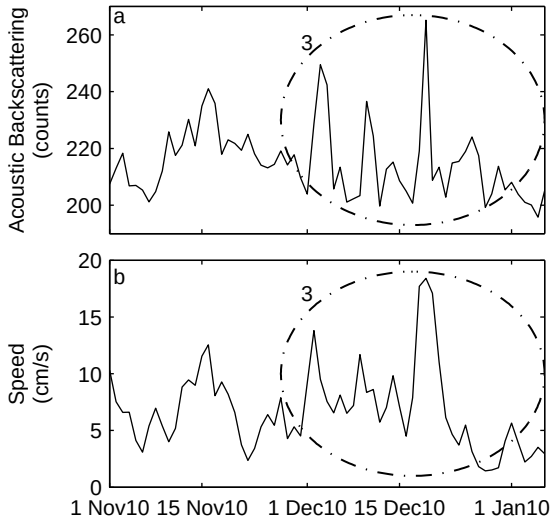

Figure 4.7: Acoustic backscattering (a) and speed (b) measured by the 900 m current meter during the third episode.

mechanism suggested are then better observed in the data. A vorticity increase (dark gray bands in Fig. 4.8) would trigger an increase in the re-suspended material and would force *A. antennatus* to move away from the fishing ground, probably towards greater depths, leading to a decrease in the catches of this species. This scenario would remain unchanged until the eddy effects disappear and the sediments once again precipitate to the sea floor (soft gray bands in Fig. 4.8). Once all the sediments are completely settled down, the water conditions would become suitable to allow the individuals to return to the depths where they can be caught (white bands in Fig. 4.8). Four episodes appear to follow one

after another in the period shown.

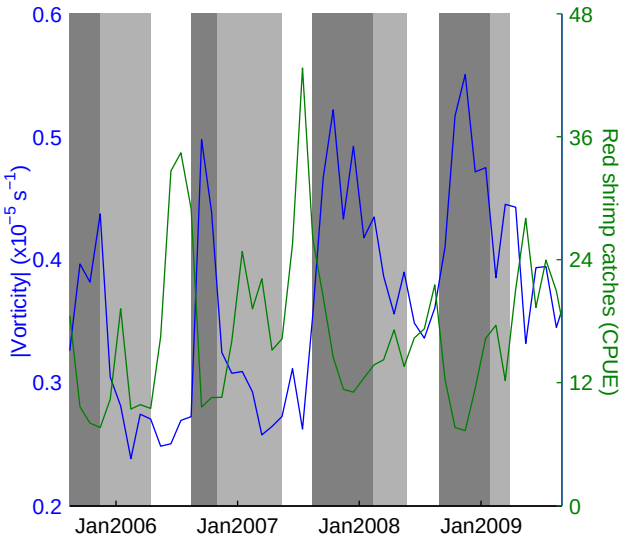

Figure 4.8: Zoom of the Fig. 4.2, where the effect of the vorticity (blue) on the Aristeus antennatus *CPUEs (green) can be seen. The colored bands indicate the amount of particles that would be re-suspended.*

Company et al. [2008] described a similar but stronger phenomenon in the submarine canyon system off the north-eastern Iberian Peninsula. They found a correlation between the strong currents associated with intense downslope shelf dense water current events and the disappearance of *A. antennatus* from its fishing grounds, exerting a negative effect on the catches reporting and a temporary collapse of its fishery. An increase in the mortality rated after exposure to high turbidity has also been detected for Penaeid shrimps at juvenile and adult stages [*Lin et al.*, 1992]. Both downslope shelf dense water current events and mesoscale eddies have been reported to enhance organic-matter flux and deposition, increasing suspending particulate matter concentrations with the transport of organic matter from coastal zones to the deep ocean or by resuspension of bottom sediments [*Bosley et al.*, 2004; *Canals et al.*, 2006; *Washburn et al.*, 1993]. Life forms as diverse as phytoplankton, protozoans, crustaceans, fish, sea snakes, marine mammals and birds are found to alter their distributions in the presence of such flow patterns [*Owen*, 1981], which can be responsible for enhancing benthic productivity and biodiversity inside canyon habitats [*Rowe et al.*, 1982; *Schlacher et al.*, 2007; *Vetter et al.*, 2010]. The presence of a significant amount of suspended sediment has also been related to the higher occurrence of juveniles and females of the deep-water pandalid shrimp species, genus Plesionika [*Puig et al.*, 2001] and the regions where the intermediate nepheloid layers detach from the seabed have been defined as potential deep-water nursery habitats for these species. The

transportation of the particulate organic matter associated with the downslope shelf dense water current appears to be positive for recruitment of red shrimp in the north-eastern Ibearian Peninsula [*Company et al.*, 2008], with a positive increase in the landings 3-5 years after these events, preceded by an increase in the number of juveniles. However, this last effect has not been detected off the Balearic Islands, probably because of the slight difference in the feeding strategies of the species between the north-eastern Iberian Peninsula and the Balearic Islands. *A. antennatus* has a highly varied diet, being among the mega-benthic species mainly preying on the benthos in the deep Mediterranean [*Cartes*, 1994; *Cartes and Carrassón*, 2004]. However, benthic preys are particularly significant off the north-eastern Iberian Peninsula, where the submarine canyons enhance such types of food availability. Conversely, the trophic webs off the Balearic Islands show an impoverishment of the benthos biomass and depend more directly on food of planktonic origin, enhancing the consumption of micro-nektonic preys [*Cartes et al.*, 2008; *Maynou and Cartes*, 2000]. In this sense, the positive effects of downslope shelf dense water current and sediment resuspension in the long term should be also more marked off north-eastern Iberian Peninsula than off the Balearic Islands.

Although the mechanism suggested is somehow speculative because we have to rely on indirect data (backscattering) to deduce bottom turbidity, we have shown several evidences that the presence of enough energetic eddies may cause bottom turbidity increases in the fishing ground. Still another indirect evidence supporting the mechanism suggested comes from the analysis of other demersal species caught in the same region that also appear to be related to vorticity changes in the area. The correlations found for each species (Fig. 4.9) are different from those observed for *A. antennatus* but consistent with the suggested mechanism where vorticity affects the seabed by increasing the bottom water turbidity.

Other decapod crustaceans, *Geryon longipes* and *Nephrops norvegicus*, the more sedentary and benthic species, show a significant positive correlation to the vorticity events at around 0.4 and 0.5, respectively. These two species are closely connected to the bottom, as reflected by their feeding behavior and biological characteristics. *G. longipes* preys on a broad range of benthic invertebrates [*Cartes*, 1993] and *N. norvegicus* shows a scavenging activity [*Cristo and Cartes*, 1998] and has been related to the sediment characteristics [*Maynou and Sardà*, 1997]. Unlike *A. antennatus*, it is likely that these two species may take some advantage of the re-suspended matter.

Galeus melastomus, which has more mobility than the previously considered epi-benthic species, feeds on the mesopelagic preys with the occasional occurrence of benthic feeding activity and scavenging in the adult phase [*Fanelli et al.*, 2009]. This species showed a lower correlation (0.33) with the vorticity time series.

Finally, *Micromesistius poutassou* and *Phycis blennoides*, the two bentho-

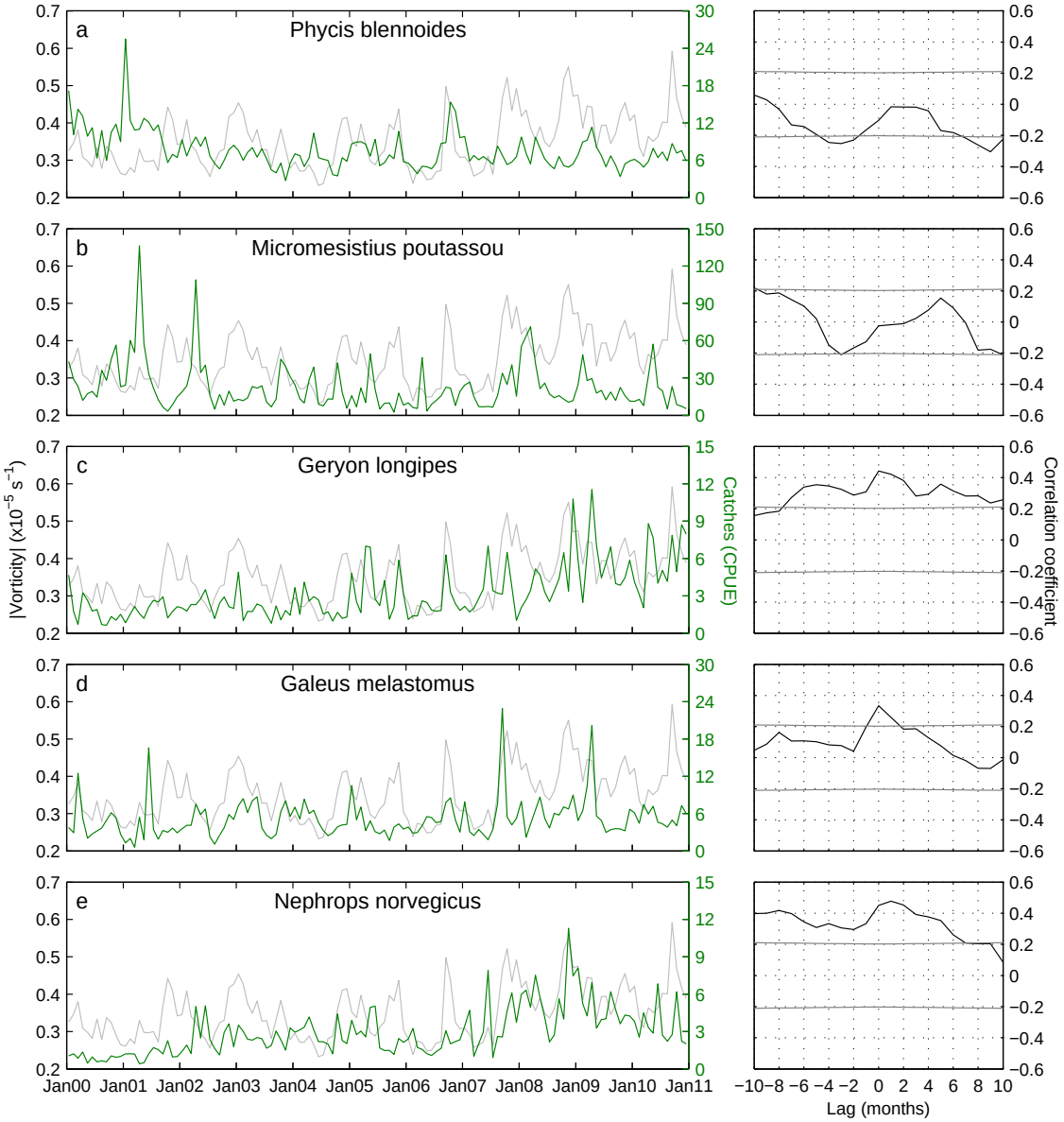

Figure 4.9: Time series of CPUEs for five demersal species (by catch) from the deep water trawl fishery and its correlation with the absolute value of surface vorticity.

pelagic teleosts with greater capacity of movement above the bottom, are expected to be less affected by bottom water turbidity. In fact, no significant correlations between the CPUEs and vorticity have been found.

4.4 Summary and Conclusions

A reasonable good negative correlation is noted between the monthly CPUE of the adult *A. antennatus* bottom trawl yields in the fishing grounds off northern Mallorca and the mean surface vorticity in the surrounding area. We have shown that the eddies causing the vorticity events may reach the bottom, increasing the current velocities, which in turn would trigger sediment resuspension and increased bottom water turbidity. Such a change in the water conditions would force adult *A. antennatus* individuals to move away from the fishing ground, probably downwards, to greater depths. This proposed mechanism is similar, although lower in magnitude, to the one suggested by *Company et al.* [2008] in the downslope shelf dense water current events of the submarine canyons in the northern Catalan margin, off the north-eastern Iberian Peninsula. In the Balearic Islands, where these geomorphological structures do not exist and where there is no river runoff, the eddies would be the triggering factor.

Other deep water demersal species found along with the catch of the red shrimp fishery, possessing different behavior and feeding habits, exhibit different responses to these events, but all of them are consistent with the eddy generation near bottom velocities increase and bottom water turbidity.

A final hypothesis could also be suggested from the results obtained. The seasonal migration of most of the fishing fleet of Mallorca, targeting the red shrimp in the Sóller fishing grounds during the summer has been explained by the highest abundance of large spawning females in this area during this season [*Guijarro et al.*, 2008], similar to other areas off the north-eastern Iberian Peninsula [*Sardà et al.*, 1994, 1997]. In light of this, the absence of these large aggregations in the Sóller fishing grounds during the rest of the year could be related to the particular behavior of the species. However, it is worth noting that, according to *Amores et al.* [2013], the vorticity episodes are much more intense off northern Mallorca during the winter time (October to March) than in the summer. This fact could be an additional factor explaining the decrease in the availability of the red shrimp to fishing exploitation during these months. However, off southern Mallorca, yields from the bottom trawl fishery targeting to red shrimp remain more stable [*Guijarro et al.*, 2008].

Acknowledgments

This research has been partially sponsored by the IDEADOS project (CMT2008-04489-C03-01 and 03). The work of A. Amores has been funded by a JAE-PreDoc grant from Consejo Superior de Investigaciones Científicas (CSIC) and co-funded by Programa Operativo FSE 2007 2013. The authors are grateful to the fishermen associations in Palma and the Autonomous Government of the Balearic Islands

for providing landing data. The authors also wish to express their gratitude to the IDEADOS team for their collaboration in the data acquisition process and the crews of the R/V Odón de Buen and F/V Punta des Vent for their valuable assistance during the mooring deployment.

Bibliography

Amores, A., S. Monserrat, and M. Marcos (2013), **Vertical structure and temporal evolution of an anticyclonic eddy in the Balearic Sea (western Mediterranean)**, *J. Geophys. Res. Oceans*, *118*, 2097–2106, doi: 10.1002/jgrc.20150.

Arrobas, I., and A. Ribeiro-Cascalho (1987), On the biology and fishery of Aristeus antennatus (Risso, 1816) in the south Portuguese coast, *Inv. Pesq.*, *51 (suppl. 1)*, 233–243.

Beentjesa, M. P., and J. A. Renwick (2001), The Relationship between Red Cod, Pseudophycis Bachus, Recruitment and Environmental Variables in New Zealand, *Environmental Biology of Fishes*, *61*(3), 315–328, doi: 10.1023/A:1010943906264.

Bombace, G. (1975), Considerazioni sulla distribuzione delle popolazioni di livello batiale con particolare riferimento a quelle bentoniche, *Pubbl. Staz. Zool. Napoli*, *39 (suppl 1)*, 7–21.

Bosley, K. L., J. W. Lavelle, R. D. Brodeur, W. W. Wakefield, R. L. Emmett, E. T. Baker, and K. M. Rehmke (2004), Biological and physical processes in and around Astoria submarine Canyon, Oregon, USA, *Journal of Marine Systems*, *50*(12), 21 – 37, doi: 10.1016/j.jmarsys.2003.06.006.

Canals, M., P. Puig, X. D. de Madron, S. Heussner, A. Palanques, and J. Fabres (2006), Flushing submarine canyons, *Nature*, *444 (7117)*, 354–357, doi: 10.1038/nature05271.

Carbonell, A., M. Carbonell, M. Demestre, A. Grau, and S. Monserrat (1999), The red shrimp Aristeus antennatus (Risso, 1816) fishery and biology in the Balearic Islands, Western Mediterranean, *Fisheries Research*, *44*, 1–13, doi: 10.1016/S0165-7836(99)00079-X.

Cartes, J. E. (1993), Diets of deep-sea brachyuran crabs in the Western Mediterranean Sea, *Marine Biology*, *117*, 449–457, doi: 10.1007/BF00349321.

Cartes, J. E. (1994), Influence of depth and season on the diet of the deep-water aristeid Aristeus antennatus along the continental slope (400 to 2300 m) in the Catalan Sea (western Mediterranean), *Marine Biology*, *120*, 639–648, doi: 10.1007/BF00350085.

Cartes, J. E., and M. Carrassón (2004), Influence of trophic variables on the depth-range distributions and zonation rates of deep-sea megafauna: the case of the Western Mediterranean assemblages, *Deep Sea Research Part I: Oceanographic Research Papers*, *51*, 263–279, doi: 10.1016/j.dsr.2003.10.001.

Cartes, J. E., V. Papiol, and B. Guijarro (2008), The feeding and diet of the deep-sea shrimp Aristeus antennatus off the Balearic Islands (Western Mediterranean): Influence of environmental factors and relationship with the biological cycle, *Progress in Oceanography*, *79*, 37–54, doi: 10.1016/j.pocean.2008.07.003.

Company, J. B., P. Puig, F. Sardà, A. Palanques, M. Latasa, and R. Scharek (2008), Climate influence on deep sea populations, *PLoS ONE*, *3*, e1431, doi: 10.1371/journal.pone.0001431.

Cristo, M., and J. E. Cartes (1998), A comparative study of the feeding ecology of Nephrops norvegicus (L.), (Decapoda: Nephropidae) in the bathyal Mediterranean and the adjacent Atlantic, *Scientia Marina*, *62 (Suppl. 1)*, 81–90, doi: 10.3989/scimar.1998.62s181.

Demestre, M., and P. Martín (1993), Optimum exploitation of a demersal resource in the western Mediterranean: the fishery of the deep-water shrimp Aristeus antennatus (Risso, 1816), *Scientia Marina*, *57 (2-3)*, 175–182.

Fanelli, E., J. Rey, P. Torres, and L. G. de Sola (2009), Feeding habits of blackmouth catshark Galeus melastomus Rafinesque, 1810 and velvet belly lantern shark Etmopterus spinax (Linnaeus, 1758) in the western Mediterranean, *J. Appl. Ichthyol.*, *25 (Suppl. 1)*, 83–93, doi: 10.1111/j.1439-0426.2008.01112.x.

Ghidalia, W., and F. Bourgois (1961), Influence of temperature and light on the distribution of shrimps in medium and great depths, *Gfcm Studies and Reviews*, *16*, 49.

Guijarro, B., and E. Massutí (2006), Selectivity of diamond- and square-mesh codends in the deepwater crustacean trawl fishery off the Balearic Islands (western Mediterranean), *ICES J. Mar. Sci.*, *63 (1)*, 52–67, doi: 10.1016/j.icesjms.2005.08.011.

Guijarro, B., E. Massutí, J. Moranta, and P. Díaz (2008), Population dynamics of the red shrimp Aristeus antennatus in the Balearic Islands (western Mediterranean): Short spatio-temporal differences and influence of environmental factors, *Journal of Marine Systems*, *71 (3-4)*, 385–402, doi: 10.1016/j.jmarsys.2007.04.003.

Guijarro, B., E. Fanelli, J. Moranta, J. E. Cartes, and E. Massutí (2012), Small-scale differences in the distribution and population dynamics of pandalid shrimps in the western Mediterranean in relation to environmental factors, *Fisheries Research*, *119-120*, 33–47, doi: 10.1016/j.fishres.2011.12.001.

Hyder, P., K. Bigelow, R. Brainard, M. Seki, J. Firing, and P. Flament (2009), Migration and Abundance of Bigeye Tuna (*Thunnus obesus*), and Other Pelagic Species, Inferred from Catch Rates and Their Relation to Variations in the Ocean Environment, *SOEST*, *09-02*.

Ivanov, V., G. Shapiro, J. Huthnance, D. Aleynik, and P. Golovin (2004), Cascades of dense water around the world ocean, *Progress in Oceanography*, *60*(1), 47 – 98, doi: 10.1016/j.pocean.2003.12.002.

Kai, E. T., and F. Marsac (2010), Influence of mesoscale eddies on spatial structuring of top predators communities in the Mozambique Channel, *Progress in Oceanography*, *86*(12), 214 – 223, doi: 10.1016/j.pocean.2010.04.010.

Lin, H.-P., G. Charmantier, P. Thuet, and J.-P. Trilles (1992), Effects of turbidity on survival, osmoregulation and gill Na^+-K^+ ATPase in juvenile shrimp *Penaeus japonicus*, *Marine Ecology Progress Series*, *90*, 31–37.

Lohrmann, A. (2001), Monitoring sediment concentration with acoustic backscattering instruments, *Nortek Tech. notes*, *No. N4000712*.

Massutí, E., S. Monserrat, P. Oliver, J. Moranta, J. L. López-Jurado, M. Marcos, J. M. Hidalgo, B. Guijarro, A. Carbonell, and P. Pereda (2008), The influence of oceanographic scenarios on the population dynamics of demersal resources in the western Mediterranean: Hypothesis for hake and red shrimp off Balearic Islands, *Journal of Marine Systems*, *71 (3-4)*, 421–438, doi: 10.1016/j.jmarsys.2007.01.009.

Maynou, F. (2008), Environmental causes of the fluctuations of red shrimp (Aristeus antennatus) landings in the Catalan Sea, *Journal of Marine Systems*, *71 (3-4)*, 294–302, doi: 10.1016/j.jmarsys.2006.09.008.

Maynou, F., and J. E. Cartes (2000), Community structure of bathyal decapod crustaceans off south-west Balearic Islands (western Mediterranean): seasonality and regional patterns in zonation, *Journal of the Marine Biological Association of the United Kingdom*, *80*, 789–798.

Maynou, F., and F. Sardà (1997), Nephrops norvegicus population and morphometrical characteristics in relation to substrate heterogeneity, *Fisheries Research*, *30 (1-2)*, 139–149, doi: 10.1016/S0165-7836(96)00549-8.

Moranta, J., A. Quetglas, E. Massutí, B. Guijarro, M. Hidalgo, and P. Diaz (2008), Spatio-temporal variations in deep-sea demersal communities off the Balearic Islands (western Mediterranean), *Journal of Marine Systems*, *71 (3-4)*, 346–366, doi: 10.1016/j.jmarsys.2007.02.029.

Owen, R. W. (1981), Fronts and eddies in the sea: mechanisms, interactions and biological effects, *Analysis of marine ecosystems*, pp. 197–233.

Palamara, L., J. Manderson, J. Kohut, M. J. Oliver, S. Gray, and J. Goff (2012), Improving habitat models by incorporating pelagic measurements from coastal ocean observatories, *Marine Ecology Progress Series*, *447*, 15–30, doi: 10.3354/meps09496.

Palmer, M., A. Quetglas, B. Guijarro, J.Moranta, F. Ordines, and E. Massutí (2009), Performance of artificial neural networks and discriminant analysis in predicting fishing tactics from multispecific fisheries, *Canadian Journal of Fisheries and Aquatic Sciences*, *66*, 224–237, doi: 10.1139/F08-208.

Papaconstantinou, C., and K. Kapiris (2001), Distribution and population structure of the red shrimp (Aristeus antennatus) on an unexploited fishing ground in the Greek Ionian Sea, *Aquatic Living Resources*, *14*, 303–312, doi: 10.1016/S0990-7440(01)01128-7.

Puig, P., J. B. Company, F. Sardà, and A. Palanques (2001), Responses of deep-water shrimp populations to intermediate nepheloid layer detachments on the Northwestern Mediterranean continental margin, *Deep Sea Research Part I: Oceanographic Research Papers*, *48*, 21952207, doi: 10.1016/S0967-0637(01)00016-4.

Ramos, A. G., J. Santiago, P. Sangra, and M. Canton (1996), An application of satellite-derived sea surface temperature data to the skipjack (Katsuwonus pelamis Linnaeus, 1758) and albacore tuna (Thunnus alalunga Bonaterre, 1788) fisheries in the north-east Atlantic, *International Journal of Remote Sensing*, *17*(4), 749–759, doi: 10.1080/01431169608949042.

Relini, G., and L. O. Relini (1987), The decline of red-shrimp stocks in the gulf of Genoa, *Investigacion Pesquera*, *51*, 245260.

Relini, M., P. Maiorano, G. D'Onghia, L. O. Relini, A. Tursi, and M. Panza (2000), A pilot experiment of tagging the deep shrimp Aristeus antennatus (Risso, 1816), *Scientia Marina*, *64*, 357–361, doi: 10.3989/scimar.2000.64n3357.

Rowe, G. T., P. T. Polloni, and R. L. Haedrich (1982), The deep-sea macrobenthos on the continental margin of the northwest Atlantic Ocean, *Deep Sea Research Part A. Oceanographic Research Papers*, *29*(2), 257 – 278, doi: 10.1016/0198-0149(82)90113-3.

Sardà, F., J. E. Cartes, and W. Norbis (1994), Spatia-temporal structure of the deep-water shrimp Aristeus antennatus (Decapoda: Aristeidae) population in the western Mediterranean, *Fishery Bulletin*, *92*, 599–607.

Sardà, F., F. Maynou, and L. Talló (1997), Seasonal and spatial mobility patterns of rose shrimp Aristeus antennatus in the Western Mediterranean: results of a long-term study, *Marine Ecology Progress Series*, *159*, 133–141, doi: 10.3354/meps159133.

Sardà, F., J. B. Company, and F. Maynou (2003), Deep-sea shrimp (Aristeus antennatus Risso 1816) in the Catalan sea: a review and perspectives, *J. Northw. Atl. Fish. Sci*, *31*, 117–136.

Sardà, F., G. D'Onghia, C. Y. Politou, J. B. Company, P. Maiorano, and K. Kapiris (2004), Deep-sea distribution, biological and ecological aspects of Aristeus antennatus (Risso, 1816) in the western and central Mediterranean Sea, *Scientia Marina*, *68*, 117–127, doi: 10.3989/scimar.2004.68s3117.

Sardà, F., J. B. Company, N. Bahamón, G. Rotllant, M. M. Flexas, J. D. Sánchez, D. Zúñiga, J. Coenjaerts, D. Orellana, G. Jordà, J. Puigdefábregas, A. Sánchez-Vidal, A. Calafat, D. Martín, and M. Espino (2009), Relationship between environment and the occurrence of the deep-water rose shrimp Aristeus antennatus (Risso, 1816) in the Blanes submarine canyon (NW Mediterranean), *Progress in Oceanography*, *82*, 227–238, doi: 10.1016/j.pocean.2009.07.001.

Schlacher, T. A., M. A. Schlacher-Hoenlinger, A. Williams, F. Althaus, J. N. A. Hooper, and R. Kloser (2007), Richness and distribution of sponge megabenthos in continental margin canyons off southeastern Australia, *Marine Ecology Progress Series*, *340*, 73–88, doi: 10.3354/meps340073.

Thomson, R. E., E. E. Davis, M. Heesemann, and H. Villinger (2010), Observations of long-duration episodic bottom currents in the Middle America Trench: Evidence for tidally initiated turbidity flow, *J. Geophys. Res.*, *115*, C10,020, doi: 10.1029/2010JC006166.

Vetter, E. W., C. R. Smith, and F. C. de Leo (2010), Hawaiian hotspots: enhanced megafaunal abundance and diversity in submarine canyons on the oceanic islands of Hawaii, *Marine Ecology*, *31*(1), 183–199, doi: 10.1111/j.1439-0485.2009.00351.x.

Washburn, L., M. S. Swenson, J. L. Largier, P. M. Kosro, and S. R. Ramp (1993), Cross-Shelf Sediment Transport by an Anticyclonic Eddy Off Northern California, *Science*, *261*(5128), 1560–1564, doi: 10.1126/science.261.5128.1560.

Zainuddin, M., H. Kiyofuji, K. Saitoh, and S.-I. Saitoh (2006), Using multi-sensor satellite remote sensing and catch data to detect ocean hot spots for albacore (Thunnus alalunga) in the northwestern North Pacific, *Deep Sea Research Part II: Topical Studies in Oceanography*, *53*(34), 419 – 431, doi: 10.1016/j.dsr2.2006.01.007.

Summary and Discussion

In this thesis, the relationship between hydrodynamics and some fishing resources has been studied using data collected from two mooring lines, satellite images and reports from the official sale bills of OP Mallorca Mar, the fishery producer organization of Mallorca.

In the first chapter, entitled *Hydrodynamic comparison between the north and south of Mallorca Island*, the hydrodynamic similarities and differences between north (Sóller) and south (Cabrera) of Mallorca Island have been studied. One mooring line was deployed in each area and satellite data were used in the analysis. The mooring lines were installed in two different zones. The Sóller mooring line was deployed in the middle of a steep slope, dominated by the Balearic Current and located within the Balearic subbasin. On the other hand, the Cabrera mooring was placed in a flatter zone, near the Mallorca Channel, in the northern part of the Algerian subbasin, where there is no clear dominant currents.

It was observed that Sóller area was hydrodynamically more active than the zone from Cabrera. This statement was supported by a greater variability in all the recorded variables (temperature, salinity, current velocity, etc) and at all the depths (with the only exception of the 900 m salinity).

The current in Sóller had a dominant direction (in contrast with Cabrera that it had no clear direction with lower recorded speed values) in both 500 m and 900 m and non-near-zero mean speed values. This fact hinders fixing a lower limit of the Balearic Current, because its effects extend down to the seabed. This is important in two main aspects: the dynamic height calculation and the transport estimation. As regards the former, fixing a zero velocity level around 500 m is not accurate enough, since we have observed 4.5 cm/s mean velocities between 500 m and 900 m. The non-zero speed values at the intermediate and deep layers also affect the classical transport estimation of the Balearic Current. The transport of this current is usually calculated by taking an area 35-50 km in width and 200-250 m in depth (coinciding with the Balearic Front) and giving them transport values ranging from 0.3 Sv up to 0.9 Sv [*Font et al.*, 1988; *García-Ladona et al.*, 1995; *Pinot et al.*, 2002; *Ruiz et al.*, 2009]. However, when computing the transport from 300 m to 900 m, with a width half of the width used in the upper layers

(17.5-25 km, trying to take into consideration the presence of the slope) and 4.5 cm/s as mean velocity, values from 0.48 Sv to 0.68 Sv are obtained. These transport values obtained for the intermediate and deep layers are comparable to the transport in the upper layers and they should possibly be taken into account for subsequent computations of the Balearic subbasin transports.

Using daily SSH images, it was demonstrated that Sóller region had a greater number of surface eddies than Cabrera area. The presence of the Balearic Current over the Sóller mooring line made the difference, as the instabilities of this current appeared to be the common source of most of the eddies. These eddies were not only more frequent but also more intense and were observed to reach down to the bottom in several occasions.

The most intense eddies have also been observed in the frequency domain. The *strong* currents associated with those eddies tilted the mooring sinking the instruments and transferring the inertial frequency present in the currents to the pressure record. In addition, the inertial frequencies, 3.7 h, 3 h and 2 h period oscillations with, a priori, unknown origin were measured. The 3.7 h oscillation was associated with some trapped wave travelling around Mallorca Island or the whole Balearic Islands Archipelago (as it appeared in the spectra from both Sóller and Cabrera pressure records) meanwhile the other two periods detected (3 h and 2 h) were related to some resonance between Mallorca Island and the Ibearian Peninsula as they only appeared in the Sóller spectrum.

In the second chapter entitled *Vertical structure and temporal evolution of an anticyclonic eddy in the Balearic Sea (western Mediterranean)*, the main features of the more intense eddy registered in Sóller during our experiment were studied. This eddy, which was the 6th most intense and the 8th with the largest radius since 1992, modified the hydrodynamic properties in the whole water column ($\sim$1000 m), remaining around 1 month (November$-$December 2010) in the region and causing a complete reversal of the current direction at 500 m and a change of 90° in 900 m with respect to the along-slope main direction under unperturbed conditions. The velocities measured were higher at 900 m than at 500 m, in both, mean values (7 cm/s and 4 cm/s respectively) and maximum values (up to 26 cm/s at 900 m). The water distribution during the eddy life included Western Mediterranean Intermediate Waters (WIW) between 300 m and 700 m, displacing the resident Levantine Intermediate Waters (LIW) to deeper levels. The 90° downslope turn in the bottom currents at 900 m, could be related to turbidity currents generated by the eddy resuspending sediments from the seabed. This turbid water would become heavier than the water below, and it would fall downslope.

This last possibility (among other factors) has been studied in the third chapter (*Environmental factors controlling particulate mass fluxes on the Mallorca continental slope (Western Mediterranean Sea)*). The sediments collected by the

traps deployed at the mooring lines have been further analyzed. It has been shown that wind forcing and mesoscale processes (such as anticyclonic eddies and bottom trapped waves) appear as major drivers of the mass fluxes on Mallorca's continental slope. When comparing both sites, Sóller and Cabrera, it has been observed that they were both affected by the wind as a common forcing (which would provoke a primary production enhancement), reason explaining why they present similar temporal behaviour. However, greater values of TFM were clearly measured in Sóller. The presence of the permanent Balearic Current, characteristic not present in Cabrera site, and its associated mesoscale instabilities surely play a role. Besides wind and the effect of the Balearic Current, Sóller site was probably also affected by bottom-trapped topographic waves that enhance bottom sediment resuspension, increasing total mass fluxes of material at 900 m water depth.

In the fourth chapter entitled *Influence of the hydrodynamic conditions on the accessibility of the demersal species to the deep water trawl fishery off the Balearic Islands (western Mediterranean)*, the relationship between the hydrodynamics and fishing resources at Sóller fishing ground was studied. More precisely, a reasonable good negative correlation was found between the monthly CPUE of the adult *A. antennatus* and the mean surface vorticity in the surrounding area. The suggested triggering mechanism involves all the knowledge learnt from the previous chapters: the eddies causing the vorticity events may reach the sea bottom, increasing the current velocities, which in turn would let loose sediment resuspension and increased bottom water turbidity. Such a change in the water conditions would force adult *A. antennatus* individuals to move away from the fishing ground, probably downwards, to greater depths where they cannot be caught. This mechanism is consistent with the results found for other demersal species such as the decapod crustaceans *G. longipes* and *N. norvegicus*, *G. melastomus* and the two bentho-pelagic teleosts *M. poutassou* and *P. blennoides*.

Bibliography

Font, J., J. Salat, and J. Tintoré (1988), Permanent features in the general circulation of the Catalan Sea, *Oceanol. Acta*, *9*, 51–57.

García-Ladona, E., A. Castellón, J. Font, and J. Tintoré (1995), The Balearic current and volume transports in the Balearic basin, *Oceanologica Acta*, *19*, 489–497.

Pinot, J. M., J. L. López-Jurado, and M. Riera (2002), The canales experiment (19961998): interannual, seasonal, and mesoscale variability of the circulation

in the Balearic Channels, *Prog. Oceanogr.*, *55(3-4)*, 335–370, doi: 10.1016/S0079-6611(02)00139-8.

Ruiz, S., A. Pascual, B. Garau, F. Yannice, A. Álvarez, and J. Tintoré (2009), Mesoscale dynamics of the Balearic Front, integrating glider, ship and satellite data, *J. Mar. Syst.*, *78*, S3S16, doi: 10.1016/j.jmarsys.2009.01.007.

Conclusions

The main conclusions of this study are listed below:

- Sóller is hydrodynamically more active than Cabrera due to:
  - Greater velocities with higher variability.
  - Higher variability in both, temperature and salinity time series.
  - Greater number of eddies.
- The constant direction of the currents in Sóller and the nonzero mean speed values, hinder the lower limit fixation of the Balearic Current. This is important in two main aspects:
  - When calculating the dynamic height.
  - When computing the transport of the Balearic Current.
- A spectral analysis shows a 3.7 h period peak at both locations (Sóller and Cabrera) and other (3 h and 2 h) two just observed in the Sóller spectrum. The 3.7 h peak is surely related to some trapped wave around the island or the whole archipelago. The other two peaks could be associated with some resonance modes between mainland and Mallorca island.
- The number of eddies detected in Sóller were more than twice than in Cabrera. We have associated this fact with the presence of the Balearic Current and its associated instabilities, feature not present in the Cabrera site.
- Some of the eddies detected in Sóller extended their effects down to the bottom, as they were clearly detected at 900 m depth. On the contrary, the eddies detected in Cabrera affected just down to 300 m, as they were not detected in the instruments deployed at 500 m depth.
- The characteristics of one of the most intense eddies (6th in terms of circulation and the 8th with the largest radius) detected in Sóller since 1992 are the following:

  - It was developed from an instability of the Balearic Current.
  - Its core was formed by Western Mediterranean Intermediate Waters (WIW), which displaced the resident waters (LIW) to greater depths.
  - It affected to the velocities of the whole water column being greater at 900 m than at 500 m depth, reaching values up to 26 cm/s near the seabed.
  - A complete reversal of the current was observed at 500 m meanwhile a 90° downslope gyre was measured at 900 m depth.
  - This downslope gyre could be related to turbidity currents developed from resuspended sediments.

- An analysis of the evolution of the measured Total Flux Mass (TFM) in Sóller and Cabrera suggests that wind is the common forcing governing both sites TFM variability through an enhancement of Primary Production (PP).

- The Sóller TFM was found to be, in average, 2.8 times greater than Cabrera. The presence of the Balearic Current in Sóller could explain this difference since it is the source of the triggering factors such as the previous mentioned eddy.

- The presence of more intense eddies in Sóller and the possible influence of bottom-trapped waves could induce bottom sediment resuspensions.

- This generated sediments could affect to the ecosystems as it is shown by the reasonable good negative correlation found between monthly CPUE of the adult *A. antennatus* individuals in the fishing grounds off northern Mallorca and the mean surface vorticity (a proxy for the measured eddies) of the surrounding area.

- The suggested mechanism explaining this correlation could be:

  1. The eddies (main source of vorticity) present in the Sóller region, may reach the bottom and trigger sediment resuspension and increase bottom water turbidity.
  2. This change in the water conditions would force the adult individuals of *A. antennatus* to move away from the fishing ground, probably downwards, towards greater depths.
  3. This movement to greater depths would hinder to the bottom trawl fishery catching the adult individuals of *A. antennatus*.

- Other deep water demersal species analyzed exhibit different responses to the influence of the vorticity, but all of them consistent with the proposed mechanism.
- Besides the particular behavior of *A. antennatus* species, the vorticity episodes, much more intense during winter time in this zone, could be an additional factor explaining the decrease in the availability of large red shrimp individuals during these months at Sóller.

Future Work

Results from this thesis suggest two different scenarios where future work may be developed.

First, previous studies, such as the one developed by *Quetglas et al.* [2012], have shown that the population dynamics of a given species can be affected by climate oscillations. The effect of climate variability on fishing ecosystems is indeed one of the major questions addressed in the recently started research project *ECLIPSAME* (CTM2012-37701). It is hypothesized, once the previous point is clarified, that it will be useful to make projections of the influence of future climate conditions on fishing resources.

One of the main results of this thesis has been to relate the evolution of adult *A. antennatus* CPUE in the fishing ground of northern Mallorca to the surface vorticity of the surrounding area. In the light of this result and the previous mentioned *ECLIPSAME* project goals, if we would be able to know the future evolution of the vorticity in the area used for the study, we could intuit the effects of the climate oscillations over the evolution of the adult *A. antennatus* CPUE's.

Following this purpose, climate change models (such as the ones developed by the CIRCE project, `http://www.circeproject.eu/`) could be used for inferring, not only the typical oceanographic variables such as the thermosteric sea level [*Marcos and Amores*, 2014], but also for the future evolution of the vorticity in the area of interest. The first step for knowing its future evolution would be to validate the observations from the past, so we should compare the vorticity time series extracted from satellite observations with the vorticity calculated from the models. If a direct comparison between the observations and the vorticity calculated from the historical runs of the models is not good enough, one could always find a proxy (for example, the mean speed of the Balearic Current, as the eddies are mainly generated from an instability of this current) to compare the model outputs and the observations. Once we could reproduce the observed results with the model outputs, we would be in a good position to study the possible future evolution of the adult red shrimp CPUE in Sóller.

As a second possibility, in the frequency domain study developed in chapter 1, several frequencies with unknown origin were detected. These frequencies (3.7 h, 3 h and 2 h) seem to be related to some kind of resonance between the Balearic Islands and the Iberian Peninsula or to trapped waves in the shelf surrounding the islands. For determining if the observed frequencies are indeed related to resonant modes, three different approaches can be taken into account:

- The problem could be dealt analytically, trying to use some kind of artificial and simple bathymetry following the scheme developed by *Liu et al.* [2002].

- A 2D shallow water equation model (as the one used in *Monserrat et al.* [2014]) could be used to confirm this hypothesis or to find the real origin of these oscillations as this models are usually used to study other kinds of resonant waves such as meteotsunamis [*Vilibić et al.*, 2013]. This option should be the simplest one as the model could be performed with the *real* bathymetry of the Western Mediterranean (from the Strait of Gibraltar to the Sicilian Channel) and just with one layer (see for example *de la Asunción et al.* [2013]).

- A *complete* ocean model, such as the *Regional Ocean Modeling System (ROMS,* `https://www.myroms.org/`*)*, could be additionally used to assess this problem. This solution would give us more information, as this model includes physical algorithms and several coupled models for biogeochemical, bio-optical, sediment and sea ice applications among other features. Although this option could seem, a priori, the best, using the 2D shallow water equation would give us the required information by the simplest way and without possible spurious contamination from other processes running in the model.

Bibliography

de la Asunción, M., M. J. Castro, E. Fernández-Nieto, J. M. Mantas, S. O. Acosta, and J. M. González-Vida (2013), Efficient GPU implementation of a two waves TVD-WAF method for the two-dimensional one layer shallow water system on structured meshes, *Computers & Fluids*, *80*(0), 441 – 452, doi: 10.1016/j.compfluid.2012.01.012.

Liu, P. L.-F., S. Monserrat, and M. Marcos (2002), Analytical simulation of edge waves observed around the Balearic Islands, *Geophysical Research Letters*, *29*(17), 28–1–28–4, doi: 10.1029/2002GL015555.

Marcos, M., and A. Amores (2014), **Quantifying anthropogenic and natural contributions to thermosteric sea level rise**, *Geophysical Research Letters*, *41*.

Monserrat, S., I. Fine, A. Amores, and M. Marcos (2014), **Tidal influence on high frequency harbor oscillations in a narrow entrance bay**, *Submitted to Natural Hazards*, *XX*, XX.

Quetglas, A., F. Ordines, M. Hidalgo, S. Monserrat, S. Ruiz, A. Amores, J. Moranta, and E. Massutí (2012), **Synchronous combined effects of fishing and climate within a demersal community**, *ICES Journal of Marine Science*, doi: 10.1093/icesjms/fss181.

Vilibić, I., K. Horvath, N. Strelec Mahović, S. Monserrat, M. Marcos, A. Amores, and I. Fine (2013), **Atmospheric processes responsible for generation of the 2008 Boothbay meteotsunami**, *Natural Hazards*, doi: 10.1007/s11069-013-0811-y.

Appendix A: characteristics of the water masses.

The properties of the water masses mentioned along the text and their position in a Temperature-Salinity diagram (TS) are the following:

Water mass	Acronym	Potential Temperature (° C)		Salinity	
		Minim value	Maxim value	Minim value	Maxim value
Western Mediterranean Intermediate Waters	WIW	12.50	13.00	37.90	38.30
Levantine Intermediate Waters	LIW	13.00	13.50	38.45	38.60
Western Mediterranean Deep Waters	WMDW	12.70	12.90	38.40	38.50

Table A.1: Properties of the water masses.

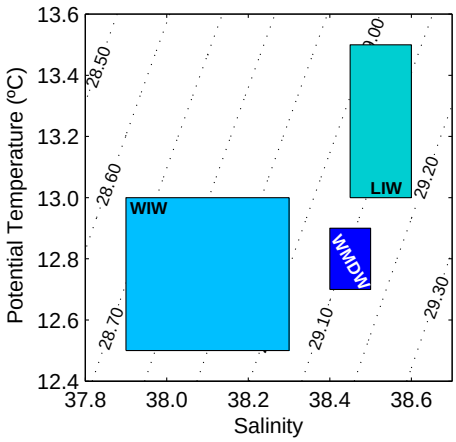

Figure A.1: TS diagram with the main Western Mediterranean water masses.

Appendix B: features of the moored instruments.

The next table is a summary of the instruments used and their main features:

Type	Main Variables	Accuracy	Resolution	Depth
CTD Seabird 37	Conductivity	$300\,\mu S \cdot m^{-1}$	$10\,\mu S \cdot m^{-1}$	300 m 500 m 700 m 900 m
	Temperature	$2 \cdot 10^{-3}\,^{\circ}C$	$0.1 \cdot 10^{-3}\,^{\circ}C$	
	Pressure	0.1% scale range	0.002% scale range	
Current meter Nortek Aquadopp	3 speed comp. (N, E, ↑↓)	1% measured value	$0.1\,cm \cdot s^{-1}$	500 m 900 m
	Temperature	$0.1^{\circ}C$	$0.01^{\circ}C$	
	Pressure	0.5% scale range	0.005% scale range	
Sediment trap PPS3/3 Technicap	Total Mass Flux (TMF)	.....	.....	900 m

Table B.1: Main characteristics of the moored instruments.

(a) CTD *(b) Current meter* *(c) Sediment trap*

Figure B.1: Moored instruments

List of Figures

1 Map showing the main characteristics of the ocean circulation in the Balearic subbasin. The positions of the moorings are marked with an S inside a star for Sóller mooring and a C inside a square for Cabrera mooring. Isobaths are plotted between 500 m and 2500 m with a step of 500 m. Black arrows indicate the permanent currents, while the grey ones indicate the temporal features. . . . 2

2 Scheme of the moorings configuration. 5

1.1 Map showing the main characteristics of the ocean circulation in the Balearic subbasin. The positions of the moorings are marked with an S inside a star for Sóller mooring and a C inside a square for Cabrera mooring. Isobaths are plotted between 500 m and 2500 m with a step of 500 m. Black arrows indicate the permanent currents, while the grey ones indicate the temporal features. The enclosed areas are 0.5°radius circles where the occurrence of eddies is checked (they seem to appear as ellipsoids due to the map projection). The bathymetric profiles correspond to the red lines indicated in the map. 13

1.2 Temperature time series after been filtered with a 24h low pass running average filter. The first column shows the measurements from the Sóller mooring and the second column shows the data registered at Cabrera. Each row corresponds to an increasing depth (300 m, 500 m, 700 m and 900 m). Colors indicate the time evolution to facilitate the comparison with other diagrams. Black patches indicate when an eddy was detected. The grey patch in the Sóller time series indicates the presence of two eddies at the same time. 16

1.3 Similar to Fig. 1.2 but for the salinity time series. 17

1.4 Ratios between the Sóller and Cabrera standard deviations at different depths. Temperature standard deviation ratios are shown in blue and the salinity standard deviation ratios in red. 18

1.5 The first two panels show the mean features (circulation, radius and duration) of all the eddies detected in each zone. Each following frame shows the features of every individual eddy for Cabrera (in red) and Sóller (in blue) with the same numbering as from Figs. 1.2 and 1.3. The trajectory from the starting point in green to the ending point in yellow is also indicated. The enclosed areas are the zones where the occurrence of eddies has been checked. Note that the sixth and seventh eddies in Sóller were simultaneous for some time but they have been plotted in different frames. 19

1.6 Temperature Salinity (TS) diagrams. Data have been smoothed by using a 24h low pass running average filter. The colors are the same than those used in Figs. 1.2 and 1.3 and they indicate the time evolution. 20

1.7 Progressive Vector Diagrams (PVD) for the current meters of both moorings. Data have been smoothed by using a 24h low pass running average filter. The scale relationship between the PVD scales is visible inside the Sóller 900 m PVD. The colors are the same than those used in Figs. 1.2 and 1.3 and indicate the time evolution. 21

1.8 Speed time series for the current meters of both moorings (panel *a* and *c* are from 500m depth and *b* and *d* are from 900m depth). Data have been smoothed by using a 24h low pass running average filter. The colors are the same as those used in Figs. 1.2 and 1.3 and indicate the time evolution. Black patches reveal when an eddy is detected. The grey patch in the Sóller time series indicates the presence of two eddies at the same time. 22

1.9 The number of times that a direction was measured (black histogram) and the corresponding mean speed for this orientation (red line) for each location and depth. 23

1.10 Velocity wavelets from Sóller at 500 m (a) and 900 m (c) and for Cabrera at 500 m (b) and 900 m (d) during the entire recording period. The vertical strips correspond to the mooring maintenances. The mother function used in wavelet computations is Morlet. . . . 24

1.11 Pressure wavelets from Sóller at 300 m (a) and 900 m (c) and for Cabrera at 300 m (b) and 900 m (d) during the entire recording period. The vertical strips correspond to the mooring maintenances. The mother function used in wavelet computations is Morlet. . . . 24

1.12 Pressure spectra for Sóller, at all available depths, for a period when an eddy was present in the area exerting a significant influence on the mooring (a) (from 18/11/2009 to 14/3/2010) and when no eddy was observed in the zone (b) (from 1/4/2010 to 26/7/2010). The main tide components are indicated in grey; the peaks with a possible resonant origin are indicated in red; the peaks related with the inertial frequency are indicated in green. 25

1.13 Comparison between the 900 m depth pressure spectra from Sóller (red) and Cabrera (blue) during the period between April 1 and July 26, 2010. The main tide components are indicated in grey; the peaks with a possible resonant origin are indicated in red. . . 26

2.1 Map of the characteristics of the ocean circulation in the Balearic subbasin. The position of the mooring is marked with an S inside a star. Isobaths are plotted between 500 and 2500 m with a step of 500 m. Solid arrows indicate permanent currents, while dashed arrows are temporal features. 35

2.2 Sea surface height (SSH) images of the formation, development, and subsequent disappearance of the eddy. Colors indicate SSH (in cm); vectors are the direction and modulus of the geostrophic currents associated to the SSH field; and the star with an S inside shows the mooring position. The dark enclosed area delimits the perimeter of the eddy following the criteria in *Nencioli et al.* [2010] (see text). 40

2.3 Main features of the eddy: the equivalent radius (black), the maximum SSH value (blue), and the circulation (red). In the inset map, the white line shows the trajectory of the eddy, and the red enclosed area shows the evolution of its surface location. The mooring position is marked with a star with an S inside. The thick black rectangle delimits the area used for the study of the recurrence of the phenomenon (see text for details). 41

2.4 SST images of the same moments of the first four SSH images. Colors indicate the temperature of the sea surface; and the star with an S inside represents the mooring position. The dark enclosed area delimits the perimeter of the eddy following the criteria in *Nencioli et al.* [2010] 42

2.5 Progressive vector diagram (PVD) of the current meters at (a) 500 m and (b) 900 m depth from 10 November 2010 to 5 January 2011. 43

2.6 Currents measured in (a and b) 500 m and (c and d) 900 m decomposed along (see Figures 2.6a and 2.6c) and across (see Figures 2.6b and 2.6d) the coast components. The original record is presented in black and grey, and the 2 day low-pass-filtered series is presented in red. 43
2.7 Time series of (a) salinity, (b) temperature, (c) potential density, and (d) pressure recorded by the Seabird37 at (1) 300 m and (2) 700 m from 10 November 2010 to 5 January 2011. The original record is presented in black and grey, and the 2 day low-pass-filtered series is presented in red. 44
2.8 *TS* diagram of 300m (series with stars) and 700m (dotted series) recorded from 10 November 2010 to 5 January 2011. The original record is presented in black and grey, and the 2 day low-pass-filtered series is presented in red. 45
2.9 (a) Temporal evolution of the vertical structure of the density interpolating the values in depth using splines and density time series (without mean value) as measured for the moored instruments at (b) 300 m, (c) 500 m, (d) 700 m, and (e) 900 m. 45
2.10 Clockwise wavelet of currents at (a) 500 m and (b) 900 m. f is the inertial frequency (18.73 h). Units are dB. 46

3.1 Map of the zone of interest. Black arrows show the permanent currents of the zone. Sóller and Cabrera moorings are marked with an S surrounded by a star and with a C surrounded by a square. The decomposition in along- and across-slope components is indicated on the mooring position. The position of the Dragonera wind buoy is shown by a blue buoy. Orange dots mark the location of the HIRLAM model wind points used. Isobaths are plotted between 500 m and 2500 m with a step of 500 m. 57
3.2 TMF recorded by the sediment trap at Sóller a), TMF collected by the trap at Cabrera b), Wind speed time series from the positions marked as orange dots in Fig. 3.1 c), Chl-a time series from satellite observations d) and Phytopigments recorded by the sediment traps e). Grey bands correspond to two selected intervals when large amounts of TFM were recorded. 62
3.3 The lithogenic fraction (brown) and the organic matter (OM) fraction (green) recorded in Sóller a), the total kinetic energy (KE) computed for the current meters from 500 m (black line) and 900 m (grey line) b) and the along-slope KE (uKE) c) and across-slope KE (vKE) d) measured in Sóller. Panels e), f) g) and h) show the same magnitudes but as measured in Cabrera 64

3.4 Velocity wavelets from the 900 m depth current meter at Sóller. The mother function is Morlet. 65

4.1 Map of the studied area in the western Mediterranean. The unbroken line encloses Sóller fishing grounds where *Aristeus antennatus* is exploited and the broken line corresponds to the zone where the time series of vorticity has been calculated. Mooring location is indicated by a star. 75
4.2 a) Monthly averaged time series of vorticity (black) and *Aristeus antennatus* CPUEs (green). b) Correlation between these two series, showing the maximum correlation (-0.35) around lag 0. Black line represents the 95% confidence level. 80
4.3 a) Derivative time series of vorticity (black) and *Aristeus antennatus* CPUEs (green). In the series of the vorticity derivative, the negative values have been fixed at 0, while the positive values of the derivative CPUEs series have been set at 0. Notice that the last one has suffered a change of sign. b) Correlation between these two series show the maximum value (0.48) at lag 0. Black line represents the 95% confidence level. 81
4.4 Sea Surface Height (SSH) image from December 1, 2010. It shows an eddy in the region analyzed. The star shows the mooring position. 82
4.5 24h low-pass filtered speed series of 500 (a) and 900 (b) m depth current meters of the mooring for the whole recorded period. Blue indicates the low speed values degrading to red, which indicates the high values. (c) and (d) are the progressive vector diagrams for 500 and 900 m depth, respectively. The different colors coincide temporally with the speed time series. Enclosed areas represent moments where an eddy is present in the zone. Ellipse number 1 highlight an eddy which is strongly present at 500 m depth, but weakly present at 900 m; number 2 ellipse shows an eddy which reached to 500 m depth, although not right up to 900 m; and number 3 ellipse illustrates an eddy which arrived strongly to the 500 and 900 m depths. Note that in the PVDs the ratio between the scales of x and y axis is 2:1. 83
4.6 Total Flux Mass (TFM) collected by the sediment trap during the whole sampling time. The gap in the data is due to the unavailability of ship for carrying out the mooring maintenance. The dashed ellipses show the increment of TFM due to the eddies reported in Fig. 4.5. 84
4.7 Acoustic backscattering (a) and speed (b) measured by the 900 m current meter during the third episode. 84

4.8 Zoom of the Fig. 4.2, where the effect of the vorticity (blue) on the *Aristeus antennatus* CPUEs (green) can be seen. The colored bands indicate the amount of particles that would be re-suspended. 85
4.9 Time series of CPUEs for five demersal species (by catch) from the deep water trawl fishery and its correlation with the absolute value of surface vorticity. 87

A.1 TS diagram with the main Western Mediterranean water masses. 107

B.1 Moored instruments 109

List of Tables

2.1 List of events that fulfill the selection criteria from 1992 to 2011 . 48

A.1 Properties of the water masses. 107

B.1 Main characteristics of the moored instruments. 109

Global Bibliography

Acosta, J., M. Canals, J. López-Martínez, A. Muñoz, P. Herranz, R. Urgeles, C. Palomo, and J. L. Casamor (2003), The Balearic Promontory geomorphology (western Mediterranean): morphostructure and active processes, *Geomorphology*, *49*(34), 177 – 204, doi: 10.1016/S0169-555X(02)00168-X.

Álvarez, A., J. Tintoré, and A. Sabatés (1996), Flow modification and shelf-slope exchange induced by a submarine canyon off the northeast Spanish coast, *J. Geophys. Res.*, *101*, 12,043–12,055, doi: 10.1029/95JC03554.

Amores, A., and S. Monserrat (2014), **Hydrodynamic comparison between the north and south of Mallorca Island**, *J. Marine Systems*, doi: 10.1016/j.jmarsys.2014.01.005.

Amores, A., S. Monserrat, and M. Marcos (2013a), **Vertical structure and temporal evolution of an anticyclonic eddy in the Balearic Sea (western Mediterranean)**, *J. Geophys. Res. Oceans*, *118*, 2097–2106, doi: 10.1002/jgrc.20150.

Amores, A., L. Rueda, S. Monserrat, B. Guijarro, C. Pasqual, and E. Massutí (2013b), **Influence of the hydrodynamic conditions on the accessibility of Aristeus antennatus and other demersal species to the deep water trawl fishery off the Balearic Islands (western Mediterranean)**, *J. Marine Systems*, doi: 10.1016/j.jmarsys.2013.11.014.

Arrobas, I., and A. Ribeiro-Cascalho (1987), On the biology and fishery of Aristeus antennatus (Risso, 1816) in the south Portuguese coast, *Inv. Pesq.*, *51 (suppl. 1)*, 233–243.

Balbín, R., M. M. Flexas, J. L. López-Jurado, M. Peña, A. Amores, and F. Alemany (2012), **Vertical velocities and biological consequences at a front detected at the Balearic Sea**, *Cont. Shelf Res.*, *47*, 28–41, doi: 10.1016/j.csr.2012.06.008.

Beentjesa, M. P., and J. A. Renwick (2001), The Relationship between Red Cod, Pseudophycis Bachus, Recruitment and Environmental Variables in New Zealand, *Environmental Biology of Fishes*, *61*(3), 315–328, doi: 10.1023/A:1010943906264.

Bombace, G. (1975), Considerazioni sulla distribuzione delle popolazioni di livello batiale con particolare riferimento a quelle bentoniche, *Pubbl. Staz. Zool. Napoli*, *39 (suppl 1)*, 7–21.

Bosley, K. L., J. W. Lavelle, R. D. Brodeur, W. W. Wakefield, R. L. Emmett, E. T. Baker, and K. M. Rehmke (2004), Biological and physical processes in and around Astoria submarine Canyon, Oregon, USA, *Journal of Marine Systems*, *50*(12), 21 – 37, doi: 10.1016/j.jmarsys.2003.06.006.

Bouffard, J., L. Renault, S. Ruiz, A. Pascual, C. Dufau, and J. Tintoré (2012), Sub-surface small-scale eddy dynamics from multi-sensor observations and modeling, *Prog. Oceanogr.*, *106*, 62–79, doi: 10.1016/j.pocean.2012.06.007.

Browman, H. I., and K. I. Stergiou (2004), Perspectives on ecosystem-based approaches to the management of marine resources, *Mar Ecol Prog Ser*, *274*, 269–303.

Canals, M., P. Puig, X. D. de Madron, S. Heussner, A. Palanques, and J. Fabres (2006), Flushing submarine canyons, *Nature*, *444 (7117)*, 354–357, doi: 10.1038/nature05271.

Carbonell, A., M. Carbonell, M. Demestre, A. Grau, and S. Monserrat (1999), The red shrimp Aristeus antennatus (Risso, 1816) fishery and biology in the Balearic Islands, Western Mediterranean, *Fisheries Research*, *44*, 1–13, doi: 10.1016/S0165-7836(99)00079-X.

Carrère, L., and F. Lyard (2003), Modelling the barotropic response of the global ocean to atmospheric wind and pressure forcing Comparisons with observations, *Geophys. Res. Lett.*, *30*, doi: 10.1029/2002GL016473.

Cartes, J. E. (1993), Diets of deep-sea brachyuran crabs in the Western Mediterranean Sea, *Marine Biology*, *117*, 449–457, doi: 10.1007/BF00349321.

Cartes, J. E. (1994), Influence of depth and season on the diet of the deep-water aristeid Aristeus antennatus along the continental slope (400 to 2300 m) in the Catalan Sea (western Mediterranean), *Marine Biology*, *120*, 639–648, doi: 10.1007/BF00350085.

Cartes, J. E., and M. Carrassón (2004), Influence of trophic variables on the depth-range distributions and zonation rates of deep-sea megafauna: the case of the Western Mediterranean assemblages, *Deep Sea Research Part I: Oceanographic Research Papers*, *51*, 263–279, doi: 10.1016/j.dsr.2003.10.001.

Cartes, J. E., V. Papiol, and B. Guijarro (2008), The feeding and diet of the deep-sea shrimp Aristeus antennatus off the Balearic Islands (Western Mediterranean): Influence of environmental factors and relationship with the biological cycle, *Progress in Oceanography*, *79*, 37–54, doi: 10.1016/j.pocean.2008.07.003.

Cartes, J. E., M. Hidalgo, V. Papiol, E. Massutí, and J. Moranta (2009), Changes in the diet and feeding of the hake Merluccius merluccius at the shelf-break of the Balearic Islands: Influence of the mesopelagic-boundary community, *Deep Sea Research Part I: Oceanographic Research Papers*, *56*(3), 344 – 365, doi: 10.1016/j.dsr.2008.09.009.

Company, J. B., F. Sardà, P. Puig, J. E. Cartes, and A. Palanques (2003), Duration and timing of reproduction in decapod crustaceans of the NW Mediterranean continental margin: is there a general pattern?, *Marine Ecology Progress Series*, *261*, 201–216.

Company, J. B., P. Puig, F. Sardà, A. Palanques, M. Latasa, and R. Scharek (2008), Climate influence on deep sea populations, *PLoS ONE*, *3*, e1431, doi: 10.1371/journal.pone.0001431.

Cook, R. M., A. Sinclair, and G. Stefansson (1997), Potential collapse of North Sea cod stocks, *Nature*, *385*, 521–522, doi: 10.1038/385521a0.

Cristo, M., and J. E. Cartes (1998), A comparative study of the feeding ecology of Nephrops norvegicus (L.), (Decapoda: Nephropidae) in the bathyal Mediterranean and the adjacent Atlantic, *Scientia Marina*, *62 (Suppl. 1)*, 81–90, doi: 10.3989/scimar.1998.62s181.

Danovaro, R., A. Dell'Anno, M. Fabiano, A. Pusceddu, and A. Tselepides (2001), Deep-sea ecosystem response to climate changes: the eastern Mediterranean case study, *Trends in Ecology & Evolution*, *16*(9), 505 – 510, doi: 10.1016/S0169-5347(01)02215-7.

D'Asaro, E. A. (1995), Upper-ocean inertial currents forced by a strong storm. Part III: Interaction of inertial currents and mesoscale eddies, *J. Phys. Oceanogr.*, *25*, 2953–2958.

de la Asunción, M., M. J. Castro, E. Fernández-Nieto, J. M. Mantas, S. O. Acosta, and J. M. González-Vida (2013), Efficient GPU implementation of

a two waves TVD-WAF method for the two-dimensional one layer shallow water system on structured meshes, *Computers & Fluids*, *80*(0), 441 – 452, doi: 10.1016/j.compfluid.2012.01.012.

Demestre, M., and P. Martín (1993), Optimum exploitation of a demersal resource in the western Mediterranean: the fishery of the deep-water shrimp Aristeus antennatus (Risso, 1816), *Scientia Marina*, *57 (2-3)*, 175–182.

Emery, W. J., and R. E. Thomson (1998), *Data Analysis Methods in Physical Oceanography*, Pergamon, Netherlands, pp. 500509.

Estrada, M., and J. Salat (1989), Phytoplankton assemblages of deep and surface water layers in a Mediterranean frontal zone, *Scientia Marina*, *53 (2-3)*, 203–214.

Fabres, J., A. Calafat, A. Sanchez-Vidal, M. Canals, and S. Heussner (2002), Composition and spatio-temporal variability of particle fluxes in the Western Alboran Gyre, Mediterranean Sea, *Journal of Marine Systems*, *33-34*, 431–456, doi: 10.1016/S0924-7963(02)00070-2.

Falkowski, P., R. J. Scholes, E. Boyle, J. Canadell, D. Canfield, J. Elser, N. Gruber, K. Hibbard, P. Högberg, S. Linder, F. T. Mackenzie, B. I. Moore, T. Pedersen, Y. Rosenthal, S. Seitzinger, V. Smetacek, and W. Steffen (2000), The global carbon cycle: a test of our knowledge of earth as a system, *Science*, *290*, 291–6.

Fanelli, E., J. Rey, P. Torres, and L. G. de Sola (2009), Feeding habits of blackmouth catshark Galeus melastomus Rafinesque, 1810 and velvet belly lantern shark Etmopterus spinax (Linnaeus, 1758) in the western Mediterranean, *J. Appl. Ichthyol.*, *25 (Suppl. 1)*, 83–93, doi: 10.1111/j.1439-0426.2008.01112.x.

Flexas, M., X. D. de Madron, M. A. Garcia, M. Canals, and P. Arnau (2002), Flow variability in the Gulf of Lions during the MATER HFF experiment (MarchMay 1997), *Journal of Marine Systems*, *33-34*, 197–214, doi: 10.1016/S0924-7963(02)00059-3.

Font, J., J. Salat, and J. Tintoré (1988), Permanent features in the general circulation of the Catalan Sea, *Oceanol. Acta*, *9*, 51–57.

Gage, J. D., and P. A. Tyler (1991), *Deep-Sea Biology: A Natural History of Organisms at the Deep-Sea Floor*, p. 504, Cambridge University Press, London.

García, E., J. Tintoré, J. M. Pinot, J. Font, and M. Manriquez (1994), Surface Circulation and Dynamics of the Balearic Sea, *Coastal Estuarine Stud.*, *46*, 73–91, doi: 10.1029/CE046p0073.

García-Ladona, E., A. Castellón, J. Font, and J. Tintoré (1995), The Balearic current and volume transports in the Balearic basin, *Oceanologica Acta*, *19*, 489–497.

Ghidalia, W., and F. Bourgois (1961), Influence of temperature and light on the distribution of shrimps in medium and great depths, *Gfcm Studies and Reviews*, *16*, 49.

Guijarro, B., and E. Massutí (2006), Selectivity of diamond- and square-mesh codends in the deepwater crustacean trawl fishery off the Balearic Islands (western Mediterranean), *ICES J. Mar. Sci.*, *63 (1)*, 52–67, doi: 10.1016/j.icesjms.2005.08.011.

Guijarro, B., E. Massutí, J. Moranta, and P. Díaz (2008), Population dynamics of the red shrimp Aristeus antennatus in the Balearic Islands (western Mediterranean): Short spatio-temporal differences and influence of environmental factors, *Journal of Marine Systems*, *71 (3-4)*, 385–402, doi: 10.1016/j.jmarsys.2007.04.003.

Guijarro, B., E. Fanelli, J. Moranta, J. E. Cartes, and E. Massutí (2012), Small-scale differences in the distribution and population dynamics of pandalid shrimps in the western Mediterranean in relation to environmental factors, *Fisheries Research*, *119-120*, 33–47, doi: 10.1016/j.fishres.2011.12.001.

Hidalgo, M., E. Massutí, J. Moranta, J. Cartes, J. Lloret, P. Oliver, and B. Morales-Nin (2008a), Seasonal and short spatial patterns in European hake (Merluccius merluccius L.) recruitment process at the Balearic Islands (western Mediterranean): The role of environment on distribution and condition, *Journal of Marine Systems*, *71*(34), 367 – 384, doi: 10.1016/j.jmarsys.2007.03.005.

Hidalgo, M., J. Tomás, H. Høie, B. Morales-Nin, and U. S. Ninnemann (2008b), Environmental influences on the recruitment process inferred from otolith stable isotopes in Merluccius merluccius off the Balearic Islands, *Aquat Biol*, *3(3)*, 195 – 207, doi: 10.3354/ab00081.

Honjo, S., S. J. Manganini, R. A. Krishfield, and R. Francois (2008), Particulate organic carbon fluxes to the ocean interior and factors controlling the biological pump: A synthesis of global sediment trap programs since 1983, *Progress in Oceanography*, *76*, 217–285, doi: 10.1016/j.pocean.2007.11.003.

Hyder, P., K. Bigelow, R. Brainard, M. Seki, J. Firing, and P. Flament (2009), Migration and Abundance of Bigeye Tuna (*Thunnus obesus*), and Other Pelagic Species, Inferred from Catch Rates and Their Relation to Variations in the Ocean Environment, *SOEST*, *09-02*.

Ivanov, V., G. Shapiro, J. Huthnance, D. Aleynik, and P. Golovin (2004), Cascades of dense water around the world ocean, *Progress in Oceanography*, *60*(1), 47 – 98, doi: 10.1016/j.pocean.2003.12.002.

Kai, E. T., and F. Marsac (2010), Influence of mesoscale eddies on spatial structuring of top predators communities in the Mozambique Channel, *Progress in Oceanography*, *86*(12), 214 – 223, doi: 10.1016/j.pocean.2010.04.010.

Lee, C., S. Wakeham, and C. Arnosti (2004), Particulate Organic Matter in the Sea: The Composition Conundrum, *AMBIO: A Journal of the Human Environment*, *33*, 565–575, doi: 10.1579/0044-7447-33.8.565.

Lin, H.-P., G. Charmantier, P. Thuet, and J.-P. Trilles (1992), Effects of turbidity on survival, osmoregulation and gill Na^+-K^+ ATPase in juvenile shrimp *Penaeus japonicus*, *Marine Ecology Progress Series*, *90*, 31–37.

Liu, P. C., and G. S. Miller (1996), Wavelet transforms and ocean current data analysis, *J. Atmos. Oceanic Technol.*, *13*, 1090–1099.

Liu, P. L.-F., S. Monserrat, and M. Marcos (2002), Analytical simulation of edge waves observed around the Balearic Islands, *Geophysical Research Letters*, *29*(17), 28–1–28–4, doi: 10.1029/2002GL015555.

Liu, Y., C. Dong, Y. Guan, D. Chen, J. McWilliams, and F. Nencioli (2012), Eddy analysis in the subtropical zonal band of the North Pacific Ocean, *Deep Sea Res., Part I 68*, 54–67, doi: 10.1016/j.dsr.2012.06.001.

Lohrmann, A. (2001), Monitoring sediment concentration with acoustic backscattering instruments, *Nortek Tech. notes*, *No. N4000712*.

Lopez-Fernandez, P., S. Bianchelli, A. Pusceddu, A. Calafat, R. Danovaro, and M. Canals (2013), Bioavailable compounds in sinking particulate organic matter, Blanes Canyon, NW Mediterranean Sea: Effects of a large storm and sea surface biological processes, *Progress in Oceanography*, *118*(0), 108 – 121, doi: 10.1016/j.pocean.2013.07.022.

López-García, M. J., C. Millot, J. Font, and E. García-Ladona (1994), Surface circulation variability in the Balearic Basin, *J. Geophys. Res.*, *99(C2)*, 3285–3296, doi: 10.1029/93JC02114.

López-Jurado, J. L., M. Marcos, and S. Monserrat (2008), Hydrographic conditions affecting two fishing grounds of Mallorca island (Western Mediterranean): during the IDEA Project (20032004), *Journal of Marine Systems*, *71*, 303–315, doi: 10.1016/j.jmarsys.2007.03.007.

Marcos, M., and A. Amores (2014), **Quantifying anthropogenic and natural contributions to thermosteric sea level rise**, *Geophysical Research Letters*, *41*.

Martín, J., J.-C. Miquel, and A. Khripounoff (2010), Impact of open sea deep convection on sediment remobilization in the western Mediterranean, *Geophysical Research Letters*, *37*, 13,60413,610, doi: 10.1029/2010GL043704.

Massutí, E., S. Monserrat, P. Oliver, J. Moranta, J. L. López-Jurado, M. Marcos, J. M. Hidalgo, B. Guijarro, A. Carbonell, and P. Pereda (2008), The influence of oceanographic scenarios on the population dynamics of demersal resources in the western Mediterranean: Hypothesis for hake and red shrimp off Balearic Islands, *Journal of Marine Systems*, *71 (3-4)*, 421–438, doi: 10.1016/j.jmarsys.2007.01.009.

Massutí, E., M. Olivar, S. Monserrat, L. Rueda, and P. Oliver (2014), Towards understanding the influence of environmental conditions on demersal resources and ecosystems in the western Mediterranean: Motivations, aims and methods of the IDEADOS project, *Journal of Marine Systems*, doi: 10.1016/j.jmarsys.2014.01.013.

Maynou, F. (2008), Environmental causes of the fluctuations of red shrimp (Aristeus antennatus) landings in the Catalan Sea, *Journal of Marine Systems*, *71 (3-4)*, 294–302, doi: 10.1016/j.jmarsys.2006.09.008.

Maynou, F., and J. E. Cartes (2000), Community structure of bathyal decapod crustaceans off south-west Balearic Islands (western Mediterranean): seasonality and regional patterns in zonation, *Journal of the Marine Biological Association of the United Kingdom*, *80*, 789–798.

Maynou, F., and F. Sardà (1997), Nephrops norvegicus population and morphometrical characteristics in relation to substrate heterogeneity, *Fisheries Research*, *30 (1-2)*, 139–149, doi: 10.1016/S0165-7836(96)00549-8.

Mertens, C., and F. Schott (1998), Interannual variability of deep-water formation in the northwestern Mediterranean, *J. Phys. Oceanogr.*, *28*, 1410–1424, doi: 10.1175/1520-0485(1998)028⟨1410:IVODWF⟩2.0.CO;2.

Millot, C. (1985), Evidence of a several-day propagating wave, *Journal of Physical Oceanography*, *15*, 258–272.

Millot, C. (1994), *Models and data: A synergetic approach in the western Mediterranean Sea*, Kluwer Acad., Dordrecht, Netherlands, pp. 407425.

Millot, C. (1999), Circulation in the Western Mediterranean Sea, *Journal of Marine Systems*, *20*, 423–442, doi: 10.1016/S0924-7963(98)00078-5.

Millot, C., M. Benzohra, and I. Taupier-Letage (1997), Circulation off Algeria inferred from the Mediprod-5 current meters, *Deep Sea Research Part I: Oceanographic Research Papers*, *44*, 1467–1495, doi: 10.1016/S0967-0637(97)00016-2.

Monserrat, S., J. L. López-Jurado, and M. Marcos (2008), A mesoscale index to describe the regional circulation around the Balearic Islands, *J. Mar. Syst.*, *71*, 413–420, doi: 10.1016/j.jmarsys.2006.11.012.

Monserrat, S., I. Fine, A. Amores, and M. Marcos (2014), **Tidal influence on high frequency harbor oscillations in a narrow entrance bay**, *Submitted to Natural Hazards*, *XX*, XX.

Moranta, J., A. Quetglas, E. Massutí, B. Guijarro, M. Hidalgo, and P. Diaz (2008), Spatio-temporal variations in deep-sea demersal communities off the Balearic Islands (western Mediterranean), *Journal of Marine Systems*, *71 (3-4)*, 346–366, doi: 10.1016/j.jmarsys.2007.02.029.

Mortlock, R. A., and P. N. Froelich (1989), A simple method for the rapid determination of biogenic opal in pelagic marine sediments, *Deep Sea Research Part A. Oceanographic Research Papers*, *36*(9), 1415 – 1426, doi: 10.1016/0198-0149(89)90092-7.

Nencioli, F., C. Dong, T. Dickey, L. Washburn, and J. C. McWilliams (2010), A vector geometry-based eddy detection algorithm and its application to a high-resolution numerical model product and high-frequency radar surface velocities in the southern California bight, *J. Atmos. Oceanic Technol.*, *27*, 564–579, doi: 10.1175/2009JTECHO725.1.

OBrien, M. C., H. Melling, T. F. Pedersen, and R. W. Macdonald (2013), The role of eddies on particle flux in the Canada Basin of the Arctic Ocean, *Deep Sea Research Part I: Oceanographic Research Papers*, *71*, 1–20, doi: 10.1016/j.dsr.2012.10.004.

Owen, R. W. (1981), Fronts and eddies in the sea: mechanisms, interactions and biological effects, *Analysis of marine ecosystems*, pp. 197–233.

Palamara, L., J. Manderson, J. Kohut, M. J. Oliver, S. Gray, and J. Goff (2012), Improving habitat models by incorporating pelagic measurements from coastal ocean observatories, *Marine Ecology Progress Series*, *447*, 15–30, doi: 10.3354/meps09496.

Palmer, M., A. Quetglas, B. Guijarro, J.Moranta, F. Ordines, and E. Massutí (2009), Performance of artificial neural networks and discriminant analysis in predicting fishing tactics from multispecific fisheries, *Canadian Journal of Fisheries and Aquatic Sciences*, *66*, 224–237, doi: 10.1139/F08-208.

Papaconstantinou, C., and K. Kapiris (2001), Distribution and population structure of the red shrimp (Aristeus antennatus) on an unexploited fishing ground in the Greek Ionian Sea, *Aquatic Living Resources*, *14*, 303–312, doi: 10.1016/S0990-7440(01)01128-7.

Pascual, A., B. B. Nardelli, G. Lanicol, M. Emelianov, and D. Gomis (2002), A case of an intense anticyclonic eddy in the Balearic Sea (western Mediterranean), *J. Geophys. Res.*, *107(C11)*, 3183, doi: 10.1029/2001JC000913.

Pasqual, C., A. Sanchez-Vidal, D. Zúñiga, A. Calafat, M. Canals, X. D. de Madron, P. Puig, S. Heussner, A. Palanques, and N. Delsaut (2010), Flux and composition of settling particles across the continental margin of the Gulf of Lion: the role of dense shelf water cascading, *Biogeosciences*, *7*, 217–231, doi: 10.5194/bg-7-217-2010.

Pasqual, C., A. Amores, M. Flexas, S. Monserrat, and A. Calafat (2013), **Environmental factors controlling particulate mass fluxes on the Mallorca continental slope (Western Mediterranean Sea)**, *Accepted in J. Marine Systems*, *XXX*, XXX, doi: XXX.

Pedlosky, J. (1979), *Geophysical fluid dynamics*, Springer-Verlag, New York and Berlin, pp. 624.

Pinot, J. M., J. Tintoré, and D. Gomis (1994), Quasi-synoptic mesoscale variability in the Balearic Sea, *Deep Sea Research Part I: Oceanographic Research Papers*, *41 (5-6)*, 897–914, doi: 10.1016/0967-0637(94)90082-5.

Pinot, J. M., J. L. López-Jurado, and M. Riera (2002), The canales experiment (19961998): interannual, seasonal, and mesoscale variability of the circulation in the Balearic Channels, *Prog. Oceanogr.*, *55(3-4)*, 335–370, doi: 10.1016/S0079-6611(02)00139-8.

Puig, P., J. B. Company, F. Sardà, and A. Palanques (2001), Responses of deep-water shrimp populations to intermediate nepheloid layer detachments on the Northwestern Mediterranean continental margin, *Deep Sea Research Part I: Oceanographic Research Papers*, *48*, 21952207, doi: 10.1016/S0967-0637(01)00016-4.

Puillat, I., I. Taupier-Letage, and C. Millot (2002), Algerian Eddies lifetime can near 3 years, *Journal of Marine Systems*, *31*(4), 245 – 259, doi: http://dx.doi.org/10.1016/S0924-7963(01)00056-2.

Pusceddu, A., G. Sarà, M. Armeni, M. Fabiano, and A. Mazzola (1999), Seasonal and spatial changes in the sediment organic matter of a semi-enclosed marine system (W-Mediterranean Sea), *Hydrobiologia*, *397*, 59–70, doi: 10.1023/A:1003690313842.

Pusceddu, A., S. Bianchelli, M. Canals, A. Sanchez-Vidal, X. D. D. Madron, S. Heussner, V. Lykousis, H. de Stigter, F. Trincardi, and R. Danovaro (2010), Organic matter in sediments of canyons and open slopes of the Portuguese, Catalan, Southern Adriatic and Cretan Sea margins, *Deep Sea Research Part I: Oceanographic Research Papers*, *57*(3), 441 – 457, doi: 10.1016/j.dsr.2009.11.008.

Quetglas, A., F. Ordines, M. Hidalgo, S. Monserrat, S. Ruiz, A. Amores, J. Moranta, and E. Massutí (2012), **Synchronous combined effects of fishing and climate within a demersal community**, *ICES Journal of Marine Science*, doi: 10.1093/icesjms/fss181.

Raimbault, P., B. Coste, M. Boulhadid, and B. Boudjellal (1993), Origin of high phytoplankton concentration in deep chlorophyll maximum (DCM) in a frontal region of the Southwestern Mediterranean Sea (algerian current), *Deep Sea Research Part I: Oceanographic Research Papers*, *40 (4)*, 791–804, doi: 10.1016/0967-0637(93)90072-B.

Ramos, A. G., J. Santiago, P. Sangra, and M. Canton (1996), An application of satellite-derived sea surface temperature data to the skipjack (Katsuwonus pelamis Linnaeus, 1758) and albacore tuna (Thunnus alalunga Bonaterre, 1788) fisheries in the north-east Atlantic, *International Journal of Remote Sensing*, *17*(4), 749–759, doi: 10.1080/01431169608949042.

Relini, G., and L. O. Relini (1987), The decline of red-shrimp stocks in the gulf of Genoa, *Investigacion Pesquera*, *51*, 245260.

Relini, M., P. Maiorano, G. D'Onghia, L. O. Relini, A. Tursi, and M. Panza (2000), A pilot experiment of tagging the deep shrimp Aristeus antennatus (Risso, 1816), *Scientia Marina*, *64*, 357–361, doi: 10.3989/scimar.2000.64n3357.

Rio, M.-H., P.-H. Poulain, A. Pascual, E. Mauri, G. Larnicol, and R. Santoleri (2007), A mean dynamic topography of the mediterranean sea computed from

altimetric data, in-situ measurements and a general circulation model, *J. Mar. Syst.*, *65*, 484–508, doi: 10.1016/j.jmarsys.2005.02.006.

Rowe, G. T., P. T. Polloni, and R. L. Haedrich (1982), The deep-sea macrobenthos on the continental margin of the northwest Atlantic Ocean, *Deep Sea Research Part A. Oceanographic Research Papers*, *29*(2), 257 – 278, doi: 10.1016/0198-0149(82)90113-3.

Rubio, A., B. Barnier, M. E. G. Jordà, and P. Marsaleix (2009), Origin and dynamics of mesoscale eddies in the Catalan Sea (NWMediterranean): Insight from a numerical model study, *J. Geophys. Res.*, *114*, C06,009, doi: 10.1029/2007JC004245.

Ruiz, S., A. Pascual, B. Garau, F. Yannice, A. Álvarez, and J. Tintoré (2009), Mesoscale dynamics of the Balearic Front, integrating glider, ship and satellite data, *J. Mar. Syst.*, *78*, S3S16, doi: 10.1016/j.jmarsys.2009.01.007.

Sammari, C., C. Millot, and L. Prieur (1995), Aspects of the seasonal and mesoscale variabilities of the Northern Current in the western Mediterranean Sea inferred from the PROLIG-2 and PROS-6 experiments, *Deep Sea Research Part I: Oceanographic Research Papers*, *42 (6)*, 893–917, doi: 10.1016/0967-0637(95)00031-Z.

Sanchez-Vidal, A., M. Canals, A. Calafat, G. Lastras, R. Pedrosa-Pàmies, M. Menéndez, R. Medina, J. B. Company, B. Hereu, J. Romero, and T. Alcoverro (2012), Impacts on the Deep-Sea Ecosystem by a Severe Coastal Storm, *PLoS ONE 7(1)*, *e30395*, doi: 10.1371/journal.pone.0030395.

Sardà, F., J. E. Cartes, and W. Norbis (1994), Spatia-temporal structure of the deep-water shrimp Aristeus antennatus (Decapoda: Aristeidae) population in the western Mediterranean, *Fishery Bulletin*, *92*, 599–607.

Sardà, F., F. Maynou, and L. Talló (1997), Seasonal and spatial mobility patterns of rose shrimp Aristeus antennatus in the Western Mediterranean: results of a long-term study, *Marine Ecology Progress Series*, *159*, 133–141, doi: 10.3354/meps159133.

Sardà, F., J. B. Company, and F. Maynou (2003), Deep-sea shrimp (Aristeus antennatus Risso 1816) in the Catalan sea: a review and perspectives, *J. Northw. Atl. Fish. Sci*, *31*, 117–136.

Sardà, F., G. D'Onghia, C. Y. Politou, J. B. Company, P. Maiorano, and K. Kapiris (2004), Deep-sea distribution, biological and ecological aspects of

Aristeus antennatus (Risso, 1816) in the western and central Mediterranean Sea, *Scientia Marina*, *68*, 117–127, doi: 10.3989/scimar.2004.68s3117.

Sardà, F., J. B. Company, N. Bahamón, G. Rotllant, M. M. Flexas, J. D. Sánchez, D. Zúñiga, J. Coenjaerts, D. Orellana, G. Jordà, J. Puigdefábregas, A. Sánchez-Vidal, A. Calafat, D. Martín, and M. Espino (2009), Relationship between environment and the occurrence of the deep-water rose shrimp Aristeus antennatus (Risso, 1816) in the Blanes submarine canyon (NW Mediterranean), *Progress in Oceanography*, *82*, 227–238, doi: 10.1016/j.pocean.2009.07.001.

Schlacher, T. A., M. A. Schlacher-Hoenlinger, A. Williams, F. Althaus, J. N. A. Hooper, and R. Kloser (2007), Richness and distribution of sponge megabenthos in continental margin canyons off southeastern Australia, *Marine Ecology Progress Series*, *340*, 73–88, doi: 10.3354/meps340073.

Simpson, J. H., and J. Sharples (2012), *Introduction to the Physical and Biological Oceanography of Shelf Seas*, p. 424, Cambridge University Press, U.K.

Stabholz, M., X. D. D. Madron, M. Canals, A. Khripounoff, I. Taupier-Letage, P. Testor, S. Heussner, P. Kerhervé, N. Delsaut, L. Houpert, G. Lastras, and B. Dennielou (2013), Impact of open-ocean convection on particle fluxes and sediment dynamics in the deep margin of the Gulf of Lions, *Biogeosciences*, *10*(2), 1097–1116, doi: 10.5194/bg-10-1097-2013.

Thomson, R. E., E. E. Davis, M. Heesemann, and H. Villinger (2010), Observations of long-duration episodic bottom currents in the Middle America Trench: Evidence for tidally initiated turbidity flow, *J. Geophys. Res.*, *115*, C10,020, doi: 10.1029/2010JC006166.

Tintoré, J., D.-P. Wang, and P. E. L. Violette (1990), Eddies and thermohaline intrusions of the shelf-slope front off Northeast Spain, *J. Geophys. Res.: Oceans*, *95*, 1627–1633, doi: 10.1029/JC095iC02p01627.

Vetter, E. W., C. R. Smith, and F. C. de Leo (2010), Hawaiian hotspots: enhanced megafaunal abundance and diversity in submarine canyons on the oceanic islands of Hawaii, *Marine Ecology*, *31*(1), 183–199, doi: 10.1111/j.1439-0485.2009.00351.x.

Vilibić, I., K. Horvath, N. Strelec Mahović, S. Monserrat, M. Marcos, A. Amores, and I. Fine (2013), **Atmospheric processes responsible for generation of the 2008 Boothbay meteotsunami**, *Natural Hazards*, doi: 10.1007/s11069-013-0811-y.

Violette, P. E. L., J. Tintoré, and J. Font (1990), The surface circulation of the Balearic Sea, *J. Geophys. Res.*, *95*, 1559–1568, doi: 10.1029/JC095ic02p01559.

Volkov, D. L., G. Larnicol, and J. Dorandeu (2007), Improving the quality of satellite altimetry data over continental shelves, *J. Geophys. Res.*, *112*, C06,020, doi: 10.1029/2006JC003765.

Wainright, S. C. (1990), Sediment-to-water fluxes of particulate material and microbes by resuspension and their contribution to the planktonic food web, *Marine ecology progress series*, *62 (3)*, 271–281.

Washburn, L., M. S. Swenson, J. L. Largier, P. M. Kosro, and S. R. Ramp (1993), Cross-Shelf Sediment Transport by an Anticyclonic Eddy Off Northern California, *Science*, *261*(5128), 1560–1564, doi: 10.1126/science.261.5128.1560.

Zainuddin, M., H. Kiyofuji, K. Saitoh, and S.-I. Saitoh (2006), Using multi-sensor satellite remote sensing and catch data to detect ocean hot spots for albacore (Thunnus alalunga) in the northwestern North Pacific, *Deep Sea Research Part II: Topical Studies in Oceanography*, *53*(34), 419 – 431, doi: 10.1016/j.dsr2.2006.01.007.

Epíleg

La relació entre un director de tesi i un estudiant de doctorat és sempre una relació complexa, plena de matisos i oscil·lant de manera periòdica entre l'amor i l'odi. Però sempre passa per quatre clares etapes:

A la primera etapa, fase A, el director de tesi demana els projectes, aconsegueix els diners i escriu gaire bé la totalitat dels treballs. L'estudiant fa molta feina, la major part de la qual no serveix de gaire. Tots dos firmen els articles.

A la fase B el director segueix demanant els projectes i aconseguint els diners però la major part de la feina la fa ja l'estudiant. Els treballs els escriuen a mitges i tots dos firmen els articles.

A la fase C l'estudiant, normalment una vegada que ha acabat la tesi, comença a demanar projectes, aconseguir diners i fer la major part de la feina. Escriu gaire bé la totalitat dels treballs i tant l'antic estudiant com l'antic director firmen tots dos els articles.

A la fase D l'estudiant demana els projectes, aconsegueix el diners i fa tota la feina. Es desmarca del director, i els treballs els firma tan sols l'estudiant que ja comença a pensar en trobar un altre estudiant que l'ajudi.

La feina d'un director de tesis consisteix bàsicament en acurçar al màxim les fases A i B i en allargar tot el possible la fase C.